博 士 論 文

（Doctoral Thesis）

Microbiological Synthesis of Metalloid Tellurium Towards Biotechnology of Heavy Metal Bioremediation and Rare Metal Recycling

重金属のバイオレメディエーションおよびレアメタルリサイクリングに向けた
金属テルルの微生物による合成

2020 年

広島大学大学院先端物質科学研究科

Graduate School of Advanced Sciences of Matter
Hiroshima University

Madison Pascual Munar

目　　次
（Table of Contents）

1.　主論文（Main Thesis）

Microbiological Synthesis of Metalloid Tellurium Towards Biotechnology of Heavy Metal Bioremediation and Rare Metal Recycling

重金属のバイオレメディエーションおよびレアメタルリサイクリングに向けた金属テルルの微生物による合成

Madison Pascual Munar

2.　公表論文（Articles）

(1) Biomineralization of Metallic Tellurium by Bacteria Isolated from Marine Sediment Off Niigata Japan
Munar MP, Matsuo T, Kimura H, Takahashi H, Okamura Y
In: Endo K, Kogure T, Nagasawa H (eds)
Biomineralization, Springer, Singapore. 31, 291- 301 (2018)
DOI**:** https://doi.org/10.1007/978-981-13-1002-7_31

(2) Discovery of a Novel Gene Conferring Tellurite Tolerance Through Tellurite Reduction to *Escherichia coli* Transformant in Marine Sediment Metagenome Library
Munar MP, Takahashi H, Okamura Y
Marine Biotechnology 21, 762-772 (2019)
DOI: https://doi.org/10.1007/s10126-019-09922-w

主　論　文
(Main Thesis)

Abstract

Tellurite is a highly toxic residual from copper mining. Microbial cell-mediated reduction of this toxicant can pave the way for sustainable recovery of the semiconductor metalloid, tellurium (Te). Isolation of tellurite-reducing bacterial strains was performed in a marine sediment enrichment culture showing tellurite reduction activity. Metagenome library construction and functional screening were also employed to discover a novel tellurite-reducing gene from the marine sediment enrichment culture. Three tellurite-reducing marine mesophiles were isolated and purified into pure cultures. *Shewanella algae* Strain Hiro-1, *Pseudomonas pseudoalcaligenes* Strain Hiro-2, and *P. stutzeri* Strain Hiro-3, were identified by phylogenetic analysis using the complete 16S rDNA sequence. The three new strains showed intracellular tellurium crystals with a minimum unit size of 60 nm. The Minimum Inhibitory Concentration (MIC) of *S. algae* Hiro-1 was found to be at 15 mM sodium tellurite (Na_2TeO_3) while the two *Pseudomonas* has MIC of 6 mM Na_2TeO_3. A recombinant *Escherichia coli* Strain A1 harboring a putative tellurite-reducing gene was also identified and characterized from the metagenome library. The metagenome fragment is composed of 215 amino acid residues and had shown low sequence homology to known proteins. The probable origin of the metagenome fragment is *P. stutzeri* Hiro-3. Cloning of the Open Reading Frame (*Ps*-ORF1) into expression clones validated the role of the metagenome fragment in conferring tellurite resistance and tellurite reduction activity to *E. coli* host cells. The *E. coli* Strain A1 had shown tellurite resistance at 1 mM Na_2TeO_3. Optimal tellurite reduction activity was recorded at 37°C and pH 7.0. A chloramphenicol-susceptible A1 mutant strain with elevated MIC at 3 mM Na_2TeO_3 and with intact *Ps*-ORF1 was isolated from the metagenome library after sub-culturing in media without the antibiotics. This thesis had shown a feasible application of microbial cell-based bioremediation of toxic heavy metal consequently allowing for the recycling of rare metals like tellurium for use in technological and biomedical applications.

Thesis Contents

Chapter I

Introduction

1.1 Background of the Study

Tellurium resource is scarce. This valuable semiconductor and photoelectric metalloid has increasing significance in the development of second-generation thin-film solar cells as well as in the development of quantum dots for medical applications. Microbial cell-mediated tellurite bioremediation and recovery of tellurium offers a viable alternative as cleaner and sustainable technology in the future.

Most studies on tellurite reduction employs bacterial cells with low resistance to tellurite. Bacterial genera already reported with resistance to tellurite includes *Bacillus, Escherichia, Pseudomonas, Rhodobacter, Shewanella,* among others (Turner et al., 2012; Borghese et al., 2014). Tellurite ions generate superoxide radicals which damages biological functions of biomolecules that lead to cell death (Avazeri et al., 1997; Sabaty et al., 2001). Species-specific tellurite resistance mechanisms were developed by bacterial cells to oppose tellurite toxicity. Common mechanism includes, enzyme-mediated detoxification, exclusion of tellurite ions via efflux pumps, intracellular sequestration of tellurite ions, and volatilization of tellurite into dimethyl telluride (Arenas-Salinas et al., 2016). Several enzymes which include nitrate reductases, terminal oxidases from respiratory chain of gram-negative bacteria, catalase, and glutathione reductase were found to mediate tellurite reduction in some bacterial cells (Arenas-Salinas et al., 2016). Common features of genes with tellurite reduction activity include the presence of catalytic cysteine residues, NAD(P)H and FAD-binding motifs (Arenas-Salinas et al., 2016).

1.2 Objectives of the Study

This study aims to isolate bacterial strains with tellurite bioremediation potential. The study also aims to discover novel tellurite-reducing gene through metagenome library construction and functional screening.

1.3 Statement of the Problem and Significance of the Study

Tellurite is a highly toxic compound from copper refining that is a potential pollutant to our water resources (Borghese et al., 2014). Conversely, reduction of tellurite into elemental tellurium can provide potential resource of semiconductor metalloid for use in photovoltaic cells and other electronic devices. Exact mechanism of tellurite reduction remains unclear. Understanding this mechanism will pave the way for the development of sustainable bioremediation of tellurite and tellurium recovery technology in the future. Figure 1 shows a schematic diagram of the proposed Microbiological Approach for tellurite bioremediation and tellurium recovery.

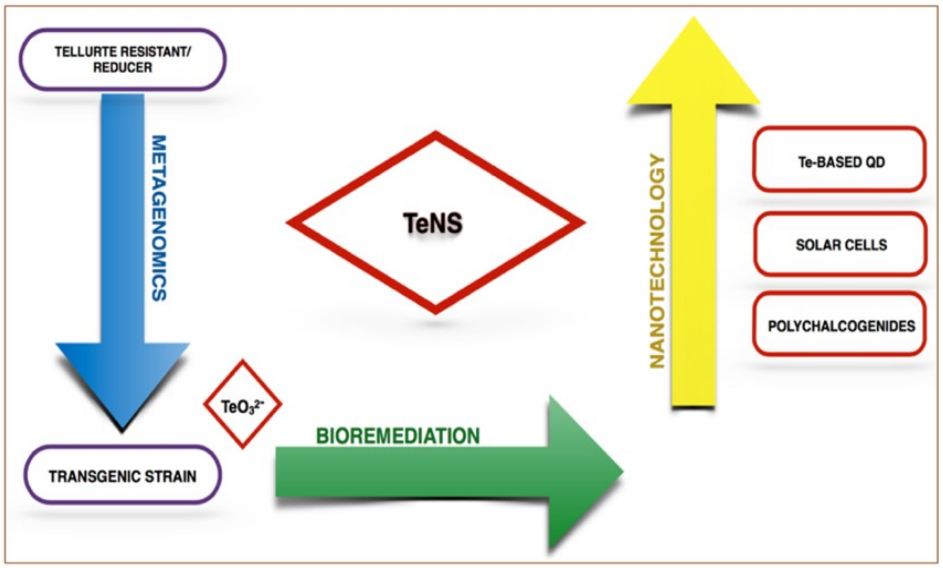

Figure 1. Microbiological Approach for tellurite bioremediation and tellurium nanostructures (TeNS) recovery. A marine sediment enrichment culture with tellurite reduction activity was used to isolate tellurite-reducing bacterial strains and as the metagenome seed culture to discover a novel tellurite-reducing gene. Tellurite-reducing bacterial strains and recombinant strains harboring a putative tellurite-reducing gene will be used for tellurite bioremediation. Tellurium crystals that formed inside the bacterial cells can be recovered and later be used into technological applications such solar cells, rechargeable batteries, and TE-based quantum dots.

1.4 Structure of Thesis, Scope and Delimitations

This thesis is composed of four Chapters which include Chapter I for the General Introduction, Chapter II covers the first paper- Isolation and Characterization of Tellurite-Reducing Bacterial Strains from Marine Sediment Enrichment Culture, Chapter III covers the second paper- Metagenome Library Construction and Functional Screening of Tellurite-Reducing Gene from Marine Sediment Microbial Community, and Chapter IV is the Over-all Conclusion and Recommendations.

In Chapter II, three new bacterial strains were isolated. These bacterial strains showed very high resistance to tellurite ions. Tellurium particle localization and morphology were also investigated in the three new marine bacterial strains. The new strains were characterized by complete 16S rDNA sequencing and phylogenetic analyses. Complete whole genome sequencing of the isolated new strains was not performed. In-depth biochemical and physicochemical analyses were not performed on the three new strains.

In Chapter III, a putative tellurite-reducing gene was screened from the metagenome library. The metagenome fragment sequence was analyzed and an Open Reading Frame (ORF) was cloned. Tellurite reduction assay validated the role of the *Ps*-ORF1 in conferring tellurite resistance and tellurite reduction activity to *Escherichia coli* transformants. Tellurium particle localization and morphology was also investigated. This thesis does not cover isolation and purification of proteins from the identified putative tellurite-reducing gene.

1.5 Review of Related Literature

1.5.1 Tellurite and its toxicity

Tellurite is known for extreme toxicity to bacterial cells primarily due to its oxidizing effect (Fleming, 1932; Taylor, 1999; Chasteen et al., 2009; Arenas-Salinas et al., 2016). Metal ions generate superoxide radicals which disturbs the functions of biomolecules (Pérez et al., 2007; Tremaroli et al., 2007; Turner et al., 2007; Martinez-Finley et al., 2012). Bacterial cells can overcome metal toxicity through expression of membrane-bound nitrate reductase or expression of cytoplasmic glutathione reductase (Avazeri et al., 1997; Sabaty et al., 2001; Turner, 2001; Turner et al., 2012; Pugin et al., 2014). Other tellurium oxyanions such as tellurate (TeO_4^{2-}) and tellurite (TeO_3^{2-}) can serve as electron acceptors in anaerobic respiration in some bacteria (Csotonyi et al., 2006; Baesman et al., 2007).

Bacterial cells have developed specific cell survival mechanisms in opposing the detrimental effects of toxic heavy metals (Narayanan and Sakthivel, 2010; Iravani, 2014). Metal-microbe interaction has potential in the bioremediation of heavy metals. Inextricably, microorganisms provide a viable and sustainable technology in metal remediation and recovery (Klaus-Joerger et al., 2001; Narayanan and Sakthivel, 2010).

1.5.2 Tellurite resistance and reduction mechanisms

Studies regarding bacterial tellurite resistance and reduction mechanisms have elucidated genes and proteins related to metal sequestration or detoxification. Metal-reducing genes (Jobling and Ritchie, 1987; Jobling and Ritchie, 1988; Hill et al., 1993; Whelan et al., 1995; Taylor, 1999; Taylor et al., 2002; Chasteen et al., 2009), cell membrane-bound flavoproteins (Moore and Kaplan, 1992; Taylor, 1999; Turner et al., 2001), and cytosolic oxidoreductases (Avazeri et al., 1997; Calderón et al., 2006; Pérez et al., 2007; Castro et al., 2008) related to tellurite resistance, reduction, susceptibility, sequestration, and detoxification were

characterized. Some tellurite-resistant bacteria were reported to utilize tellurite ions in anaerobic respiration (Lovley, 1993; Coker et al., 2012).

There are only few studies which identified the involvement of metal transport proteins in bacterial tellurite resistance and reduction mechanism. Among the few reported genes related to tellurite transport these include a manganese and iron transport gene (*mntH*), and two phosphate transport genes (*pstA* and *pstD*) (Kehres et al., 2000; Makui et al., 2000; Turner et al., 2007). Computational analysis of conserved functional domains from known tellurite reductases (TR) revealed the role of catalytic cysteine residues, NAD(P)H, and FAD-binding motifs in tellurite reduction activity (Korbekandi et al., 2009; Arenas-Salinas et al., 2016; Maltman et al., 2017).

1.5.3 Tellurium and its resources

Tellurium is from the Latin word *tellus* which means Earth thus also called the Earth metal. It was discovered by Franz-Joseph Müller von Reichenstein in 1782 (Emsley, 1989). Tellurium belongs to the Chalcogenides, Group 16 of the Periodic Table of Elements, together with oxygen, sulfur, polonium, and selenium (Arenas et al., 2014). There is no reported biological activity linked with tellurium (Ba et al., 2010). Tellurium possess thermoelectric and photoelectric properties which made it useful in developing photovoltaic cells (Mayers and Xia, 2002; Arenas et al., 2014).

Japan and Belgium were reported to be the leading producers of selenium and tellurium in the world market (Bleiwas, 2010). Tellurium are mostly recovered from copper mine tailings. The amount of extracted tellurium in a copper concentrate is generally below 100 parts per million. Roughly 50% to 60% are recovered from copper anode slimes (Simonz and Prinz, 1973). Significant increase in the market demand of tellurium encouraged countries like China and Mexico to search new possible deposits of tellurium (Bleiwas, 2010). In 2011, the value of tellurium has reached $350/kg (Trouba, 2019). The anticipation in price increase also induced researches on improving tellurium recovery.

1.5.4 Tellurium uses and important applications

Tellurium was commonly added to alloy to improve its machinability (AHP Materials, 2011). Tellurium is an important raw material for photovoltaic cells, rechargeable chalcogenide batteries, rewritable compact discs, and as quantum dots for cancer detection and treatment (Grandell and Hook, 2015; Mal et al., 2016; Zhang et al., 2019).

Chapter II

Isolation and Characterization of Tellurite-Reducing Bacterial Strains from Marine Sediment Enrichment Culture

2.1 Introduction

Tellurite reduction into pure metallic elemental tellurium (Te^0) was first observed as formation of black tellurium precipitate in the culture media (Tucker et al., 1962). Production and recovery of tellurium is important for the advancement of thin-film photovoltaic cells. However, tellurite reduction mechanism remains poorly understood. Studies conducted on tellurite reduction used bacterial strains with low tellurite resistance, and this greatly affects interpretation of results (Arenas-Salinas et al., 2016).

Escherichia coli BL21 has a very low resistance to tellurite with Minimum Inhibitory Concentration (MIC) of 4.5 μM (Aradska et al., 2013). A recombinant *E. coli* carrying nitrate reductase (*nar*) gene has developed increased tellurite resistance with MIC of 500 μM (Turner, 2001). One of the bacterial strains with very high tolerance to potassium tellurite (K_2TeO_3) is *Salinococcus* sp. Strain QW6 with MIC of 12 mM (Amoozegar et al., 2008). Other bacterial strains with high tolerance to tellurite are *Bacillus selenitireducens* with MIC of 8 mM, *Psychrobacter immobilis* with MIC of 2 mM, and *Rhodobacter capsulatus* with MIC of 1 mM (Sepahei and Rashetnia, 2009; Borghese et al., 2014; Arenas et al., 2014).

Tellurium crystal synthesis was reported in several bacterial strains. *Agrobacter, Bacillus, Erwinia*, *Escherichia*, *Geobacter*, *Pseudomonas*, *Rhodobacter*, *Selenihalanaerobacter, Shewanella, Staphylococcus*, and *Sulfurospirillum*, were reported for tellurium crystal synthesis (Moore and Kaplan, 1994; Avazeri et al., 1997; Trutko et al., 2000; Sabaty et al., 2001; Di Tomaso et al., 2002; Borsetti et al., 2003; Oremland et al., 2004; Csotonyi et al., 2006; Baesman et al., 2007; Baesman et al., 2009; Turner et al., 2012; Borghese et al., 2014). Bacterial strains with innate resistance to tellurite are potential candidates for tellurite bioremediation and tellurium recycling. Isolation and characterization of new strains with high tolerance to the metal can augment our understanding on the bacterial tellurite reduction mechanisms.

2.2 Materials and Methods

2.2.1 Isolation and cultivation

2.2.1.1 Marine sediment collection site

The marine sediment was collected at a depth of 100 meters off Niigata Bay, Japan. The marine sediment sample was provided by Dr. Takeshi Terahara of the Tokyo University of Marine Science and Technology. Figure 2 shows the images of collection site generated using the Geographical Positioning System (GPS) coordinates, 38°05’00.0”N,139°04’00.0”E, in Google Earth Engine (Gorelick et al., 2017).

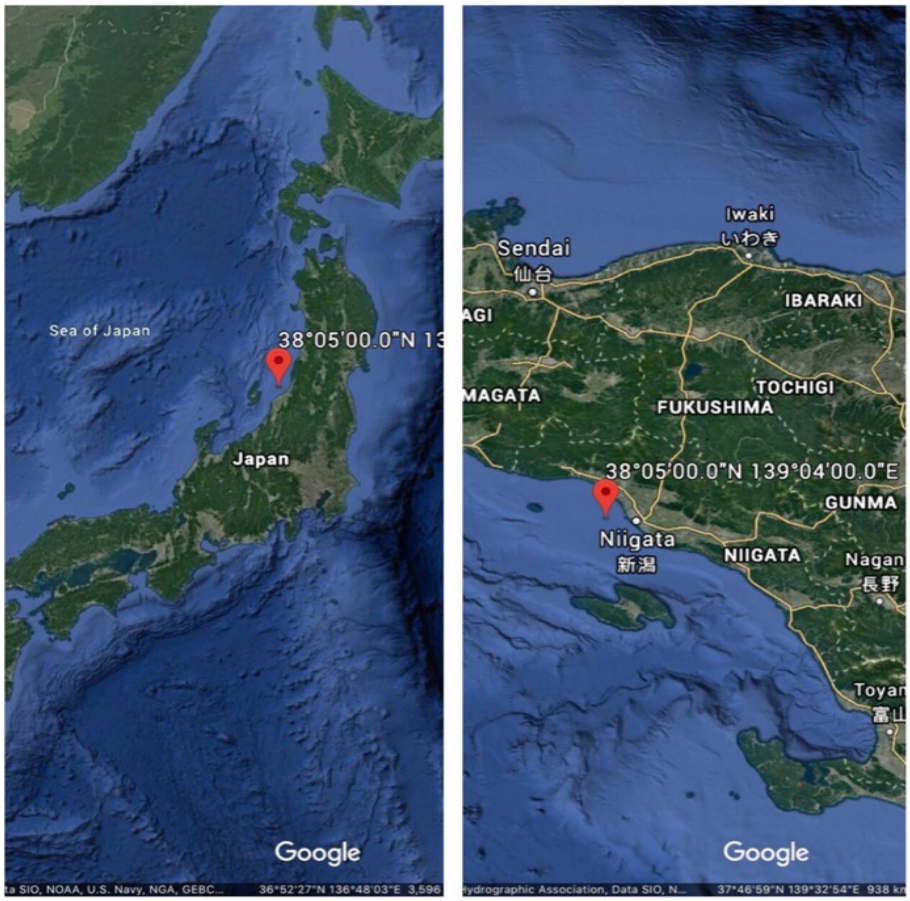

Figure 2. Collection site of the marine sediment samples in Niigata Bay, Japan.

2.2.1.2 Cultivation

The marine sediment was inoculated in RCVBN medium in 50 ml centrifuge Falcon tubes under continuous illumination for 1 month (Burgess et al., 1991). The sample was cultured in completely-filled 8-mL screw-capped tubes and incubated at 24°C with continuous illumination (38 µmol/m^2/s).

2.2.2 Tellurite reduction assay on marine sediment enrichment culture

2.2.2.1 Preparation of 100 mM sodium tellurite (Na_2TeO_3) stock solution

Stock solution of 100 mM Na_2TeO_3 (Sigma-Aldrich, USA) was prepared by dissolving the metal salt into ultrapure water (Direct-Q 3 UV Water Purification System, Merck Millipore, USA) and filter-sterilized using 0.20 µm membrane filter unit (Advantec, Toyo Roshi Keisha Ltd., Japan).

2.2.2.2 Tellurite reduction assay

One mL of the marine sediment enrichment culture was transferred into 7 mL fresh RCVBN medium amended with 1 mM sodium tellurite (Na_2TeO_3) to determine the tellurite-reducing activity. Tellurite reduction was visually recorded by the formation of black tellurium precipitate in the media (Tucker et al., 1962).

2.2.3 Characterization of marine sediment enrichment culture

2.2.3.1 Simple staining

Simple staining was performed using 0.5% crystal violet on 24-h bacterial cell culture (Moyes et al., 2009).

2.2.3.2 Identification of bacterial strains in the marine sediment enrichment culture using genus specific primers

Genomic DNA from the marine sediment enrichment culture was extracted using Hexadexyl-trimethyl-ammonium bromide (CTAB) method (Okamura et al., 2010). Polymerase Chain Reaction (PCR) using genus specific primers was performed to determine bacterial species present in the enrichment culture (Table 1). PCR mixture included 1x EmeraldAmp Max PCR Master Mix and 2 µL gDNA. Final concentration of each primers was listed in Table 2. Thermal cycling conditions include one cycle of pre-denaturation for 5 min at 94°C, followed by 28 cycles of denaturation at 94°C for 10 s, then annealing at 61°C for 20 s, and extension at 72°C for 45 s. PCR was performed using T100^{TM} Thermal Cycler (Bio-Rad, CA, USA). PCR products were electrophoresed at 100 V for 40 min (Mupid-exU, Mupid Co., Ltd., Japan). Samples were stained with UltraPower DNA Safe Dye and viewed under Blue Light Transilluminator (LEDB-SBOXH, OptoCode, Tokyo, Japan).

Table 1. Sequence of the genus specific primers used to identify the bacterial species present in the marine sediment enrichment culture.

No	Genus	Query Coverage (%)	Primer sequence (5' to 3')
1	*Marichromatium*	100	F363 GCCTGTGGTTAATACCCATG R516 TTCACATCTGACTGACCTCG
2	*Desulfovibrio*	100	F56 GCGTGGATTATCTACCTGCA R412 CGGCGTATTATTCCGCATAC
3	*Pseudomonas*	99	P-GS-F GACGGGTGAGTAATGCCTA P-GS-R CACTGGTGTTCCTTCCTATA
4	*Enterococcus*	99	F63 GGTAACCTGCCCATCAGAAG R334 ACTTTCGTCCATTGCCGAAG
5	*Oceanotoga*	99	F46 CGTAGGAATCTGCCCAAAGG R190 GCTTGGGAGTCTCTTACACT
6	*Sunxiuqinia*	99	F60 GTATGCAACCTGCCTTTGAC R373 GTTTACAACCCATAGGGCAG
7	*Vibrio*	100	F74 CCTGGGAAATTGCCCTGATG R192 CCACCTGGGCATATCCTGAC
8	*Shewanella*	99	F41 CCTGGGAATTTGCCCATTTG R159 CCACCTGGGCTTATCCATCA

Table 2. Final concentration of genus specific primers used in PCR to identify the bacterial species present in the marine sediment enrichment culture.

Genus	Primer conc. (μM/L)	Expected size (bp)
1. *Marichromatium*	1.0	150
2. *Desulfovibrio*	1.0	350
3. *Pseudomonas*	2.5	700
4. *Enterococcus*	2.5	300
5. *Oceanotoga*	1.0	150
6. *Sunxiuqinia*	0.75	300
7. *Vibrio*	1.0	100
8. *Shewanella*	1.0	100

2.2.3.3 Growth and tellurite reduction activity of marine sediment enrichment culture

The marine sediment enrichment was cultured in 8 mL RCVBN medium with or without 1-10 mM Na_2TeO_3. The marine sediment enrichment culture was incubated at 24°C under continuous illumination at various pH (pH 4.0, 7.0, 8.0, 9.0, 10.0, and 11.0). Bacterial growth was measured every 48 h for 21 d using spectrometer at OD_{660} nm (WPA CO-7500 Colorimeter, Biochrom Ltd., UK).

2.2.3.4 Effect of light on tellurite reduction activity

Tellurite reduction assay was performed in the presence of light and in complete darkness in 8-mL screw-capped tubes.

2.2.4 Investigation of spontaneous tellurite reduction in RCVBN media at various pH

Spontaneous tellurite reduction was investigated in RCVBN media at various pH. The pH tested were pH 4.0, 5.0, 6.0 7.0 8.0, 9.0, 10.0, and 11.0. The pH of RCVBN media was adjusted using 1 M HCl or 1 M NaOH.

2.2.5 Isolation of new bacterial strains

2.2.5.1 Incubation at 37℃

Plates were initially incubated anaerobically for two months at 24°C. The plates were transferred at 37°C (SANYO Incubator MIR-162, SANYO Electric Co., Ltd., Osaka, Japan), after which visible isolated bacterial colonies were observed after 24 h.

2.2.5.2 Isolation and purification

Pour plate method and streak plate method were employed to isolate tellurite-resistant and tellurite-reducing bacterial strains on RCVBN agar media with pH 7.6 at 37°C (Sanders, 2012).

2.2.5.3 Gram staining

Gram staining was performed on the three pure cultures (Smith and Hussey, 2005).

2.2.5.4 Establishing the purity of new bacterial isolates

Genomic DNA from purified isolates were extracted using DNA extraction kit (Cica Geneus, Kanto Chemical Co. Inc., Japan). Genus specific primers were used to validate purity of each isolated bacterial culture (Table 1). Simple staining was also performed and cells were viewed under oil immersion microscopy using compound microscope.

2.2.5.5 Catalase test

Catalase test was performed using 30% hydrogen peroxide (H_2O_2) on the three new isolated pure cultures to determine whether the isolates are facultative anaerobes.

2.2.6 16S rDNA analysis

2.2.6.1 16S rDNA amplification

The genomic DNA of pure cultures was extracted using DNA extraction Kit (Cica Geneus, Kanto Chemical Co. Inc., Japan). The complete sequence of 16S rDNA was amplified using PCR mix containing 10X KOD Plus-Neo Buffer, 2 mM dNTPs, 25 mM $MgSO_4$ (TOYOBO Co., Ltd., Japan), 10 µM each forward and reverse primer 16S 27F (F-5′-AGAGTTTGATCNTGGCTCAG-3′) and 16S ipRSR2 (R-5′-AAGGAGGTGATCCANCCGC-3′) (Eurofins Genomics, Tokyo Japan), 0.05 U/µL KOD Neo POL (TOYOBO Co., Ltd., Japan), and 2 µL genomic DNA. Thermal cycling conditions include one cycle of pre-denaturation for 2 min at 94°C, followed by 35 cycles of denaturation at 95°C for 10 s, then annealing at 60°C for 10 s, followed by extension at 68°C for 60 s, and final extension at 68°C for 60 s (T100^{TM} Thermal Cycler, Bio-Rad, USA).

2.2.6.2 Cloning

Amplified 16S rDNA fragments were excised from the gel and purified using Gel/PCR purification column (FAVORGEN Biotech Corp., Taiwan). Purified 16S rDNA fragments were cloned into the ZERO-Blunt TOPO vector following the kit protocol (Invitrogen, Japan). Positive transformants able to grow on LB/Kanamycin plates were used for Colony-PCR to verify insertion using M13 primers (Table 20) (Eurofins Genomics, Tokyo Japan). Thermal cycling conditions include one cycle of pre-denaturation for 5 min at 94°C, followed by 28 cycles of denaturation at 94°C for 10 s, then annealing at 70°C for 20 s, and final extension at 72°C for 45 s.

2.2.6.3 Sequencing

Positive transformants were isolated and plasmids were extracted using a Fastgene plasmid mini kit (Nippon Genetics Europe GnBH Co., Ltd., Japan) following the manufacturer's protocol. DNA sequencing was performed by Eurofins Genomics Co., Ltd. (Tokyo, Japan). SnapGene (SnapGene Software, www.snapgene.com) was used to evaluate the chromatogram and to guide trimming of erroneous bases. Error-free sequences were assembled with CodonCode Aligner (CodonCode Corporation, www.codoncode.com). DNA sequences were analyzed using Basic Local Alignment Search Tool (BLAST) in National Center for Biotechnology Information (NCBI) (Altschul et al., 1990).

2.2.6.4 Phylogenetic analysis of new bacterial strains

Phylogenetic analyses were performed using Molecular Evolutionary Genetics Analysis 6.0 (MEGA6) software (Tamura et al., 2013). Neighbor-Joining (NJ), Maximum-Likelihood (ML), and Minimum Evolution (ME) with Kimura-2-Parameter distance correction and 1000 bootstrap value were used to infer homology of the pure cultures with the reported bacterial strains in NCBI (Kimura, 1980; Felsenstein, 1985; Saitou and Nei, 1987; Rzhetsky and Nei, 1992;

Nei and Kumar, 2000). Muscle DNA alignment was used to align the assembled 16S rDNA sequences. There were 26 *Shewanella* and 24 *Pseudomonas* strains included in the analyses. The final data set included equal length of quality proofed sequences.

2.2.7 Culture characteristics of new bacterial strains

2.2.7.1 Culture characteristics of new bacterial strains and comparison with respective type strains

New bacterial strains were compared with the type strains *S. algae* NBRC 103173^T, *P. pseudoalcaligenes* NBRC 14167^T, and *P. stutzeri* NBRC 14165^T. These strains were obtained from the National Institute of Technology and Evaluation Biological Resource Center (NBRC) in Japan. Cultures were first inoculated on the recommended media and later transferred onto RCVBN plates. Cultures were also grown on plates with 200 µL 1 mM Na_2TeO_3. Cultures were incubated at 37°C for 6 d (SANYO Incubator MIR-162, SANYO Electric Co., Ltd., Osaka, Japan). Colony morphology were observed using stereomicroscope (TW-360, WRAYMER, Japan).

2.2.7.2 Optimum growth and tellurite reduction conditions of the three new isolates

Optimal growth conditions were determined for each isolated culture by assessing growth under varying pH levels (1.0, 4.0, 7.0, and 11.0) incubated at 37°C, and under varying temperatures (4°C, 25°C, 37°C, and 45°C) using pH 7.6 (SANYO Incubator MIR-162, SANYO Electric Co., Ltd., Osaka, Japan). The cultures were inoculated in RCVBN media amended with1 mM Na_2TeO_3. Bacterial concentrations were standardized using cultures incubated at the same time and with the same OD values at 550 nm. Optimum growth conditions, tellurite reduction activity, and MIC were performed using 6 mL RCVBN broth media and 1 mL inoculum in 8-mL screw-capped tubes with manual inversion

every 24 h. Bacterial growth was measured using spectrometer at OD_{550} nm (WPA CO-7500 Colorimeter, Biochrom Ltd., UK).

2.2.7.3 Comparison of culture characteristics, biochemical properties, and carbon utilization of the three new strains with respective species

Culture characteristics, biochemical properties, and carbon utilization were compared with respective strains using published literatures.

2.2.8 Tellurite reduction activity and MIC of the three new bacterial strains

Tellurite reduction activity and MIC of the three new bacterial strains were investigated in RCVBN media amended with increasing concentration of Na_2TeO_3 (1 mM, 2 mM, 4 mM, 6 mM, 8 mM, 10 mM, 12 mM, 15 mM). The samples were incubated at 37°C for 3 wk (SANYO Incubator MIR-162, SANYO Electric Co., Ltd., Osaka, Japan).

2.2.9 Temporal aspect of tellurite reduction in the three new strains

Temporal aspect of tellurite reduction activity of the three new strains was investigated in RCVBN media amended with 1 mM Na_2TeO_3. The cultures were incubated at 37°C for 31 d.

2.2.10 Observation using Transmission Electron Microscope

Tellurium crystal morphologies and localizations were observed using Transmission electron microscopy (TEM) (JEM2010, JEOL Ltd, Tokyo, Japan). The marine sediment enrichment culture was exposed to 1 mM Na_2TeO_3 for 101 d. The culture was washed twice with milliQ water through centrifugation at 10,000x g for 5 min. Washed cells were mounted on 150-mesh copper grids coated with collodion (Nisshin EM Co., Ltd., Japan).

2.3 Results

2.3.1 Marine sediment enrichment culture shows tellurite reduction activity

The marine sediment enrichment culture shows prominent purple-colored pigmentation due to the growth of a photosynthetic purple-sulfur bacterium, *Marichromatium* sp. (Figure 3, A-C2). The enrichment culture exhibits tellurite reduction activity in media amended with 1-2 mM Na_2TeO_3 (Figure 3, A-C3, A-C4).

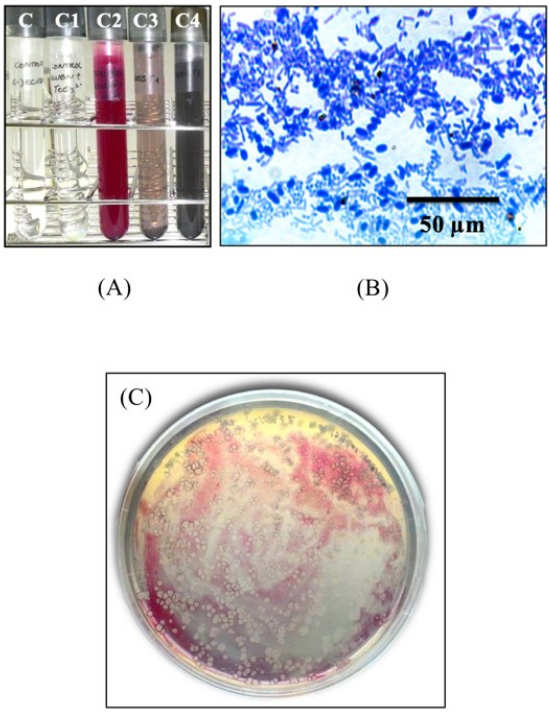

Figure 3. The marine sediment was cultivated in RCVBN media (A). Control tubes contains RCVBN media (A-C) and RCVBN amended with 1 mM Na_2TeO_3 (A-C1). Growth of purple-sulfur bacterium, *Marichromatium* sp. (A-C2). Simple staining and observation under compound microscope at 100x magnification reveal diversity of bacterial sizes and shapes (B). Plate showing growth of *Marichromatium* sp. with other unknown bacterial colonies (C).

2.3.2 Characterization of marine sediment enrichment culture

2.3.2.1 Eight bacterial strains in marine sediment enrichment culture

PCR using genus specific primers revealed eight bacterial genera present in the enrichment culture (Figure 4).

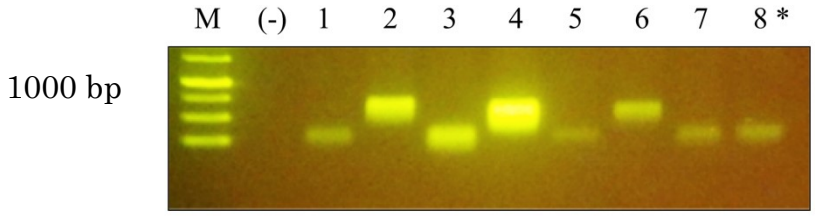

Figure 4. Eight bacterial species were identified using the genus specific primers. The bacterial genera were listed in Table 3. Ten µL of 1 Kb DNA Ready-To-Use Ladder (M) and PCR products were loaded on 1% agarose gel, electrophoresed at 100 V for 40 min. Samples were stained with UltraPower DNA Safe Dye and viewed using Blue Light Transilluminator. Negative control (-) used was Takara dH_2O. Numbers (1-8*) corresponds to the bacterial genus in Table 3.

Table 3. Bacterial Genera identified in the marine sediment enrichment culture.

* No.	Genus	Gram ID
1	*Marichromatium*	-
2	*Desulfovibrio*	-
3	*Pseudomonas*	-
4	*Enterococcus*	+
5	*Oceanotoga*	-
6	*Sunxiuqinia*	-
7	*Vibrio*	-
8	*Shewanella*	-

2.3.2.2 Growth and tellurite reduction activity of the marine sediment enrichment culture

The marine sediment enrichment culture showed highest growth at pH 8.0 which has no significant difference (*P*-value < .05) on growth at pH 9.0 and pH 10.0 (Figure 5). Lowest growth rate was recorded at pH 11.0 and has no significant difference (*P*-value < .05) with pH 4.0. Tellurite reduction activity at pH 9.0 and pH 10.0 has no significant difference (*P*-value > .05) with pH 7.0 and pH 8.0 (Figure 6). Tellurite reduction activity at pH 4.0 and pH 11.0 has significant difference (*P*-value < .05) with pH 7.0 and pH 9.0.

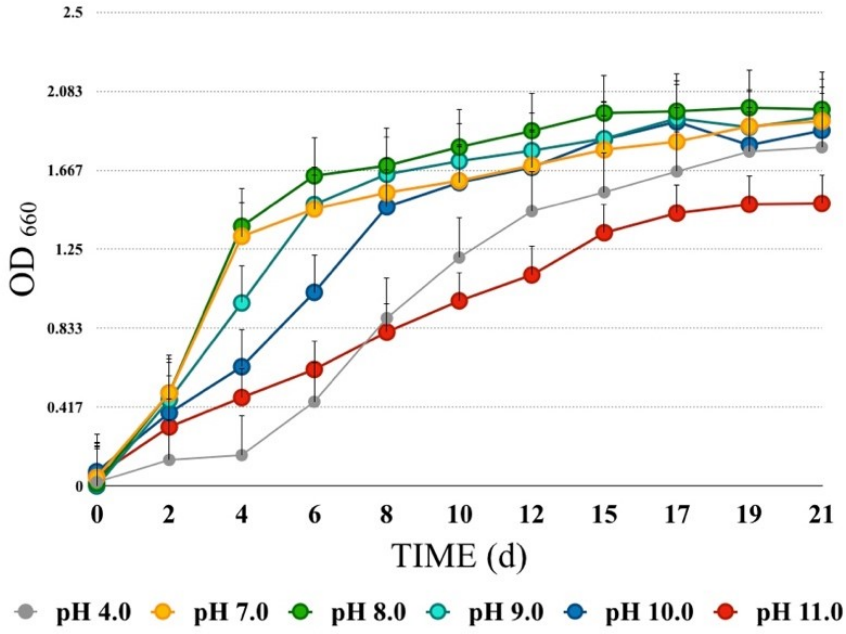

Figure 5. Optimum growth of marine sediment enrichment culture at various pH.

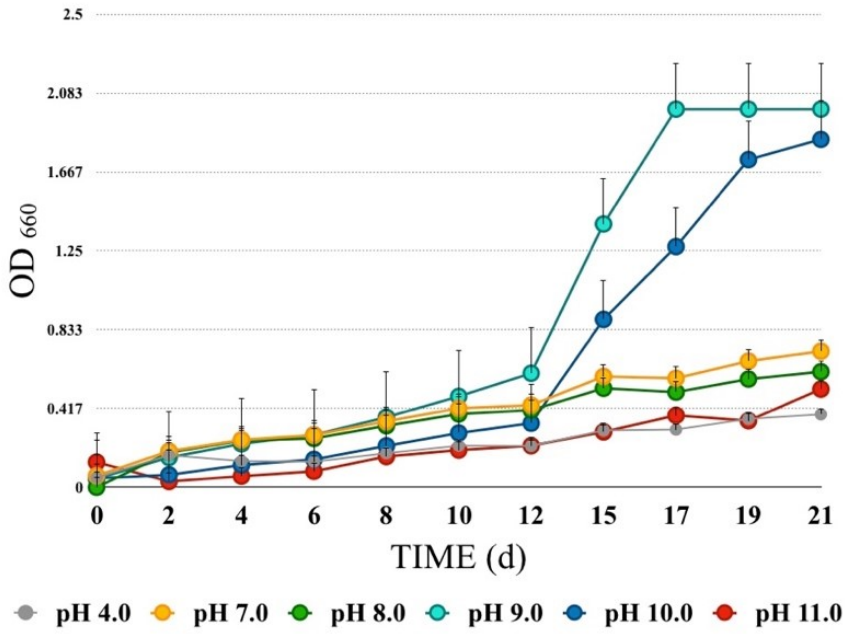

Figure 6. Optimum tellurite reduction activity of marine sediment enrichment culture at various pH.

Tellurite reduction activity from 1 mM-10 mM Na_2TeO_3 (Figure 7-A). Intense black precipitate formation was observed at pH 9.0 and pH 10.0 which coincided with reported optimum pH for tellurite reduction activity in some bacterial strains (Figure 7-B, 7-C) (Arenas-Salinas et al., 2016).

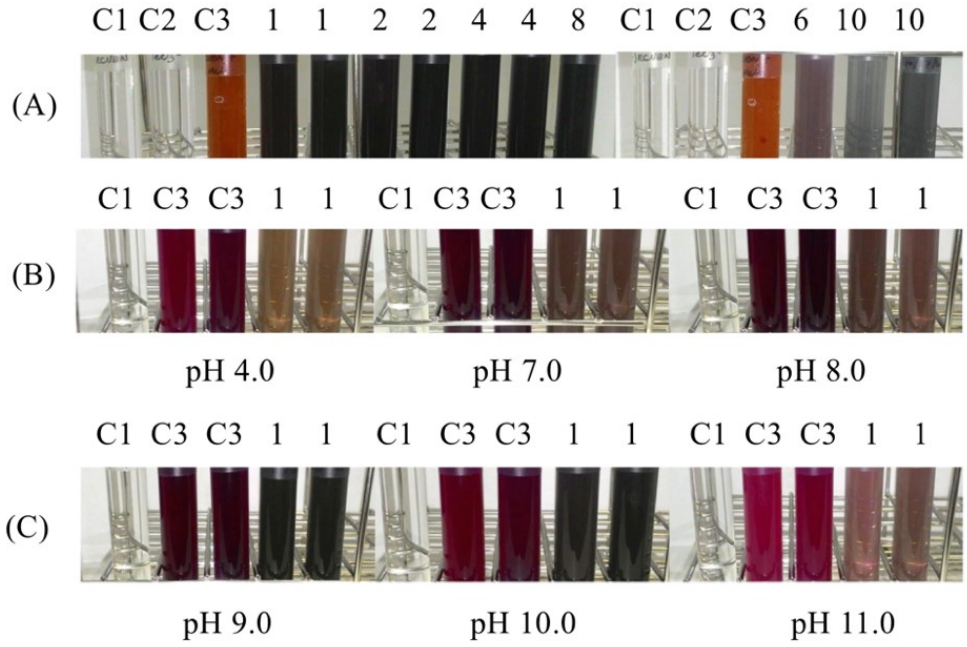

Figure 7. Tellurite reduction activity of marine sediment enrichment culture. Biochemical assay includes RCVBN media (C1), RCVBN media amended with 1 mM Na_2TeO_3 (C2), RCVBN inoculated with bacterial culture (C3), and RCVBN amended with 1 mM-10 mM Na_2TeO_3 (conc. is indicated on the label) inoculated with bacterial culture (A). Tellurite reduction activity was also assayed at various pH (B, C).

2.3.2.3 Effect of light on the growth of *Marichromatium* sp.

Marichromatium sp. grew on the tubes exposed to light, while no growth of the photosynthetic purple-sulfur bacterium was observed on tubes under complete darkness (Figure 8). However, it is noteworthy that tellurite reduction activity was both recorded on tubes exposed to light and tubes under darkness. This observation led to the hypothesis that there are other bacterial strains capable of tellurite reduction present in the marine sediment enrichment culture other than *Marichromatium* sp.

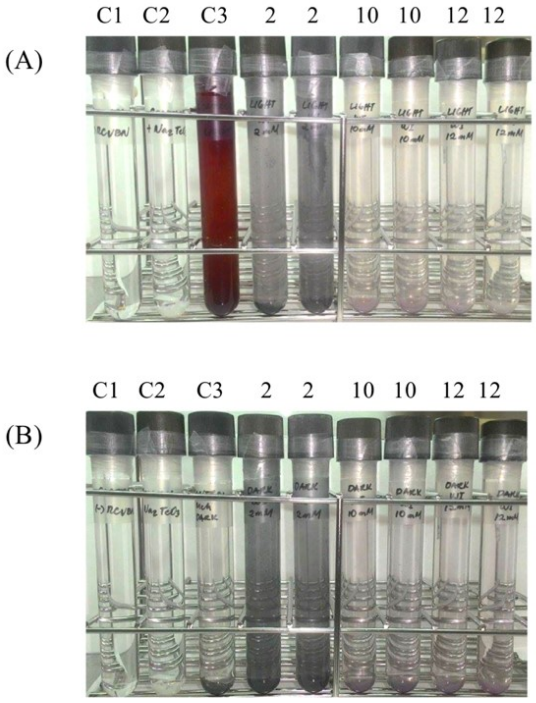

Figure 8. Effect of light on the growth of *Marichromatium* sp. Tellurite reduction assay includes RCVBN media (C1), RCVBN amended with 1 mM Na_2TeO_3 (C2), RCVBN inoculated with marine sediment enrichment culture (C3), and RCVBN amended with Na_2TeO_3 and inoculated with the marine sediment enrichment culture. Concentrations of Na_2TeO_3 (2, 10, 12 mM were labeled on tubes). Set-up incubated with light source (A), and set-up incubated under complete darkness (B).

2.3.3 Investigation of spontaneous tellurite reduction in RCVBN media at various pH

There was no visible spontaneous reduction of Na_2TeO_3 ions when added in RVCBN with varying pH (Figure 9). The brownish precipitate on pH 11 is due to adjustment of pH using 1 mM NaOH which already formed the precipitate even before the addition of Na_2TeO_3.

Figure 9. Investigation of spontaneous tellurite reduction in RCVBN media at various pH. The medium amended with Na_2TeO_3 remains clear after eight days of incubation.

2.3.4 Isolation of new bacterial strains

2.3.4.1 Incubation at 37℃

After two months of incubation at 24°C, no visible bacterial growth was observed. Plates were transferred to 37°C, after 24 h visible isolated colonies were observed. This presented an opportunity to isolate possible tellurite-resistant and tellurite-reducing bacterial strains from the marine sediment enrichment culture (Figure 10).

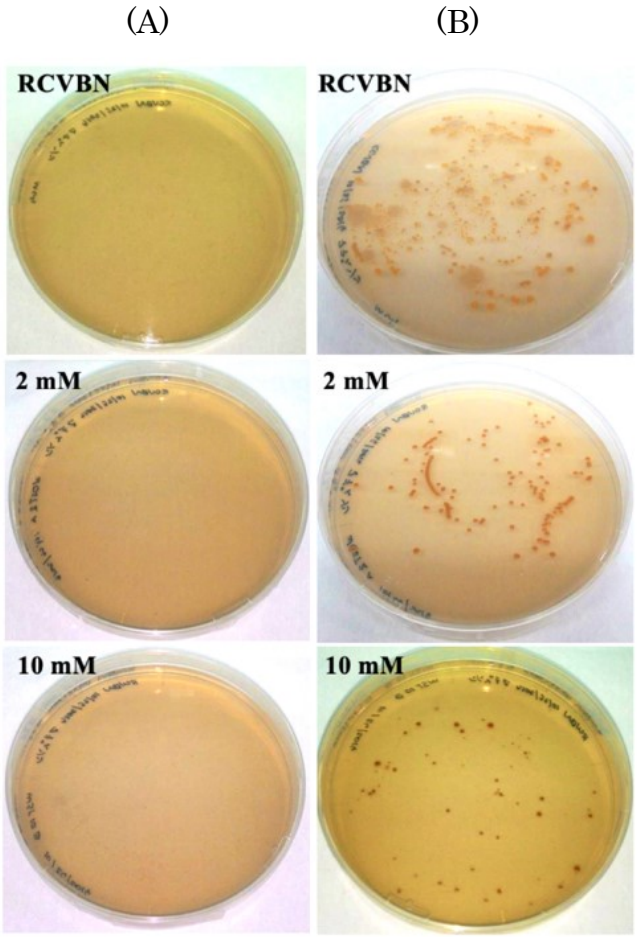

Figure 10. Isolation of tellurite-reducing bacterial strains. Plates incubated at 24°C (A). Plates incubated at 37°C (B). Concentrations of Na_2TeO_3 (mM) were indicated.

2.3.4.2 Isolation and purification of new bacterial strains

Streak plating technique was performed to purify three visible distinct colonies from the plates grown at 37°C (Figure 11).

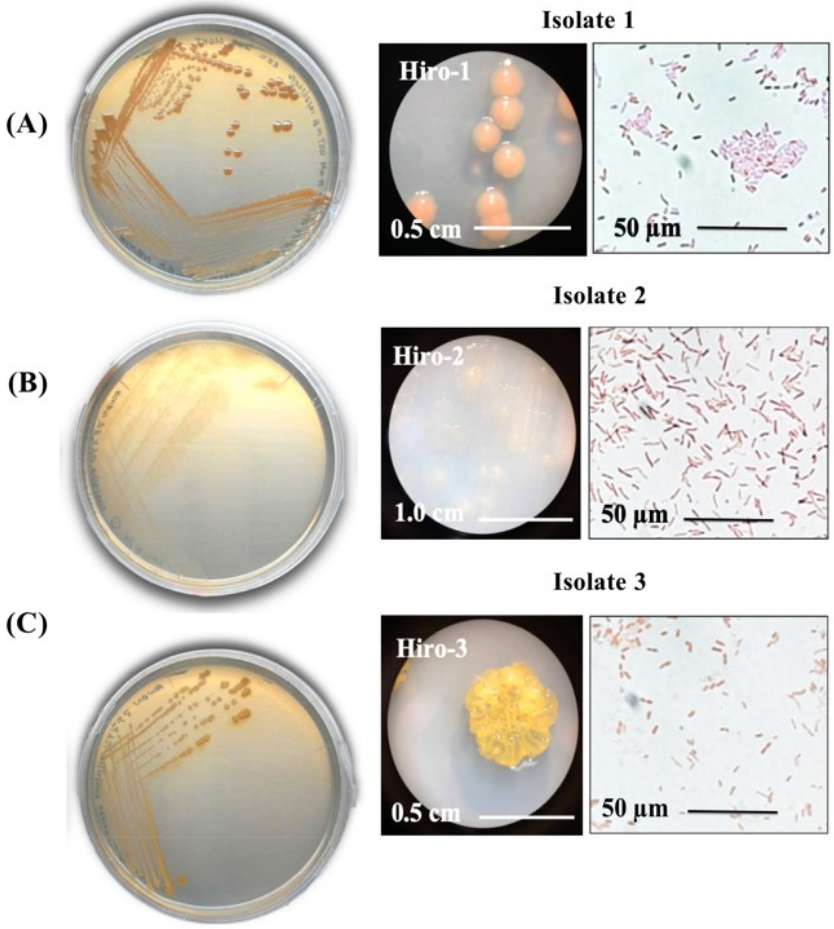

Figure 11. Isolation and purification of marine bacterial isolates (A, B, C). Gram staining revealed gram negative reaction. Observation under compound microscope at 100x magnification showed rod-shaped cells.

2.3.4.3 Establishing the purity of new bacterial strains

Purity of the new isolates were investigated using simple staining and PCR using the DNA extracted from each pure culture. Single amplicons were observed on the genus *Pseudomonas* and *Shewanella* (Figure 12).

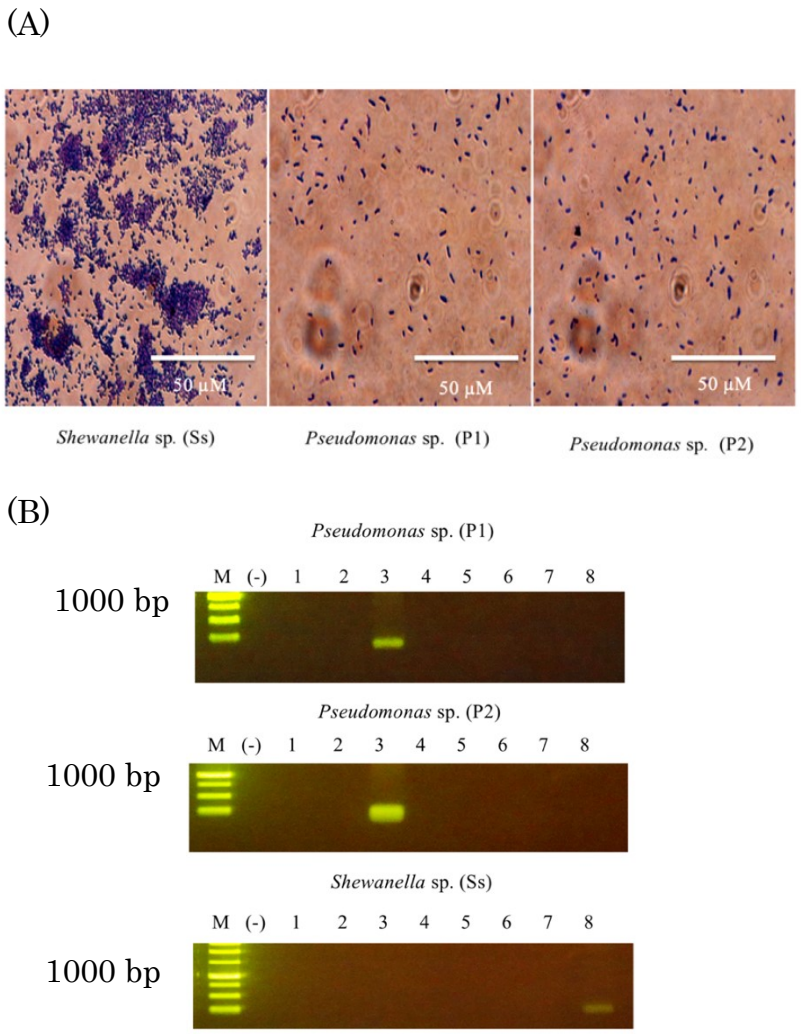

Figure 12. Microscopic observation of the three pure cultures under oil immersion microscopy at 400x magnification using compound microscope (A). PCR validated the purity of the isolates (B). Marker (M) used was a 1 Kb DNA Ready-To-Use Ladder. Lane 3 corresponds to genus *Pseudomonas* while lane 8 corresponds to genus *Shewanella*. Negative control (-) used was UltraPure H_2O.

2.3.4.4 Catalase activity of new bacterial isolates

Catalase test revealed the facultative anaerobe nature of the three new bacterial isolates (Figure 13). Presence of catalase denotes the cells are capable of breaking down H_2O_2 into H_2O and O_2 thus the observed effervescence.

Figure 13. Catalase Test on three pure cultures. Control tube (C) contains 30% H_2O_2 and test reaction contains 100 µL 30% H_2O_2 inoculated with 1 mL bacterial culture. *Shewanella* sp. (H1), *Pseudomonas* sp. (H2), and *Pseudomonas* sp. (H3) showed positive result for catalase activity denoting their facultative anaerobe nature.

2.3.5 16S rDNA analysis on the three new bacterial strains

2.3.5.1 Amplification of complete 16S rDNA

Complete 16S rDNA of the three pure cultures was amplified and cloned (Figure 14).

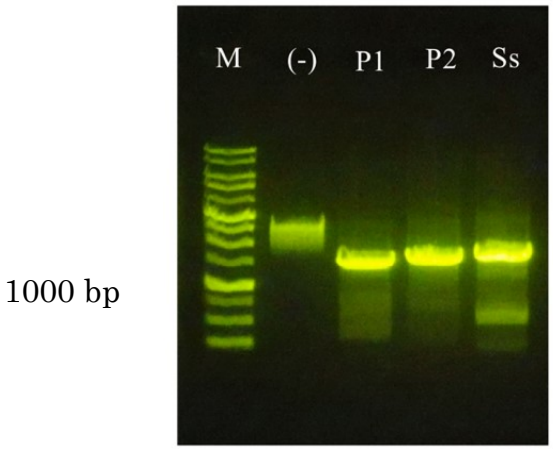

Figure 14. Amplification of complete 16S rDNA from the three new bacterial isolates. Ten µL of 1 Kb DNA Ready-To-Use Ladder (M), and PCR products from *Pseudomonas* sp. (P1), *Pseudomonas* sp. (P2) and *Shewanella* sp. (Ss) were electrophoresed at 100 V for 40 min. Negative control (-) used was UltraPure H_2O.

Plasmids harboring the complete 16S rDNA were extracted and sequenced by Eurofins Genomics, Tokyo, Japan (Figure 15).

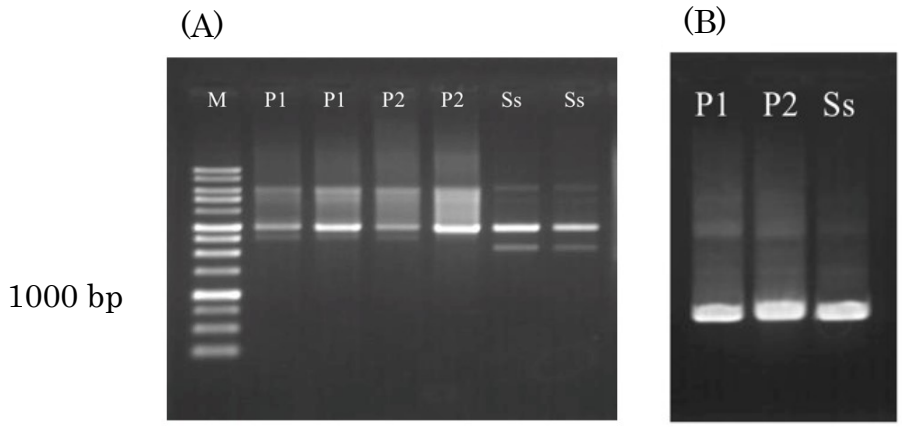

Figure 15. Plasmid extracted from clones harboring the complete 16S rDNA from the three new bacterial isolates (A). Ten µL of 1 Kb DNA Ready-To-Use Ladder (M), plasmids extracted from *Pseudomonas* sp. (P1), *Pseudomonas* sp. (P2) and *Shewanella* sp. (Ss) were electrophoresed. Confirmation of 16S rDNA insertion in plasmids by PCR using 16S rDNA primers (B).

2.3.5.2 Phylogenetic analyses on new bacterial isolates

BLAST search revealed homology of the three new isolates to *S. algae* (Query length: 1537 bp; homology: 99%; E-value: 0.00), *P. pseudoalcaligenes* (Query length: 1529 bp; homology: 99%; E-value: 0.00), and *P. stutzeri* (Query length: 1529 bp; homology: 99%; E-value: 0.00). Phylogenetic analyses suggested the three isolates were unique strains (Figure 16, 17, 18, 19, 20, 21). Thus, new strains were designated as *S. algae* strain Hiro-1 (DDBJ Accession no.: LC339942), *P. pseudoalcaligenes* strain Hiro-2 (DDBJ Accession no.: LC339940), and *P. stutzeri* strain Hiro-3 (DDBJ Accession no.: LC339941).

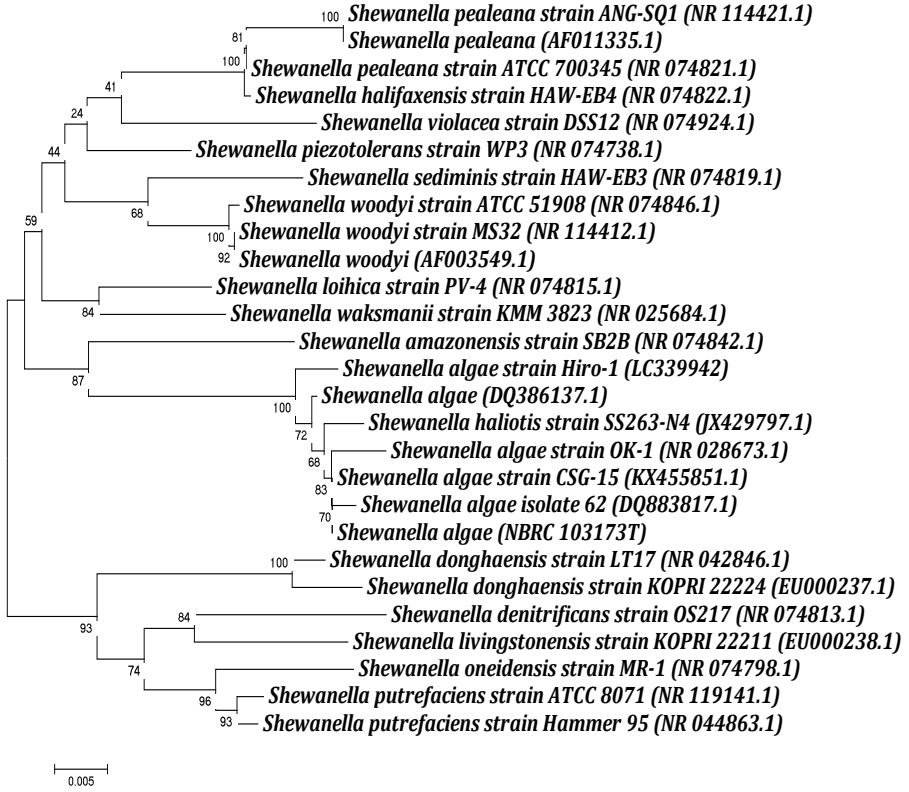

Figure 16. Unrooted Neighbor-Joining (NJ) tree of partial and complete 16S rDNA sequences from *S. algae* Hiro-1, and reported shewanellae in NCBI GenBank. Accession numbers were presented in parentheses. Numbers at nodes represent bootstrap values from 1000 resampled datasets. Scale bar indicates 0.5% sequence divergence. Kimura-2-parameter was used for distance correction.

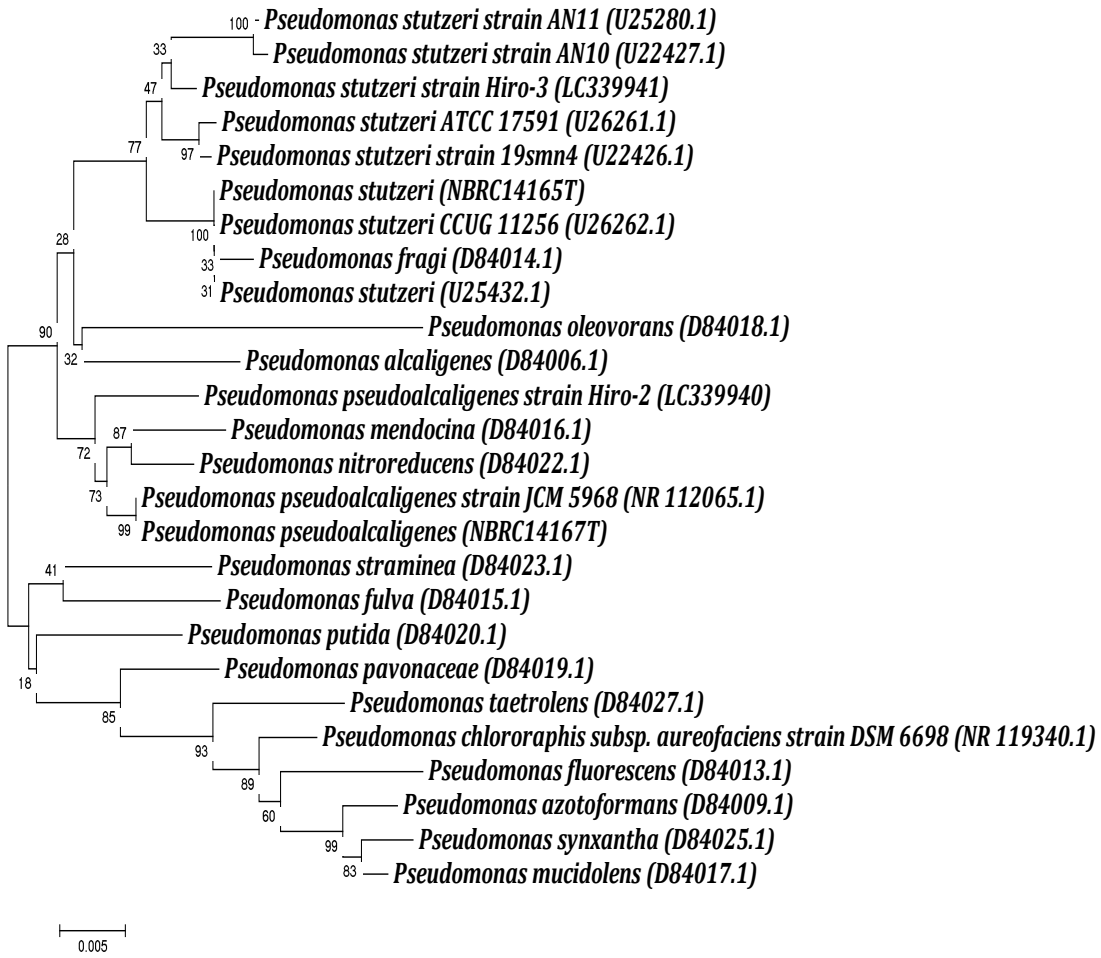

Figure 17. Unrooted Neighbor-Joining (NJ) tree based on partial and complete 16S rDNA nucleotide sequences of *P. pseudoalcaligenes* Hiro-2, and *P. stutzeri* Hiro-3 and other closely related species. Accession numbers were presented in parentheses. Numbers at nodes represent bootstrap values from 1000 resampled datasets. Scale bar indicates 0.5% sequence divergence. Kimura-2-parameter was used for distance correction.

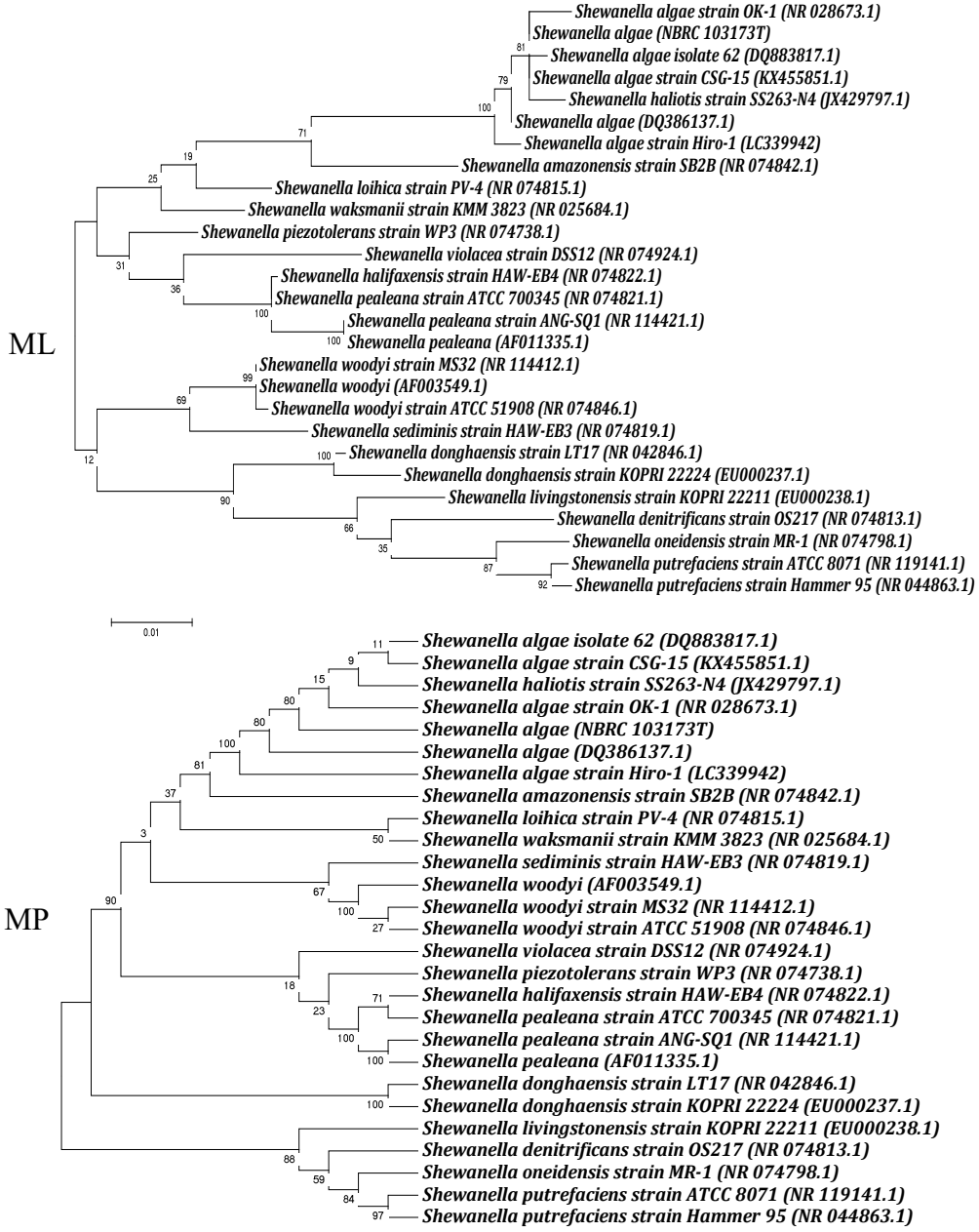

Figure 18. Unrooted Maximum-Likelihood (ML) and Maximum Parsimony (MP) trees based on partial and complete 16S rDNA nucleotide sequences of *S. algae* Hiro-1 and closely related species reported in NCBI GenBank. Accession numbers were presented in parentheses. Numbers at nodes represent bootstrap values from 1000 resampled datasets. Scale bar indicates sequence divergence. Kimura-2-Parameter was used for distance correction.

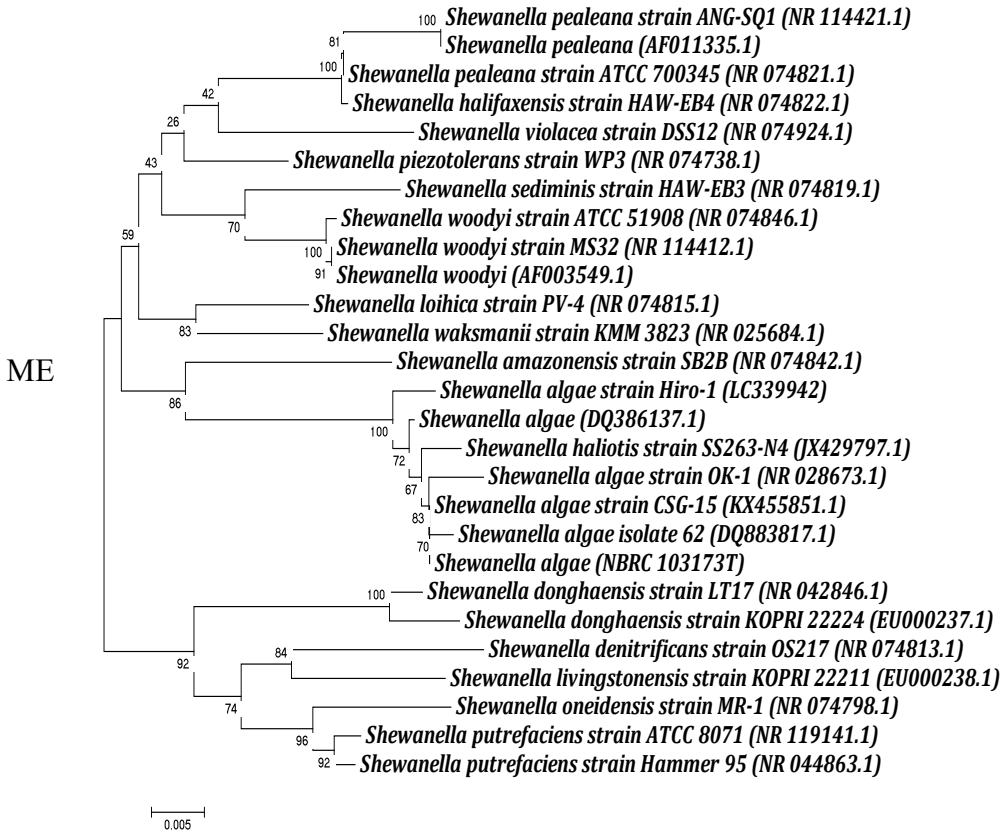

Figure 19. Unrooted Minimum Evolution (ME) tree based on partial and complete 16S rDNA nucleotide sequences of *S. algae* Hiro-1 and closely related species reported in NCBI GenBank. Accession numbers were presented in parentheses. Numbers at nodes represent bootstrap values from 1000 resampled datasets. Scale bar indicates sequence divergence. Kimura-2-Parameter was used for distance correction.

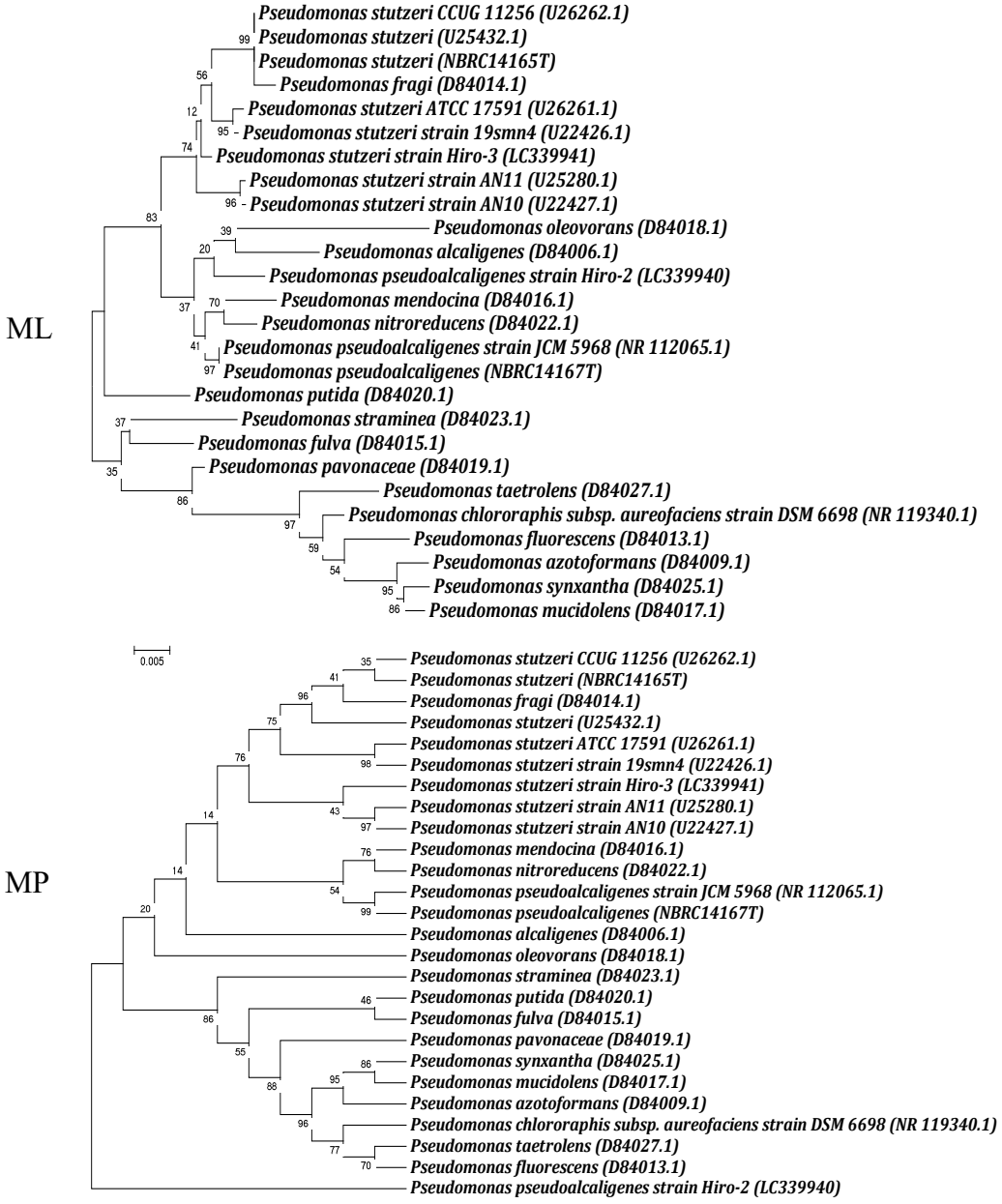

Figure 20. Unrooted Maximum-Likelihood (ML) and Maximum Parsimony (MP) trees based on partial and complete 16S rDNA nucleotide sequences of *P. pseudoalcaligenes* Hiro-2, and *P. stutzeri* Hiro-3 and closely related species reported in NCBI GenBank. Accession numbers were presented in parentheses. Numbers at nodes represent bootstrap values from 1000 resampled datasets. Scale bar indicates sequence divergence. Kimura-2-Parameter was used for distance correction.

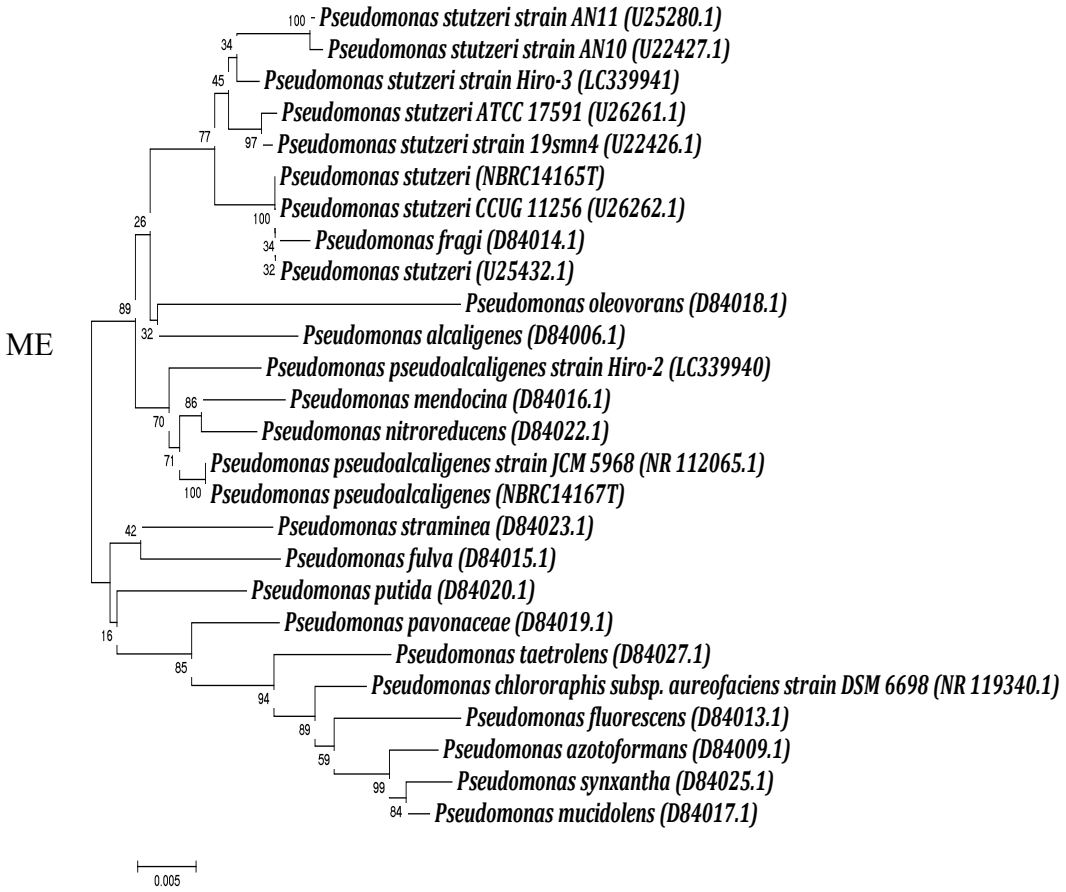

Figure 21. Unrooted Minimum Evolution (ME) tree based on partial and complete 16S rDNA nucleotide sequences of *P. pseudoalcaligenes* Hiro-2, and *P. stutzeri* Hiro-3 and closely related species reported in NCBI GenBank. Accession numbers were presented in parentheses. Numbers at nodes represent bootstrap values from 1000 resampled datasets. Scale bar indicates sequence divergence. Kimura-2-Parameter was used for distance correction.

2.3.6 Culture characteristics of new bacterial strains

2.3.6.1 Culture characteristics of new bacterial strains and comparison with respective type strains

Round colonies with entire margin, convex elevation, mucoid consistency, orange color, and about 2-5 µm in size were observed in *S. algae* Hiro-1. Colonies with irregular form, undulate margin, raised elevation, viscid consistency, translucent color, and about 2-5 µm in size were observed in *P. pseudoalcaligenes* Hiro-2. Colonies with wrinkled form, undulate margin, raised elevation, rugose consistency, yellow color, and about 2-5 µm in size were observed in *P. stutzeri* Hiro-3. The new strains showed similar colony characteristics with the NBRC type strains (Figure 22). Tellurite resistance were both observed in the three new strains and type strains.

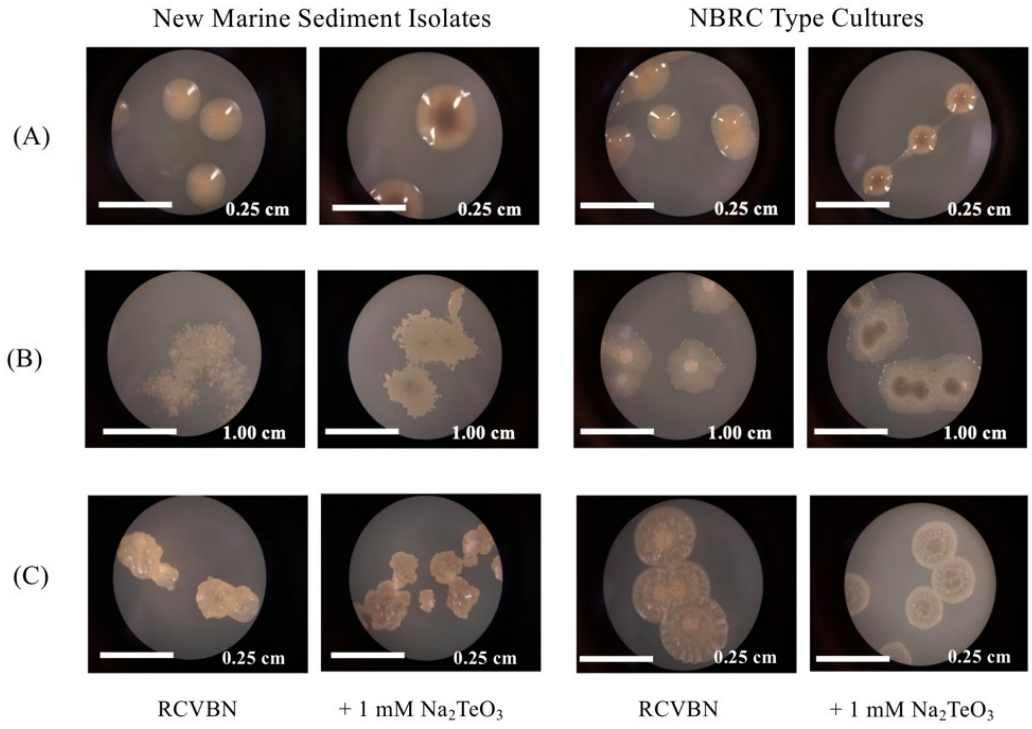

Figure 22. Comparison of new bacterial strains isolated from marine sediment enrichment culture with the respective type strains. Similar colony morphology was observed between similar species.

2.3.6.2 Optimum growth and tellurite reduction activity of the three new strains

S. algae Hiro-1 and *P. stutzeri* Hiro-3 grew optimally at pH 7.0. *P. pseudoalcaligenes* Hiro-2 grew optimally at pH 9.0 (Figure 23). No significant difference (*P*-value > .05) between the growths at 25˚C, 37˚C, and 45˚C on the three new strains (Figure 24). No observable growth was recorded at 4˚C. The three marine isolates were facultative anaerobes (Figure 25). Optimum tellurite reduction activity of *S. algae* Hiro-1 and *P. stutzeri* Hiro-3 was observed at pH 7.0 (Figure 26). Optimum tellurite reduction activity of *P. pseudoalcaligenes* Hiro-2 was observed at pH 9.0.

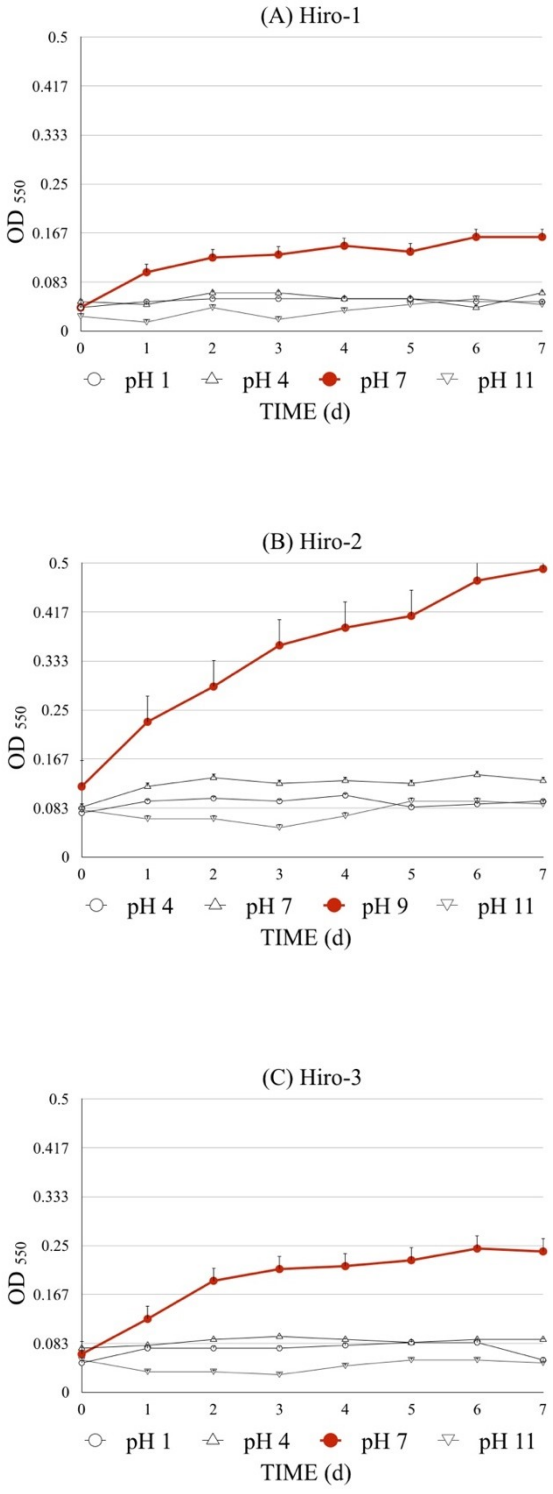

Figure 23. *S. algae* Hiro-1 (A) and *P. stutzeri* Hiro-3 (C) showed optimum growth at pH 7, while *P. pseudoalcaligenes* Hiro-2 (B) showed optimum growth at pH 9.

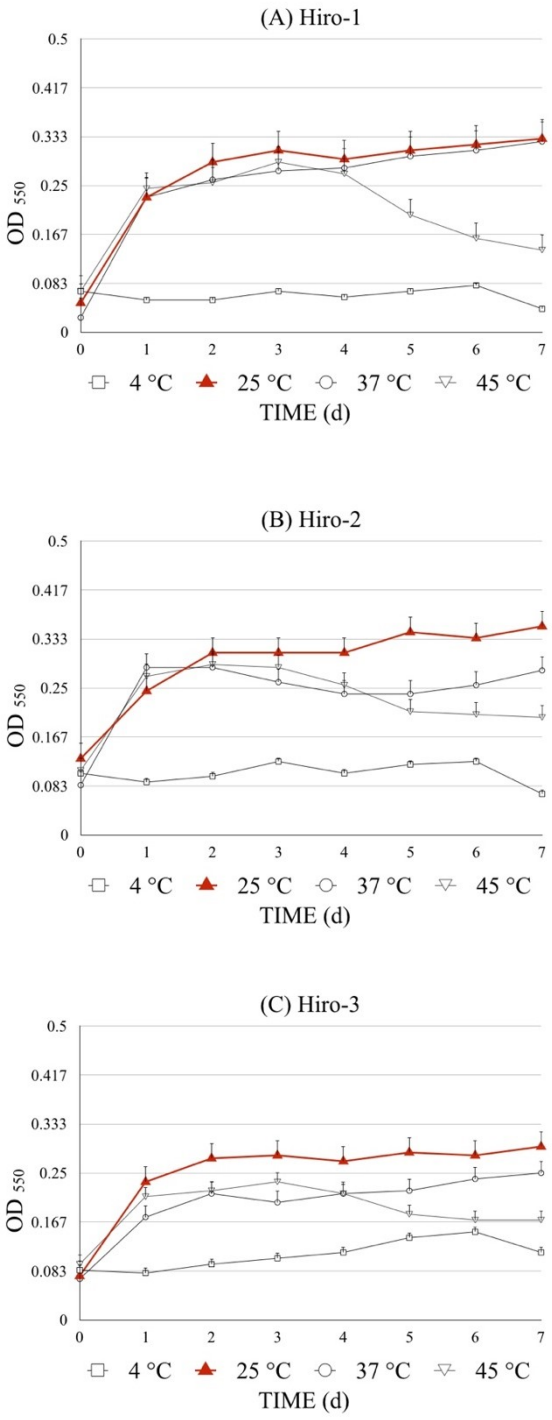

Figure 24. The three new bacterial strains are mesophiles with optimum growth at 25°C.

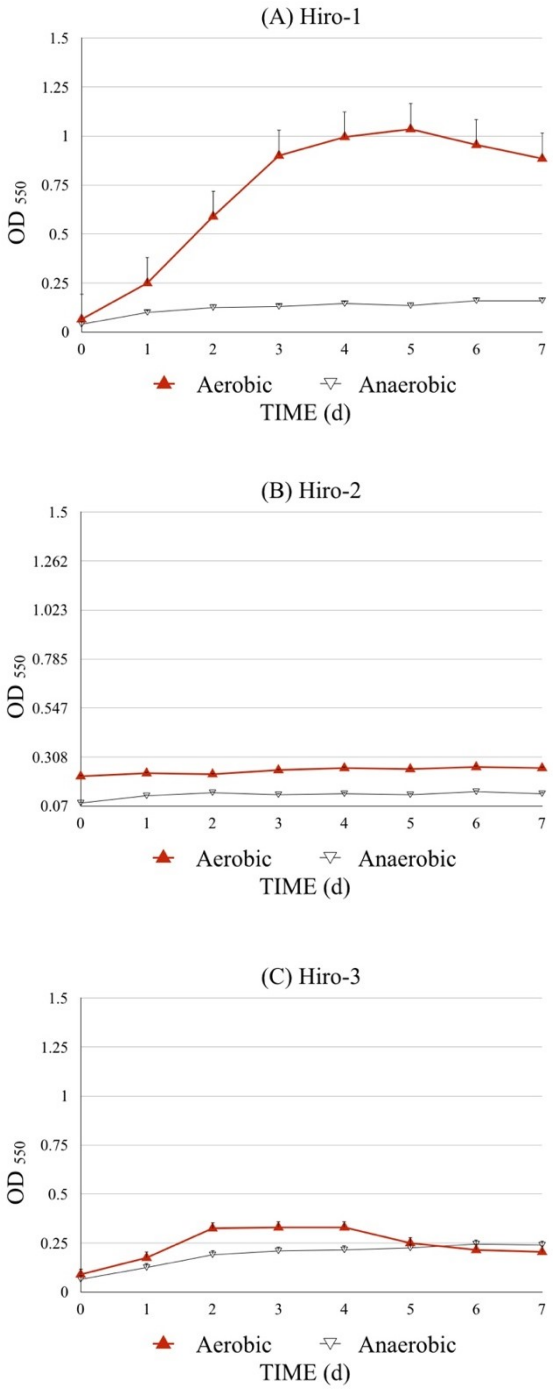

Figure 25. The three new bacterial strains are facultative anaerobes.

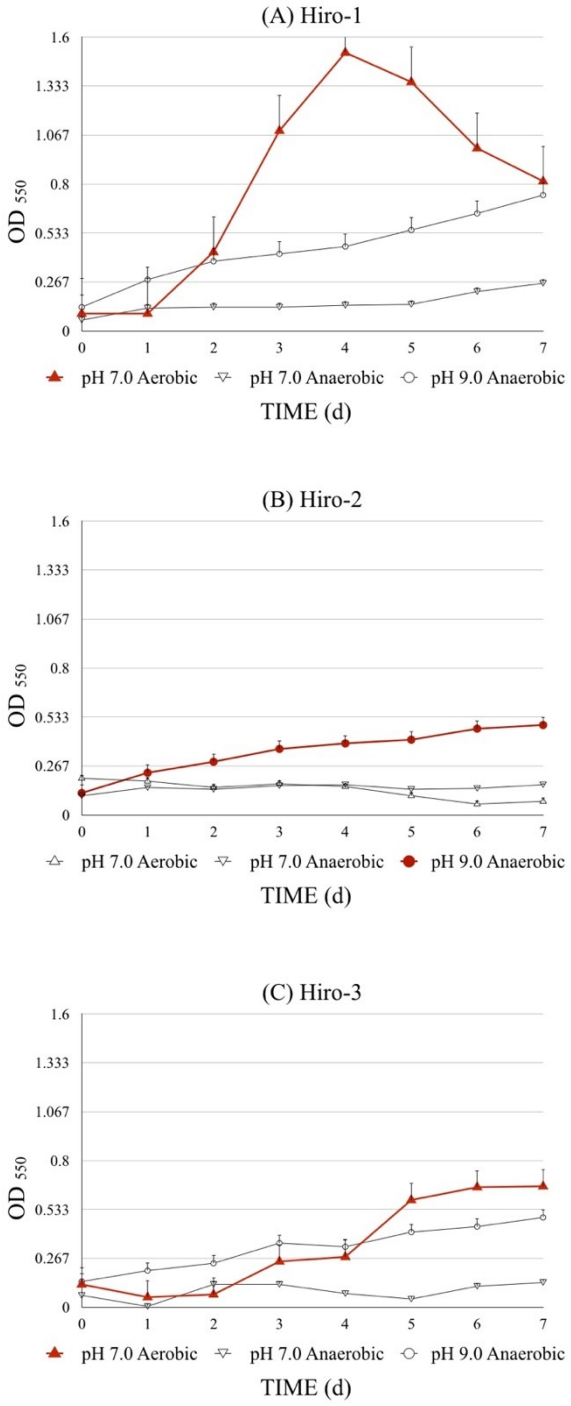

Figure 26. Optimum tellurite reduction conditions for *S. algae* Hiro-1 (A), *P. pseudoalcaligenes* Hiro-2 (B), and *P. stutzeri* Hiro-3 (C) at 1 mM Na_2TeO_3.

2.3.6.3 Comparison of culture characteristics, biochemical properties, and carbon utilization of the three new strains with respective species

Culture characteristics, biochemical properties, and carbon utilization of *S. algae* Hiro-1, *P. pseudoalcaligenes* Hiro-2, and *P. stutzeri* Hiro-3 were also compared with other shewanellae and pseudomonads (Table 4 to Table 18).

Table 4. Comparison of *S. algae* Hiro-1 with other shewanellae.

Characteristics	*S. algae* Hiro-1	*S. algae* IAM 14159 (OK-1)	*S. haliotis* DW01
Gram reaction	negative	negative	negative
Aerobicity	facultative anaerobe	ND	facultative anaerobe
Colony (a) form	(a) round	(a) ND	(a) round
(b) margin	(b) entire	(b) ND	(b) entire
(c) elevation	(c) convex	(c) ND	(c) convex
(d) consistency	(d) mucoid	(d) mucoid	(d) smooth
(e) color	(e) orange	(e) yellowish brown	(e) orange
Cell shape	rod	rod	rod
Size (μm)	2-5	ND	ND
Flagellation	ND	monotrichous	ND
Motility	ND	motile	motile
Capsule	ND	ND	ND
Isolation	Marine Sediment, Japan	Red algae, Japan	Abalone gut microflora, South Sea, Republic of Korea
References	This study	Simidu et al., 1990; Nozue et al., 1992; Holt et al., 2005	Kim et al., 2007

(ND) no data; (+) positive reaction; (-) negative reaction

Table 5. Comparison of *S. algae* Hiro-1 with other shewanellae.

Characteristics	*S. algae* Hiro-1	*S. algae* IAM 14159 (OK-1)	*S. haliotis* DW01
Catalase test	+	+	+
Oxidase test	ND	+	+
Indole production	ND	-	-
H_2S production	ND	+	+
Gelatin hydrolysis	ND	+	+
Arginine dihydrolase test	ND	-	-
Nitrate reduction	ND	+	+
Beta-hemolysis on BSA	ND	+	ND
Optimum temp. (°C)	25	ND	37
Optimum pH	7	ND	7
NaCl conc. (%)	ND	6	6
DNA G+C (%)	ND	54	53.7
Major fatty acids	ND	ND	C15-C17
References	This study	Simidu et al., 1990; Nozue et al., 1992; Holt et al., 2005	Kim et al., 2007

(ND) no data; (+) positive reaction; (-) negative reaction

Table 6. Comparison of *S. algae* Hiro-1 with other shewanellae.

Characteristics	*S. algae* Hiro-1	*S. amazonensis* SB2B	*S. loihica* PV-4
Gram reaction	negative	negative	negative
Aerobicity	facultative anaerobe	facultative anaerobe	facultative anaerobe
Colony (a) form	(a) round	(a) round	(a) round
(b) margin	(b) entire	(b) entire	(b) ND
(c) elevation	(c) convex	(c) convex	(c) slightly raised
(d) consistency	(d) mucoid	(d) smooth	(d) smooth
(e) color	(e) orange	(e) beige-pink	(e) orange
Cell shape	rod	rod	rod
Size (μm)	2-5	2-3	1.8
Flagellation	ND	monotrichous	monotrichous
Motility	ND	motile	motile
Capsule	ND	ND	ND
Isolation	Marine Sediment, Japan	Shelf muds, Amazon River delta, Amapá coast, Brazil	Iron-rich microbial mats, Seamount, Hawaii
References	This study	Venkateswaran et al., 1998	Gao et al., 2006

(ND) no data; (+) positive reaction; (-) negative reaction

Table 7. Comparison of *S. algae* Hiro-1 with other shewanellae.

Characteristics	*S. algae* Hiro-1	*S. amazonensis* SB2B	*S. loihica* PV-4
Catalase test	+	+	+
Oxidase test	ND	+	+
Indole production	ND	+	ND
H_2S production	ND	+	-
Gelatin hydrolysis	ND	+	+
Arginine dihydrolase test	ND	+	ND
Nitrate reduction	ND	+	-
Beta-hemolysis on BSA	ND	+	ND
Optimum temp. (°C)	25	37	18
Optimum pH	7	7-8	6-8
NaCl conc. (%)	ND	1-3	2
DNA G+C (%)	ND	51.7	53.8
Major fatty acids	ND	C15-C17	C12-C18
References	This study	Venkateswaran et al., 1998	Gao et al., 2006

(ND) no data; (+) positive reaction; (-) negative reaction

Table 8. Comparison of *P. pseudoalcaligenes* Hiro-2, and *P. stutzeri* Hiro-3 with other pseudomonads.

Characteristics	*P. pseudoalcaligenes* Hiro-2	*P. stutzeri* Hiro-3	*P. stutzeri*
Gram reaction	negative	negative	negative
Aerobicity	facultative anaerobe	facultative anaerobe	aerobe
Colony (a) form	(a) irregular	(a) wrinkled	(a) wrinkled
(b) margin	(b) undulate	(b) undulate	(b) undulate
(c) elevation	(c) raised	(c) raised	(c) raised
(d) consistency	(d) viscid	(d) rugose	(d) hard/dry
(e) color	(e) translucent	(e) yellow	(e) brown
Cell shape	rod	rod	rod
Size (μm)	2-5	2-5	1-3
Flagellation	ND	ND	monotrichous
Motility	ND	ND	motile
Capsule	ND	ND	ND
Isolation	Marine Sediment, Japan	Marine Sediment, Japan	Human opportunistic pathogen
References	This study	This study	Lalucat et al., 2006

(ND) no data; (+) positive reaction; (-) negative reaction

Table 9. Comparison of *P. pseudoalcaligenes* Hiro-2, and *P. stutzeri* Hiro-3 with other pseudomonads.

Characteristics	*P. pseudoalcaligenes* Hiro-2	*P. stutzeri* Hiro-3	*P. stutzeri*
Catalase test	+	+	+
Oxidase test	ND	ND	+
Indole production	ND	ND	ND
H_2S production	ND	ND	ND
Gelatin hydrolysis	ND	ND	-
Arginine dihydrolase test	ND	ND	-
Nitrite reduction	ND	ND	+
Beta-hemolysis on BSA	ND	ND	ND
Optimum temp. (°C)	25	25	35
Optimum pH	9	7	ND
NaCl conc. (%)	ND	ND	ND
DNA G+C (%)	ND	ND	60-65
Major fatty acids	ND	ND	ND
References	This study	This study	Lalucat et al., 2006

(ND) no data; (+) positive reaction; (-) negative reaction

Table 10. Comparison of *P. pseudoalcaligenes* Hiro-2, and *P. stutzeri* Hiro-3 with other pseudomonads.

Characteristics	*P. pseudoalcaligenes* Hiro-2	*P. stutzeri* Hiro-3	*P. pseudoalcaligenes* subsp. *Citrulli*
Gram reaction	negative	negative	negative
Aerobicity	facultative anaerobe	aerobe	aerobe
Colony (a) form	(a) irregular	(a) wrinkled	(a) round
(b) margin	(b) undulate	(b) undulate	(b) ND
(c) elevation	(c) raised	(c) raised	(c) slightly convex
(d) consistency	(d) viscid	(d) rugose	(d) smooth
(e) color	(e) translucent	(e) yellow	(e) transparent
Cell shape	rod	rod	rod
Size (μm)	2-5	2-5	0.5
Flagellation	ND	ND	monotrichous
Motility	ND	ND	motile
Capsule	ND	ND	ND
Isolation	Marine Sediment, Japan	Marine Sediment, Japan	Watermelon pathogen
References	This study	This study	Schaad et al., 1978

(ND) no data; (+) positive reaction; (-) negative reaction

Table 11. Comparison of *P. pseudoalcaligenes* Hiro-2, and *P. stutzeri* Hiro-3 with other pseudomonads.

Characteristics	*P. pseudoalcaligenes* Hiro-2	*P. stutzeri* Hiro-3	*P. pseudoalcaligenes* subsp. *Citrulli*
Catalase test	+	+	ND
Oxidase test	ND	ND	+
Indole production	ND	ND	ND
H_2S production	ND	ND	ND
Gelatin hydrolysis	ND	ND	-
Arginine dihydrolase test	ND	ND	-
Nitrite reduction	ND	ND	-
Beta-hemolysis on BSA	ND	ND	-
Optimum temp. (°C)	25	25	30
Optimum pH	9	7	ND
NaCl conc. (%)	ND	ND	ND
DNA G+C (%)	ND	ND	65-67
Major fatty acids	ND	ND	ND
References	This study	This study	Schaad et al., 1978

(ND) no data; (+) positive reaction; (-) negative reaction

Table 12. Comparison of *P. pseudoalcaligenes* Hiro-2, and *P. stutzeri* Hiro-3 with other pseudomonads.

Characteristics	*P. pseudoalcaligenes* Hiro-2	*P. stutzeri* Hiro-3	*P. alcaligenes*
Gram reaction	negative	negative	negative
Aerobicity	facultative anaerobe	aerobe	aerobe
Colony (a) form	(a) irregular	(a) wrinkled	(a) round
(b) margin	(b) undulate	(b) undulate	(b) wrinkled
(c) elevation	(c) raised	(c) raised	(c) flat
(d) consistency	(d) viscid	(d) rugose	(d) mucous
(e) color	(e) translucent	(e) yellow	(e) translucent
Cell shape	rod	rod	rod
Size (μm)	2-5	2-5	0.5
Flagellation	ND	ND	monotrichous
Motility	ND	ND	motile
Capsule	ND	ND	ND
Isolation	Marine Sediment, Japan	Marine Sediment, Japan	Human opportunistic pathogen
References	This study	This study	Monias, 1928; Ralston-Barrett et al., 1976

(ND) no data; (+) positive reaction; (-) negative reaction

Table 13. Comparison of *P. pseudoalcaligenes* Hiro-2, and *P. stutzeri* Hiro-3 with other pseudomonads.

Characteristics	*P. pseudoalcaligenes* Hiro-2	*P. stutzeri* Hiro-3	*P. alcaligenes*
Catalase test	+	+	+
Oxidase test	ND	ND	+
Indole production	ND	ND	-
H_2S production	ND	ND	-
Gelatin hydrolysis	ND	ND	ND
Arginine dihydrolase test	ND	ND	+
Nitrite reduction	ND	ND	+
Beta-hemolysis on BSA	ND	ND	ND
Optimum temp. (°C)	25	25	26-30
Optimum pH	9	7	ND
NaCl conc. (%)	ND	ND	ND
DNA G+C (%)	ND	ND	66-68
Major fatty acids	ND	ND	ND
References	This study	This study	Monias, 1928; Ralston-Barrett et al., 1976

(ND) no data; (+) positive reaction; (-) negative reaction

Table 14. Comparison of carbon utilization of *S. algae* Hiro-1 with other shewanellae.

Carbon source	*S. algae* Hiro-1	*S. algae* IAM 14159 (OK-1)	*S. haliotis* DW01
D-mannose	ND	-	-
Sucrose	ND	-	ND
Maltose	ND	-	ND
D-glucose	ND	+	-
Fructose	ND	-	-
Succinate	ND	ND	ND
Fumarate	ND	ND	ND
Citrate	ND	ND	-
Malate	ND	ND	+
Isolation	Marine Sediment, Japan	Red algae, Japan	Abalone gut microflora, South Sea, Republic of Korea
References	This study	Simidu et al., 1990; Nozue et al., 1992; Holt et al., 2005	Kim et al., 2007

(ND) no data; (+) positive reaction; (-) negative reaction

Table 15. Comparison of carbon utilization of *S. algae* Hiro-1 with other shewanellae.

Carbon source	*S. algae* Hiro-1	*S. amazonensis* SB2B	*S. loihica* PV-4
D-mannose	ND	ND	ND
Sucrose	ND	ND	ND
Maltose	ND	ND	ND
D-glucose	ND	ND	+
Fructose	ND	ND	ND
Succinate	ND	+	+
Fumarate	ND	+	+
Citrate	ND	+	+
Malate	ND	ND	+
Isolation	Marine Sediment, Japan	Shelf muds, Amazon River delta, Amapá coast, Brazil	Iron-rich microbial mats, active deep-sea hydrothermal Naha vent, South Rift of Loihi Seamount, Hawaii
References	This study	Venkateswaran et al., 1998	Gao et al., 2006

(ND) no data; (+) positive reaction; (-) negative reaction

Table 16. Comparison of carbon utilization of *P. pseudoalcaligenes* Hiro-2, and *P. stutzeri* Hiro-3 with other pseudomonads.

Carbon source	*P. pseudoalcaligenes* Hiro-2	*P. stutzeri* Hiro-3	*P. stutzeri*
Citrate	ND	ND	ND
Fructose	ND	ND	ND
D-mannose	ND	ND	-
Sucrose	ND	ND	-
Glucose	ND	ND	+
Maltose	ND	ND	+
Fumarate	ND	ND	+
Malate	ND	ND	+
Succinate	ND	ND	+
Isolation	Marine Sediment, Japan	Marine Sediment, Japan	Wide ecological niche, Human opportunistic pathogen
References	This study	This study	Lalucat et al., 2006; Rosselló-Mora et al., 1994

(ND) no data; (+) positive reaction; (-) negative reaction

Table 17. Comparison of carbon utilization of *P. pseudoalcaligenes* Hiro-2, and *P. stutzeri* Hiro-3 with other pseudomonads.

Carbon source	*P. pseudoalcaligenes* Hiro-2	*P. stutzeri* Hiro-3	*P. pseudoalcaligenes* subsp. *citrulli*
Citrate	ND	ND	+
Fructose	ND	ND	+
D-mannose	ND	ND	-
Sucrose	ND	ND	-
Glucose	ND	ND	-
Maltose	ND	ND	-
Fumarate	ND	ND	ND
Malate	ND	ND	ND
Succinate	ND	ND	ND
Isolation	Marine Sediment, Japan	Marine Sediment, Japan	Watermelon pathogen
References	This study	This study	Schaad et al., 1978

(ND) no data; (+) positive reaction; (-) negative reaction

Table 18. Comparison of carbon utilization of *P. pseudoalcaligenes* Hiro-2, and *P. stutzeri* Hiro-3 with other pseudomonads.

Carbon source	*P. pseudoalcaligenes* Hiro-2	*P. stutzeri* Hiro-3	*P. alcaligenes*
Citrate	ND	ND	-
Fructose	ND	ND	-
D-mannose	ND	ND	-
Sucrose	ND	ND	-
Glucose	ND	ND	-
Maltose	ND	ND	-
Fumarate	ND	ND	ND
Malate	ND	ND	ND
Succinate	ND	ND	ND
Isolation	Marine Sediment, Japan	Marine Sediment, Japan	Human opportunistic pathogen
References	This study	This study	Monias, 1928; Ralston-Barrett et al., 1976

(ND) no data; (+) positive reaction; (-) negative reaction

2.3.7 Tellurite reduction activity and MIC of three new bacterial strains

S. algae Hiro-1 showed tellurite reduction activity at 10 mM Na_2TeO_3 and MIC of 15 mM. *Pseudomonas* isolates both showed tellurite reduction activity at 4 mM Na_2TeO_3 and MIC of 6 mM (Figure 27). There was no spontaneous reduction or contamination based on the negative controls.

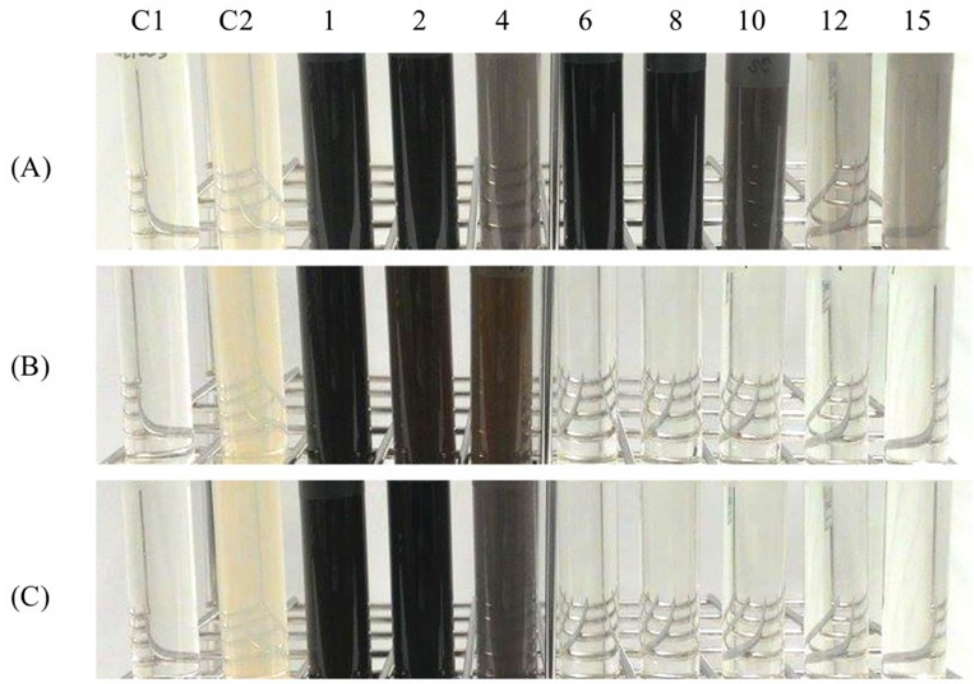

Figure 27. Tellurite reduction activity and MIC of the three new bacterial strains. Tellurite reduction assay includes RCVBN media (C1), RCVBN inoculated with pure cultures (C2), and RCVBN amended with 1-15 mM Na_2TeO_3 (conc. labeled on the tubes) and inoculated with the pure cultures, *S. algae* Hiro-1 (A), *P. pseudoalcaligenes* Hiro-2 (B), and *P. stutzeri* Hiro-3 (C).

2.3.8 Temporal aspect of tellurite reduction in the three new strains

Temporal aspect of tellurite reduction in the three new bacterial strains proceeds gradually after 4 d incubation (Figure 28).

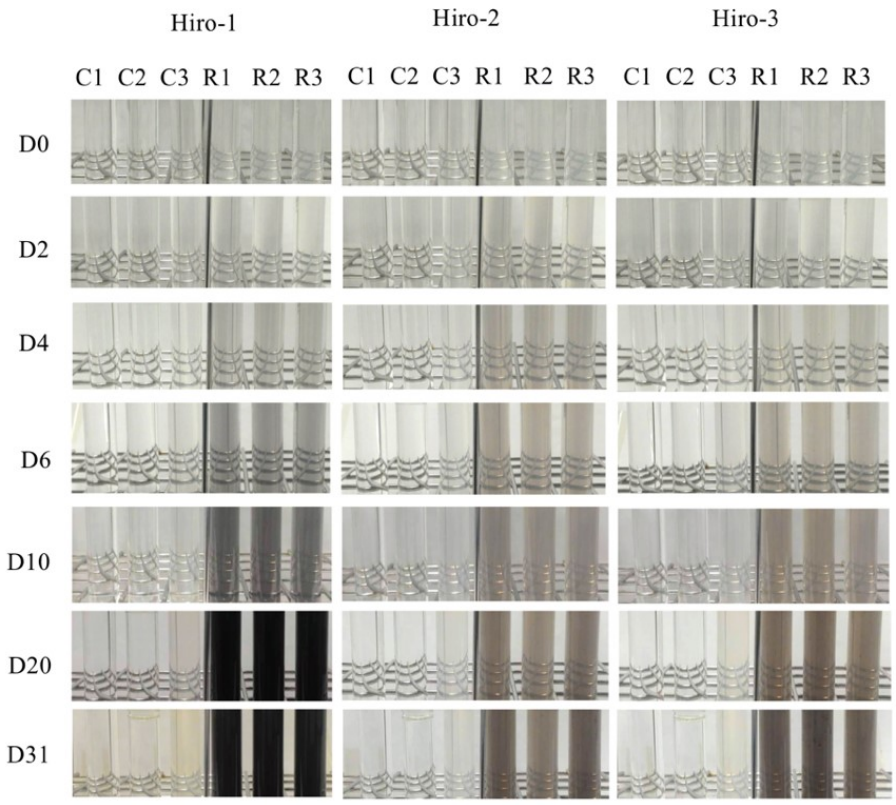

Figure 28. Gradual tellurite reduction was observed in the three new bacterial strains. Tellurite reduction assay includes RCVBN media (C1), RCVBN inoculated with 1 mM Na_2TeO_3 (C2), RCVBN inoculated with pure cultures (C3), and RCVBN amended with 1 mM Na_2TeO_3 and inoculated with pure cultures (R1, R2, R3). Days (D0-D31) of exposure are indicated.

2.3.9 Tellurium crystals in the three new strains

Intracellular tellurium crystals were observed within the cell of the three new strains. The tellurium crystals in *S. algae* Hiro-1 showed long needle crystals which formed Te rosettes (Figure 29-A). *P. pseudoalcaligenes* Hiro-2 showed needle crystals (Figure 29-B). *P. stutzeri* Hiro-3 showed rod crystals with (Figure 29-C). Both Hiro-2 and Hiro-3 showed tellurium crystals scattered within the cell cytoplasm. The minimum unit size of Te crystals is 60 nm Externally deposited crystals were also observed which could be crystals liberated from lysed cells.

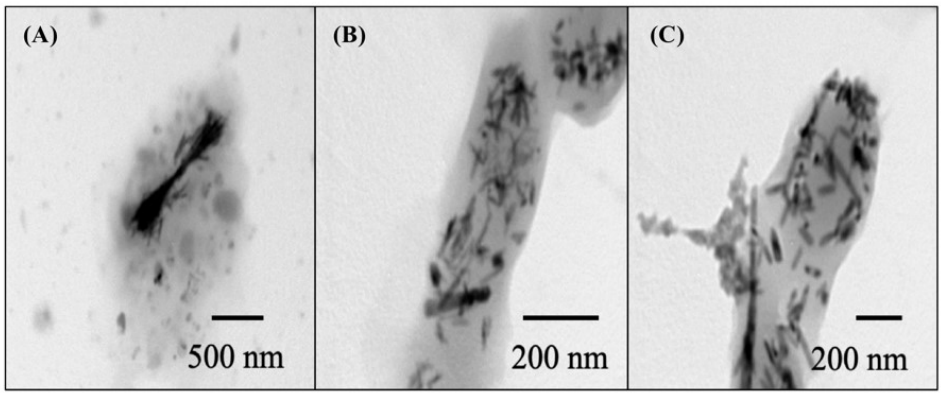

Figure 29. Intracellular tellurium crystals were observed on the three new bacterial strains, *S. algae* Hiro-1 (A), *P. pseudoalcaligenes* Hiro-2 (B), and *P. stutzeri* Hiro-3 (C).

2.4 Discussion

The three new bacterial strains showed high tolerance to tellurite and was observed to synthesis intracellular tellurium crystals. Bioremediation of uranium, plutonium, tellurite ions, nitrite, and halogenated organic compounds was reported in *S. algae* (Almagro et al., 2005; Klonowska et al., 2005). Common colony morphologies for *Shewanella* species such as mucoid and round colonies are also similar with *S. algae* Hiro-1 (Simidu et al., 1990; Nozue et al., 1992; Venkateswaran et al., 1998; Holt et al., 2005; Gao et al., 2006; Kim et al., 2007). Bioremediation of cyanide and tellurite was reported in *P. pseudoalcaligenes* and *P. stutzeri* (Romero et al., 1998). Common colony morphology for *P. pseudoalcaligenes* is translucent consistency (Monias, 1928; Ralston-Barrett et al., 1976; Schaad et al., 1978). This characteristic was also observed with *P. pseudoalcaligenes* Hiro-2. Common morphology for *P. stutzeri* is wrinkled colony (Lalucat et al., 2006). Wrinkled colonies were also observed in *P. stutzeri* Hiro-3.

Species-specific tellurium crystal formation was observed in the three new bacterial strain. Most tellurium crystals were deposited intracellularly. Crystal formation inside the cell suggests influx of metal ions into the cell cytoplasm. Unknown ion transporters or channels might be responsible in this phenomenon. After sequestration of tellurite ions inside the cell, enzyme-catalyzed reduction precedes crystal synthesis.

2.5 Conclusion

This thesis showed that the three new bacterial strains has high tolerance to tellurite ions and therefore can effectively reduce tellurite into elemental tellurium. These bacterial strains have bioremediation potential against tellurite. Simultaneously, tellurium crystals synthesized inside the cells can be recovered for use in technological and biomedical applications.

Whole genome sequencing on the three new strains may also further increase our knowledge on the identity of these marine isolates. Especially on *P. stutzeri* Hiro-3 which shows low sequence homology with other *P. stutzeri* species as shown in the phylogenetic analyses. *P. stutzeri* Hiro-3 could possibly be a new species. The gDNA of the new strains can also be used for cDNA library construction to discover novel genes related to tellurite reduction. Further investigation and optimization of growth parameters in the new strains may also increase their tellurium recovery potential.

Chapter III

Metagenome Library Construction and Functional Screening of Tellurite-Reducing Gene from Marine Sediment Microbial Community

3.1 Introduction

Available technologies for the production of tellurium (Te) requires enormous energy input and employs highly toxic chemical compounds that pollutes the environment (Borghese et al., 2014). Contrastingly, microbial synthesis of Te offers minimal energy consumption and less chemicals overcoming the negative effects of the conventional extraction methods. Understanding the fundamental mechanisms involved in tellurite reduction is prerequisite for establishing microbial-based tellurite reduction technology. Henceforth, the discovery of novel metal reductase genes will provide novel insights to better understand the intrinsic microbial cell-mediated metal reduction in nature.

Metagenomics is an indispensable tool in bridging the knowledge gaps through the discovery of novel genes. Metagenomics approach can significantly speed-up the discovery of novel genes from a microbial gene pool in a given environmental sample or enrichment culture (Thapa et al., 2017). This technique can uncover novel protein-coding genes that are previously unknown and hidden due to the limitations of microbial culture-based techniques. A putative cadmium accumulation gene was discovered from marine sponge-associated bacteria using the metagenome library construction (Mori et al., 2016). Similarly, this study employed the metagenome library construction approach coupled with activity-based screening to discover novel tellurite-reducing genes from a marine sediment enrichment culture. Biochemical assay and gene expression analysis were used to validate the activity of a putative tellurite-reducing gene. Open source computational tools were used for gene annotation and to predict proteins with possible structural similarity.

3.2 Materials and Methods

3.2.1 Construction of metagenome library

3.2.1.1 Fragmentation of metagenome

Half-liter of the marine sediment enrichment culture was grown for metagenome DNA extraction. CTAB method was used to extract metagenome DNA (Okamura et al., 2010). Metagenome DNA was treated with 1 µL of 1% RNAse after elution for 1 h. Restriction enzyme (RE) digestion was carried with 0.7 µL, 0.5 µL, 0.3 µL, and 0.2 µL *Sau*3A1 at 37°C (SANYO Incubator MIR-162, SANYO Electric Co., Ltd., Osaka, Japan) for 10 s in a 10-µL volume per reaction which contains 2 µL DNA and 2 µL RE buffer. After RE digestion, enzyme inactivation at 65°C for 20 min immediately followed. DNA fragments of 1000 bp to 3000 bp were recovered from the gel using the 1 Kb DNA Ready-To-Use Ladder (Maestrogen, Las Vegas, NV, USA) as standard reference. Excised gels containing the metagenome fragments were purified using Gel/PCR purification column (FAVORGEN Biotech Corp., Taiwan). DNA quantity (A260) and quality (A260/A280) were measured using spectrophotometer (GE NanoVue Plus Spectrophotometer, Biochrom, Harvard Bioscience, Inc., USA).

3.2.1.2 Plasmid vector

Plasmid vector pHSG398 carrying a chloramphenicol-resistance gene was used for the RE digestion (Figure 30, Table 19). Digestion reaction contains 5 µL DNA, 10 µL buffer, and 5 µL *Bam*HI in a 50-µL volume per reaction incubated at 37°C (SANYO Incubator MIR-162, SANYO Electric Co., Ltd., Osaka, Japan) in 1 h interval for 5 h. One µL of 0.1% Bovine Serum Albumin (BSA) was used to stabilize the reaction. Dephosphorylation of the plasmid vector to prevent self-ligation was performed using bacterial alkaline phosphatase (BAP). RE digested plasmids were purified as described earlier.

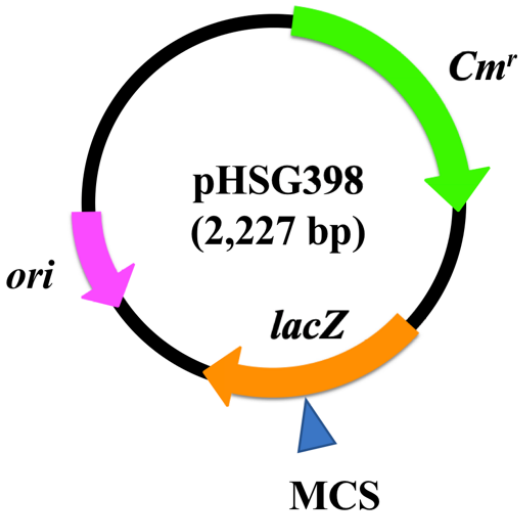

Figure 30. pHSG398 plasmid vector used for metagenome library construction. Chloramphenicol-resistance gene (*Cm*^{r}) and Multiple Cloning Site (MCS) were indicated.

Table 19. Bacterial strains and plasmids used in this study.

Strains or plasmids	Description	Sources
(A) Strains		
E. coli TOP-10	F^- *mcr*A Δ(*mrr-hsd*RMS-*mcr*BC) φ80*lac*ZΔM15 Δ*lac*X74 *rec*A1 *ara*D139 Δ(*ara-leu*)7697 *gal*U *gal*K *rps*L (Str^R) *end*A1 *nup*G	Thermo Fisher SCIENTIFIC, Waltham, MA, USA
DH5α	*deo*R, *sup*E44, *hsd*R17(r_k^-, m_k^+), *pho*A, *rec*A1, *end*A1, *gyr*A96, *thi-1*, *rel*A1, D(*lac*ZYA-*arg*F) U169, f80d*lac*ZDM15, F^-, l^-	TOYOBO, Osaka, Japan
BL21	F^-, *omp*T, *hsd*S_B（$r_B^-m_B^-$）, *gal*, *dcm*	BioDynamics Laboratory Inc., Tokyo, Japan
E. coli strain A1	Recombinant *E. coli* strain harboring the metagenome fragment	This study
S. algae Hiro-1	Tellurite-reducing bacterium	This study
P. pseudoalcaligenes Hiro-2	Tellurite-reducing bacterium	This study
P. stutzeri Hiro-3	Tellurite-reducing bacterium	This study
(B) Plasmids		
pHSG398	Cloning vector; Cm^r	Takara Bio, Japan
pHSG-A1	*Sau*3AI-digested metagenome fragment cloned into *Bam*HI-digested pHSG398; Cm^r	This study
pTrc99A	Expression vector; Amp^r	Creative Biogen, Shirley, NY, USA
pTrc99A-ORF1	PCR product encoding *Ps*-ORF1 cloned into pTrc99A; Amp^r	This study
pTrc99A-ORF2	PCR product encoding *Ps*-ORF2 cloned into pTrc99A; Amp^r	This study

3.2.1.3 Cloning

Purified *Sau*3A1digested metagenome fragments were ligated into *Bam*HI digested pHSG398 plasmid vector following the ligation protocol for T-Vector pMD20 with minor modifications. Ligation volume was doubled (2x) and ligation incubation time was also extended for 1 h. DNA Mighty Mix Ligation Kit was used for ligation. One-shot TOP-10 competent cell was used for transformation (Table 19). Sterile Lysogeny Broth (LB) was used to grow cells. Transformation tubes were manually shaken intermittently for 1 h during incubation at 37°C (SANYO Incubator MIR-162, SANYO Electric Co., Ltd., Osaka, Japan). Transformation reaction was plated in LB/ 1 mM X-GAL/ 20 µg/mL chloramphenicol (CHL) agar media using 100 µL of transformed cells. Microbiological techniques were performed under sterile conditions using Bio Clean Bench (Sanyo, Japan).

3.2.2 Metagenome library screening

3.2.2.1 Colony-PCR

Colony-PCR was performed on 20 positive transformants to check metagenome fragment insertion using M13 primers (Table 20). Oligonucleotide primers used in this study were purchased from Eurofins Genomics Co., Ltd., Tokyo, Japan. PCR mixture contains 10 µM each primer, 1x EmeraldAmp Max PCR Master Mix and one single isolated colony of positive transformant. Thermal cycling conditions include one cycle of pre-denaturation for 5 min at 94°C, followed by 28 cycles of denaturation at 94°C for 10 s, then annealing at 70°C for 20 s, and final extension at 72°C for 45 s. PCR was performed using T100^{TM} Thermal Cycler (Bio-Rad, CA, USA). PCR products were electrophoresed and visualized as described earlier.

Table 20. Primers used in this study.

Primer	Sequence (5′-3′)	Reference
M13	F- TGTAAAACGACGGCCAGT R- CAGGAAACAGCTATGACC	Yanisch-Perron et al., 1985
Ps-ORF1-HA[ab]	F-AAAAGAATTCATGGGCTGCGGTATTG CTGTGCCTGC R- GGGAAGCTTTTA*GGCATAGTCGGGCAC GTCATA*GGGATAGGGCTGGACGAGCCTGCG TTGCAGCTCG	This study
Ps-ORF2-HA[ab]	F- AAAAGAATTCATGGAGCCGAGCAGC TACAGCTTTCC R- GGGAAGCTTCTA*GGCATAACATCTGC ATCGCCA*TTG	This study
Ps-ORF1	F- ATGGGCTGCGGTATTGCTGTGCCT R- CTAGGGCTGGACGAGCCTGCGTT	This study
Ps-ORF2	F- ATGGAGCCGCTGAGCAGCTACAGC R- TTATTGATACCGGTACATCTGCAT	This study

[a] Restriction enzyme recognition sites are indicated by underline
[b] Hemagglutinin tag (HA-tag) sequences are indicated in italic letters

3.2.2.2 Functional screening of positive clones with confirmed metagenome fragment insertion

Functional screening was performed on positive clones with confirmed metagenome fragment insertion in 6 mL LB broth amended with 1 mM Na_2TeO_3 with 1 mM isopropyl β-D-thiogalactopyranoside (IPTG) solution. The assay was incubated at 37°C (SANYO Incubator MIR-162, SANYO Electric Co., Ltd., Osaka, Japan).

3.2.2.3 Plasmid extraction and RE digestion

Plasmids were extracted from a 24-h culture of the sample A1 showing tellurite reduction activity using FastGene Plasmid Mini Kit (NIPPON Genetics Europe GnBH Co., Ltd., Japan). Restriction enzymes for plasmid mapping were determined using New England BioLabs NEBcutter (NEB) (Vincze et al., 2003). Single-cut and double-cut RE digestion was performed using *Bam*HI/*Nco*I, and *Xba*I/*Dra*I. Ten µL of 1 Kb DNA Ready-To-Use Ladder (Maestrogen, Las Vegas, NV, USA), and digested fragments were electrophoresed as described earlier. After electrophoresis, the gel was stained with ethidium bromide (EtBr) for 5 min, followed by de-staining with ultrapure water for 10 min with shaking. The gel was viewed using UV Transilluminator (BioDoc-IT^{TM} Imaging System, USA).

3.2.2.4 Investigation on tellurite reduction activity of competent cells and plasmid vectors

Tellurite reduction activity of competent cells; DH5α, BL21, and plasmid vectors; pTrc99A, pGGEXP1 was investigated in 96-well clear plates (TrueLine, USA) using LB broth amended with 1 mM Na_2TeO_3. The assay was incubated at 37°C (SANYO Incubator MIR-162, SANYO Electric Co., Ltd., Osaka, Japan).

3.2.3 *in silico* analysis

3.2.3.1 Sequence assembly

Plasmids were extracted from the identified positive transformant, *E. coli* strain A1, and was sent for sequencing. DNA sequencing was performed by Eurofins Genomics Co., Ltd., Tokyo, Japan. The resulting chromatogram was visually checked of sequence gaps and errors using SnapGene (SnapGene Software, www.snapgene.com). Sequences were assembled using CodonCode Aligner (CodonCode Corporation, www.codoncode.com) and deposited in DNA Data Bank of Japan (DDBJ).

3.2.3.2 Homology search

DNA sequence of the metagenome fragment was analyzed using BLAST (Altschul et al., 1990). Bioinformatics analyses were performed using the deduced amino acid sequences of the metagenome fragment. Open Reading Frames (ORF) were determined using Expert Protein Analysis System or ExPASy (Gasteiger et al., 2003). BLASTP non-redundant protein database was used to infer protein sequence similarity. Conserved functional domains on the deduced amino acid sequence were analyzed using NCBI CDD/SPARCLE or Conserved Domain Database Subfamily Protein Architecture Labelling Engine (Marchler-Bauer and Bryant, 2004; Marchler-Bauer et al., 2011; Marchler-Bauer et al., 2015; Marchler-Bauer et al., 2017).

3.2.3.3 Prediction of structure, topology, and gene ontology

Protein structural similarity, topology, and gene ontology were inferred using different open-source computational tools such as Pfam or Protein families database (Finn et al., 2014; Finn et al., 2015), SWISS-MODEL (Guex et al., 2009; Benkert et al., 2011; Bertoni et al., 2017; Bienert et al., 2017; Waterhouse et al., 2018), Phyre^2 or Protein Homology/AnalogY Recognition Engine (Kelley and Sternberg, 2009), I-TASSER or Iterative Threading ASSEmbly Refinement (Zhang, 2008; Roy et al., 2010; Yang et al., 2015), and PSIPRED or PSI-BLAST based secondary structure PREDiction (Jones, 1999). Putative metal binding sites were predicted using MetalDetector v2.0 (Passerini et al., 2011).

3.2.4 Gene origin and phylogenetic analysis

3.2.4.1 PCR using Ps-ORF1 specific primers

Genomic DNA from previously characterized pure cultures of *S. algae* Hiro-1, *P. pseudoalcaligenes* Hiro-2, and *P. stutzeri* Hiro-3 isolated from the same metagenome seed culture were used as DNA template to validate the specificity

of the metagenome fragment to *P. stutzeri*. PCR mixture included 10 µM of *Ps*-ORF1-HA forward and reverse primers (Table 20), 1x EmeraldAmp Max PCR Master Mix and 2 µL of gDNA. Thermal cycling conditions include one cycle of pre-denaturation for 4 min at 95°C, followed by 30 cycles of denaturation at 95°C for 1 min, then annealing at 75°C for 1 min, followed by extension at 72°C for 1 min, and final extension at 72°C for 10 min. PCR products were electrophoresed and visualized as described earlier.

3.2.4.2 Phylogenetic analysis

MEGA7 software was employed to analyze nucleotide sequence relatedness to strains of *P. stutzeri* (Kumar et al., 2016). About 22 nucleotide sequences from the genus *Pseudomonas* with partial sequence similarity to PAP2/DedA family protein (1440 bp) based on BLASTN were aligned using CLUSTALW (Thompson et al., 1994). Phylogenetic tree was constructed using Unrooted Maximum-Likelihood (ML) with Kimura-2-parameter model and 1000 bootstrap value (Kimura, 1980). About 503 nucleotide base pairs were included in the final dataset.

3.2.5 Determination of responsible Open Reading Frame (ORF)

3.2.5.1 Amplification of Ps-ORFs

Determination of the gene coding sequence which is responsible on the observed tellurite reduction activity in recombinant cells was investigated by cloning the two Open Reading Frames (ORF) into expression vectors. *Ps*-ORF-expression primers were designed to amplify *Ps*-ORF1 and *Ps*-ORF2 with Hemagglutinin tag (HA-tag; YPYDVPDYA, 1.1 kDa) and *Eco*RI and *Hind*III restriction sites (Table 20). PCR mixture contained 10 µM each primer, 1x EmeraldAmp Max PCR Master Mix and 2 µL of plasmid. Thermal cycling conditions include one cycle of pre-denaturation for 4 min at 95°C, followed by 30 cycles of denaturation at 95°C for 1 min, then annealing at 75°C for 1 min,

followed by extension at 72°C for 1 min, and final extension at 72°C for 10 min. PCR products were electrophoresed and visualized as described earlier. After electrophoresis, amplicons were excised from the gel and purified as described earlier. *Ps*-ORF1 and *Ps*-ORF2 from the *E. coli* strain A1 were both cloned into expression vectors. *Ps*-ORF1 from *P. stutzeri* Hiro-3 was also cloned into expression vectors.

3.2.5.2 Cloning of Ps-ORFs

pTrc99A plasmid vector was used for expression of *Ps*-ORF1 and *Ps*-ORF2 (Figure 31). *Ps*-ORF-HA-tag fragments were ligated into pTrc99A expression vector and transformed into One-shot TOP-10 competent cells in LB media supplemented with 100 µg/mL ampicillin (AMP).

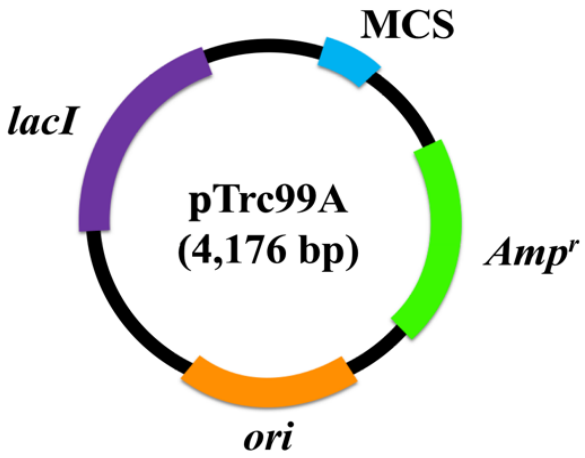

Figure 31. pTrc99A plasmid vector used for determination of responsible ORF. Ampicillin-resistance gene (*Amp*^{r}) and Multiple Cloning Site (MCS) were indicated.

3.2.5.3 Confirmation of Ps-ORF insertion

Plasmids were extracted on the positive transformants growing on LB/AMP plates. PCR was performed on the extracted plasmids to further confirm the presence of the ORFs using *Ps*-ORF1 and *Ps*-ORF2 specific primers (Table 20). PCR mixture contained 10 µM of each primer, 1x EmeraldAmp Max PCR Master Mix and 2 µL of plasmid. Thermal cycling conditions include one cycle of pre-denaturation for 4 min at 95°C, followed by 30 cycles of denaturation at 95°C for 1 min, then annealing at 78°C for 1 min, followed by extension at 72°C for 1 min, and final extension at 72°C for 10 min. PCR products were electrophoresed and visualized as described earlier.

3.2.6 Characterization of the recombinant *E. coli* stain A1

3.2.6.1 Colony morphology

Colony morphology of the *E. coli* strain A1 on LB agar with or without 1 mM Na_2TeO_3 was observed under stereomicroscope (TW-360, WRAYMER, Japan). Cultures used for observation were incubated at 37°C for 3 d (SANYO Incubator MIR-162, SANYO Electric Co., Ltd., Osaka, Japan).

3.2.6.2 E. coli strain A1 growth curve

Growth curve of the *E. coli* strain A1 was established to determine the growth phase that coincided with the occurrence of the tellurite reduction activity. *E. coli* strain A1 was inoculated in a 6 mL LB broth (pH 6.7) in 8-mL screw-capped tubes and incubated at 37°C (SANYO Incubator MIR-162, SANYO Electric Co., Ltd., Osaka, Japan). OD_{550} was measured every 1 h for 24 h using spectrometer (WPA CO-7500 Colorimeter, Biochrom Ltd., UK).

3.2.6.3 Tellurite reduction assay

Tellurite reduction activity was monitored in 8-mL screw-capped tubes. One mL of the recombinant culture was inoculated in a 6 mL LB broth with 20 µg/mL CHL amended with 1 mM Na_2TeO_3. The assay was incubated at 37°C (SANYO Incubator MIR-162, SANYO Electric Co., Ltd., Osaka, Japan). Time-course of tellurite reduction activity was recorded for 31 d.

3.2.6.4 Transmission Electron Microscopy (TEM) on E. coli strain A1

TEM was performed on *E. coli* strain A1 cells to observe tellurium crystal morphology and localization. *E. coli* strain A1 was cultured in LB broth amended with 1 mM Na_2TeO_3 and was incubated for 101 d. Four mL of the culture was collected and washed twice with milliQ water by centrifugation at 10,000x g for 5 min. Cell debris were resuspended in milliQ water and mounted on 150-mesh copper grids coated with collodion for TEM observation (Nisshin EM Co., Ltd., Japan).

3.2.6.5 Optimum temperature and pH for growth and tellurite reduction activity

Optimum temperature and pH for growth and tellurite reduction activity of the wild-type (WT), *E. coli* strain A1, and *Ps*-ORF expression clones were investigated in a 96-well clear plates (TrueLine, USA) using LB broth with or without 1 mM Na_2TeO_3. Optimum temperature was investigated using LB broth at pH 6.7. The temperatures included were 4°C, 32°C, 37°C, and 45°C. pH optimum was determined at 37°C. The pH tested were pH 7.0, pH 9.0, and pH 10.0. Samples were incubated in a shaking incubator (Maximizer MBR-420FL, TIETEC Co., Ltd., Nagoya, Japan). Bacterial growth and tellurite reduction activity were measured at OD_{550} after 48-h incubation using SpectraMAX M Series Multi-Mode Microplate Reader (Molecular Devices, USA). Unpaired *t*-test at 95% level of significance was used to statistically evaluate the growth variations on different treatments tested.

3.2.7 Isolation of a chloramphenicol-susceptible strain

Streak plate method was employed on LB agar plates for the isolation and purification of chloramphenicol-susceptible A1 mutant strain. Isolated mutant strain was cultured on LB agar plates with or without 1 mM Na_2TeO_3, and LB agar plates with or without 20 μg/mL chloramphenicol.

3.2.7.1 MIC assay on E. coli strain *A1 and A1 mutant strain*

MIC of the *E. coli* strain A1 and A1 mutant strain was assayed using 96-well clear plates in a 300-μL volume per reaction containing 1 mM-6 mM Na_2TeO_3 incubated at 37°C (SANYO Incubator MIR-162, SANYO Electric Co., Ltd., Osaka, Japan).

3.2.7.2 Validation of Ps-ORF1 presence in A1 mutant strain

Plasmid extraction on the chloramphenicol-susceptible A1 mutant strain was performed as described earlier. PCR using *Ps*-ORF1 and *Ps*-ORF2 specific primers was performed as described earlier.

3.2.7.3 Characterization of A1 mutant strain

Growth and tellurite reduction activity of A1 mutant strain were investigated in 96-well clear plates (TrueLine, USA) using LB media with or without 1 mM Na_2TeO_3. The A1 mutant strain was incubated at 4°C, 32°C, 37°C, and 45°C (SANYO Incubator MIR-162, SANYO Electric Co., Ltd., Osaka, Japan). pH tested includes pH 7, pH 9, and pH 10.

3.2.8 Cell-free tellurite reduction assay

3.2.8.1 Preparation of solubilized cells

Tellurite reduction assay using solubilized cells was performed to determine whether whole intact cells are required to observe the tellurite reduction activity in recombinant cells. Cell fractionation was performed using a 500 mL 24-h cultures. Cells were harvested by centrifugation at 10,000 g for 10 min at 4°C using High Speed Refrigerated Microcentrifuge, MX-307 (TOMY Seiko Co., Ltd., Japan). After collection, cells were resuspended in cell lysis buffer containing 0.1 M Tris-HCl and 1% Triton X-100 (Kanto Chemical, Co. Inc., Tokyo, Japan). Cells were solubilized in the lysis buffer at 4°C for overnight. Solubilized cells were sonicated at different time intervals (15 min, 45 min, 60 min) in a 15 min intermittent sonication (Branson Ultrasonic Sonifier 250, USA). Live-intact cells, whole cell lysates, and supernatant collected from the fractionated cultures were used for tellurite reduction assay using 96-well clear plates in a 200-µL volume per reaction in replicates. Tellurite reduction activity was visually observed after 6 h of incubation at 37°C (SANYO Incubator MIR-162, SANYO Electric Co., Ltd., Osaka, Japan).

3.2.8.2 Ultracentrifugation

Whole cell lysates were cleared by centrifugation at 10,000 g for 10 min in High Speed Refrigerated Microcentrifuge, MX-307 (TOMY Seiko Co., Ltd., Japan). Ultracentrifugation at 100,000 g for 1 h was performed with the cleared lysates to separate cytosolic fraction and cell membrane (Beckman-Coulter tabletop ultracentrifuge Optima Max, Beckman-Coulter, Inc., Brea, CA, USA). Tellurite reduction assay was performed on soluble and insoluble fractions using 96-well clear plates in a 200-µL volume per reaction in cell lysis buffer amended with 1 mM Na_2TeO_3. Tellurite reduction was visually observed in replicated reactions after 24 h of incubation at 37°C (SANYO Incubator MIR-162, SANYO Electric Co., Ltd., Osaka, Japan).

3.2.9 Estimation of tellurium recovery using Inductively Coupled Plasma-Optical Emission Spectroscopy (ICP-OES)

Marine sediment enrichment culture, new bacterial strains, and *E. coli* strain A1 was exposed to 1 mM Na_2TeO_3 for one week and was analyzed by ICP-OES (SRS3100, Seiko Instruments Inc., Japan). Eight mL of culture was transferred in 15 mL nunc sterile tubes and centrifuged at 20,000 g for 10 min. Supernatant was transferred in new tubes, filtered with 0.8 µm filter, this represent the extracellular Te in spent medium. On the cell sample, 8 mL 0.1M phosphate buffer was added, vortexed, centrifuged at 10,000 g for 5 min, and supernatant was collected, this represent the adsorbed ions onto the cell surface. On the cell sample 8 mL 0.01M EDTA (pH 7.5) was added, centrifuged at 20,000 g for 5 min, and supernatant was collected, this represent the remaining adsorbed ions onto the cell surface. One mL MilliQ H_2O was added to the cell sample, and was transferred to 8-mL glass tube, refrigerated at -80°C for 3 h (MDF-U364-PJ, Panasonic, Japan). The sample was freeze-dried overnight. Five hundred µL of concentrated HNO_3 and 500 µL H_2O_2 was added to the cell sample and was ash-fixed in furnace at 180°C for 3 h (Maffle Furnace FO100, Yamato Scientific Co. Ltd., Tokyo, Jaoan). Eight mL 1M HNO_3 was added to the cell sample, this represent the cell-membrane bound Te particles. Tellurium concentration was determined in the cell fraction using ICP-OES at 238.578 nm.

3.3 Results

3.3.1 Metagenome DNA extraction

Metagenome DNA from the marine sediment enrichment culture was extracted (Figure 32).

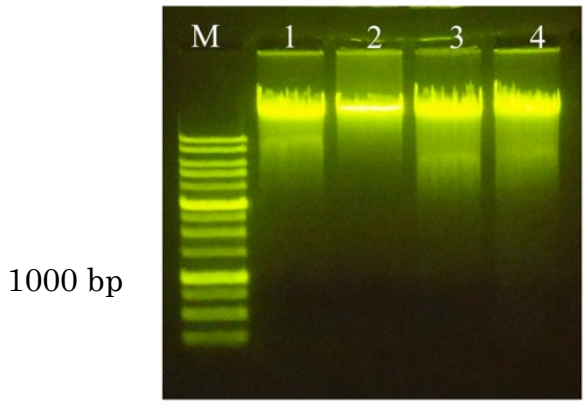

Figure 32. DNA extracted from the metagenome seed culture. Ten µL of 1 Kb DNA Ready-To-Use Ladder (M) and gDNA were loaded in 0.7% agarose gel, stained with UltraPower DNA Safe Dye, electrophoresed at 100 V for 40 min and viewed using Blue Light Transilluminator. DNA quantity (A260) and quality (A260/A280) of extracted metagenome DNA are as follows; (1): 483.0 ng/µL, 2.038; (2): 306.5 ng/µL, 2.085; (3): 535.0 ng/µL, 2.058; (4): 545.0 ng/µL, 2.034.

3.3.2 Optimization of RE digestion on metagenome DNA

Optimization of restriction enzyme digestion of the metagenome DNA was carried out using *Sau*3A1 (Figure 33, 34, 35).

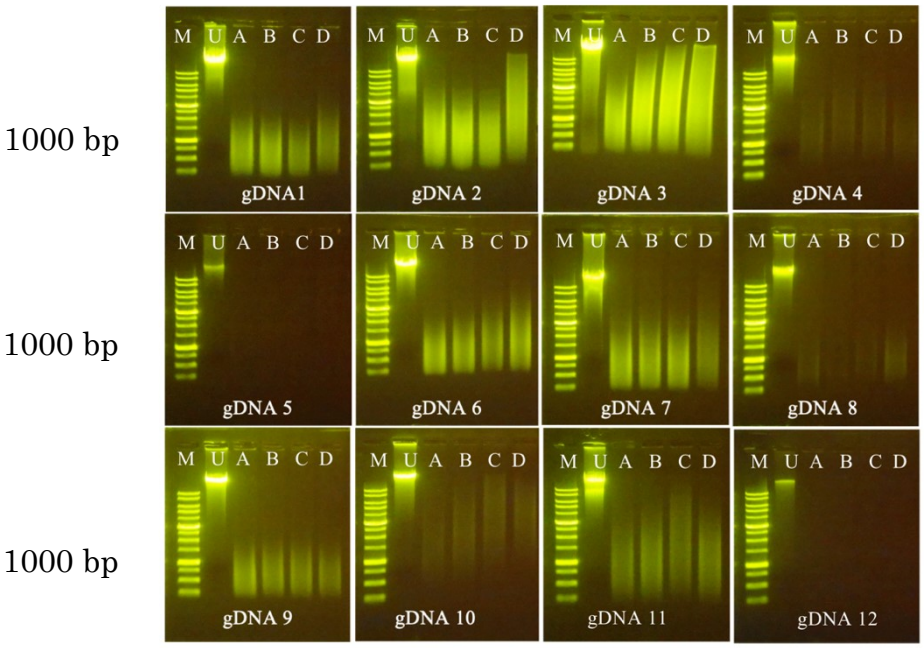

Figure 33. Optimization of RE digestion using *Sau*3A1 on metagenome DNA. Ten µL of 1 Kb DNA Ready-To-Use Ladder (M), undigested metagenome DNA (U) and metagenome DNA digested with 0.7 µL (A), 0.5 µL (B), 0.3 µL (C), and 0.2 µL (D) RE, were loaded on 0.7% agarose gel, electrophoresed at 100 V for 40 min. Samples were stained with UltraPower DNA Safe Dye and viewed using Blue Light Transilluminator. DNA quantity (A260) and quality (A260/A280) of extracted metagenome DNA are as follows; (1): 72.50 ng/µL, 1.859; (2): 483.0 ng/µL, 2.038; (3): 545.0ng/µL, 2.034; (4): 31.50 ng/µL, 1.800; (5): 20.50 ng/µL, 1.806; (6): 143.5ng/µL, 1.864; (7): 48.00 ng/µL, 1.830; (8): 27.00 ng/µL, 1.843; (9): 42.00 ng/µL, 1.826; (10): 37.00 ng/µL, 1.805; (11): 68.00 ng/µL, 1.838; (12): 30.00 ng/µL, 2.000.

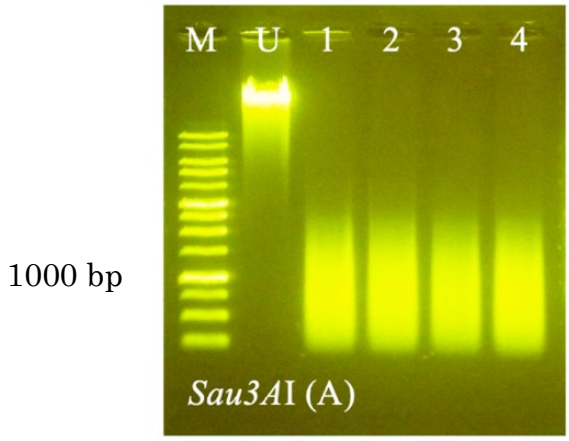

Figure 34. Optimization of RE digestion on metagenome DNA. Ten µL of 1 Kb DNA Ready-To-Use Ladder (M), undigested metagenome DNA (U) and digested metagenome DNA (1, 2, 3, 4) were loaded on 0.7% agarose gel, electrophoresed at 100 V for 40 min. Samples were stained with UltraPower DNA Safe Dye and viewed using Blue Light Transilluminator. RE digestion was performed with 0.5 µL *Sau*3A1 at 37°C for 10 s in a 50-µL volume per reaction containing 10 µL DNA and 10 µL RE buffer followed by enzyme inactivation at 65°C for 20 min.

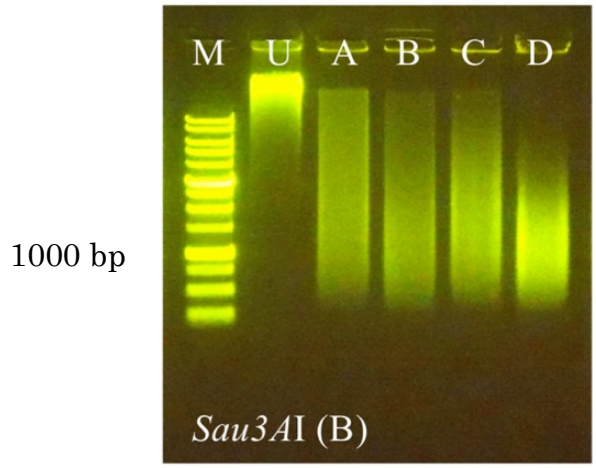

Figure 35. Optimization of RE digestion on metagenome DNA. Ten µL of 1 Kb DNA Ready-To-Use Ladder (M), undigested metagenome DNA (U) and digested metagenome DNA (A, B, C, D) were loaded on 0.7% agarose gel, electrophoresed at 100 V for 40 min. Samples were stained with UltraPower DNA Safe Dye and viewed using Blue Light Transilluminator. RE digestion was performed with 0.2 µL (A), 0.3 µL (B), 0.4 µL (C), 0.5 µL (D) *Sau*3A1 at 37°C for 10 s in a 15-µL volume per reaction containing 2 µL DNA and 2 µL RE buffer followed by enzyme inactivation at 65°C for 20 min.

3.3.3 Optimization of RE digestion on pHSG398 plasmid vector

Optimized RE digestion conditions were determined on the pHSG398 plasmid vector using *Bam*HI, *Nco*I, *Xba*I, and *Dra*I (Figure 36, 37).

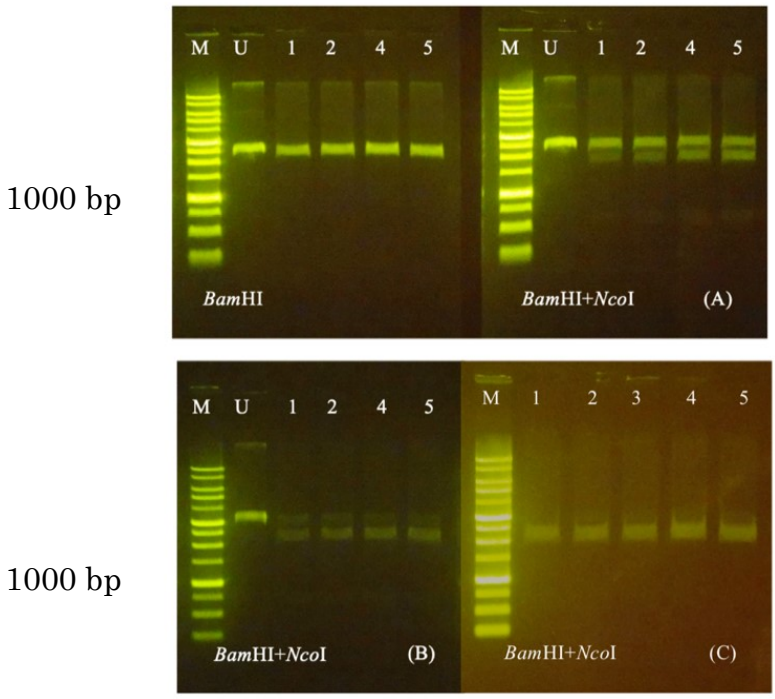

Figure 36. Optimization of RE digestion on pHSG398 plasmid vector. Ten µL of 1 Kb DNA Ready-To-Use Ladder (M), undigested pHSG398 plasmid (U) and digested pHSG398 plasmids (1, 2, 4, 5) were loaded on 0.7% agarose gel, electrophoresed at 100 V for 40 min. Samples were stained with UltraPower DNA Safe Dye and viewed using Blue Light Transilluminator. RE digestion was performed at 37°C at 10 min interval (A), 1 h interval (B), and 30 min interval (C). RE digestion was performed with 2 µL (A), 3 µL (B), 5 µL (C) RE at 37°C in a 50-µL volume per reaction containing 5 µL DNA and 10 µL RE buffer followed by enzyme inactivation at 65°C for 20 min.

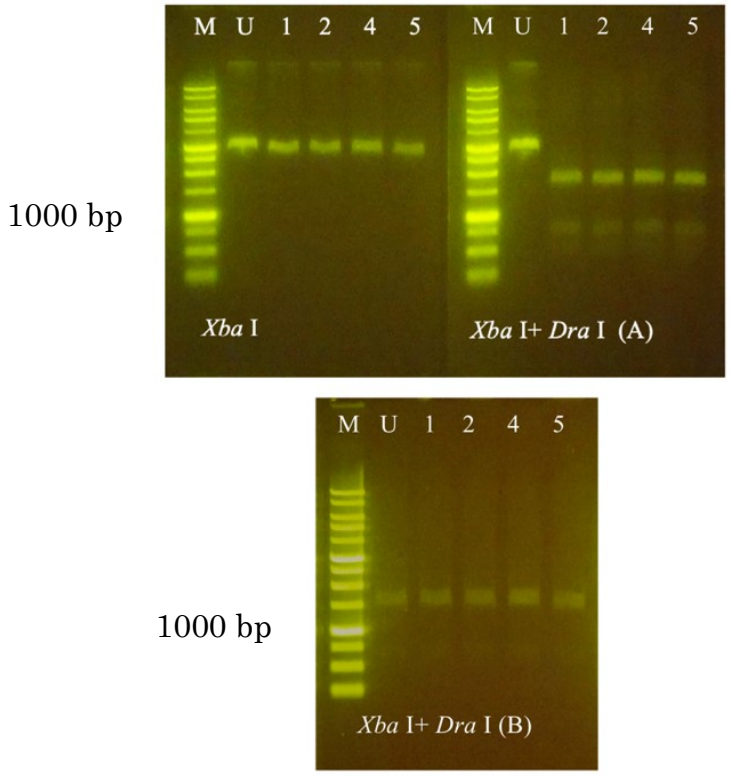

Figure 37. Optimization of RE digestion on plasmid vector**.** Ten µL of 1 Kb DNA Ready-To-Use Ladder (M), undigested pHSG398 plasmid (U) and digested pHSG398 plasmids (1, 2, 4, 5) were loaded on 0.7% agarose gel, electrophoresed at 100 V for 40 min. Samples were stained with UltraPower DNA Safe Dye and viewed using Blue Light Transilluminator. RE digestion was performed at 37°C at 10 min interval (A), and 30 min interval (B). RE digestion was performed with 2 µL (A), and 5 µL (B) RE in a 50-µL volume per reaction containing 5 µL DNA and 10 µL RE buffer followed by enzyme inactivation at 65°C for 20 min.

3.3.4 Metagenome library reveals a putative tellurite-reducing gene

Metagenome library was constructed using the optimized conditions of restriction enzyme digestion on gDNA and plasmid vector. Schematic diagram of metagenome library construction and functional screening was shown in Figure 38. The white colonies of positive transformants from the X-GAL screening showed insertional inactivation due to successful ligation of metagenome fragment into the *lac* operon Multiple Cloning Site (MCS) (Horwitz et al., 1964). Colony-PCR on positive transformants revealed metagenome fragments about 1000 bp-3000 bp. This size estimation is not accurate because the dye being used was observed to add additional weight on the bands. Twenty transformants with amplicons about 1000 bp–3000 bp were re-screened for tellurite reduction activity. One culture was screened to exhibit prominent tellurite reduction activity.

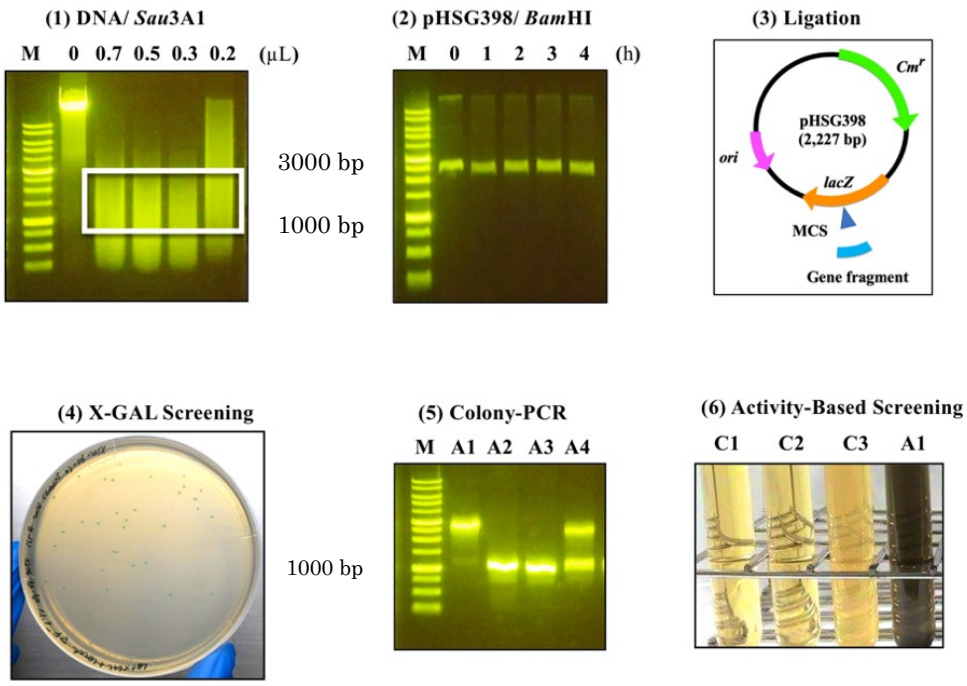

Figure 38. Metagenome library construction and functional screening of tellurite-reducing gene. Metagenome DNA was extracted from the marine sediment enrichment culture using CTAB DNA extraction method. Metagenome DNA was digested with *Sau*3AI. Fragments about 1000 bp-3000 bp (with white outline) were chosen for ligation (1). *Bam*HI digestion of pHSG398 plasmid vector (2). Ligation of metagenome fragments into the pHSG398 Multiple Cloning Site (MCS) (3). Screening of positive transformants using Blue and White Screening (4). Colony-PCR for insert confirmation on positive transformants (5). Activity-based screening includes LB media (C1), LB amended with 1 mM Na_2TeO_3 and 1 mM IPTG (C2), LB inoculated with positive transformant (C3), LB amended with 1 mM Na_2TeO_3 and 1 mM IPTG inoculated with positive transformant (A1) (6).

3.3.4.1 Blue and White screening of positive transformants

Twenty positive transformants were observed and isolated independently on RCVBN media (Figure 39, 40).

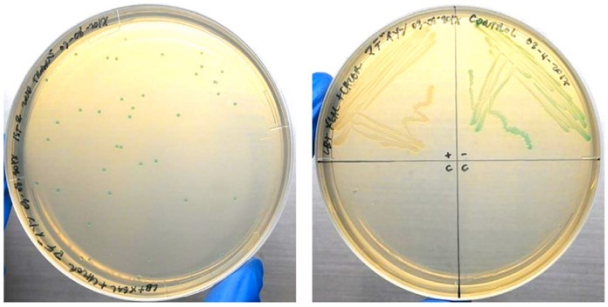

Figure 39. Blue and White screening using LB/CHL/X-GAL plates. White colonies are positive transformants whereas blue colonies are negative transformants.

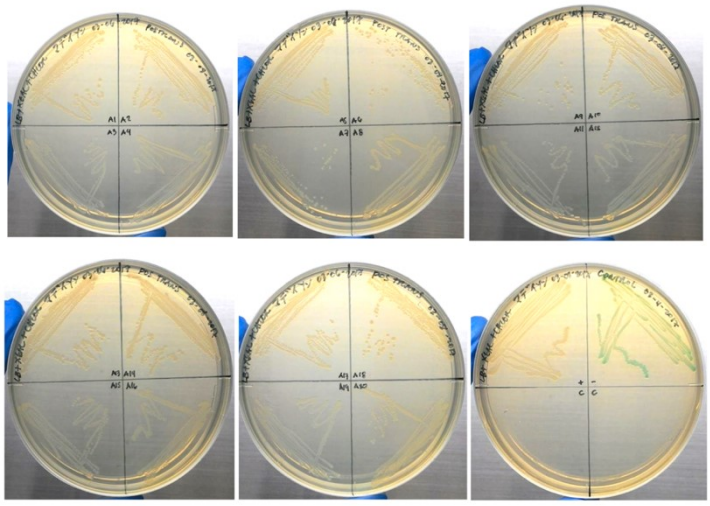

Figure 40. About 20 white colonies were isolated independently.

3.3.4.2 Colony-PCR on positive transformants

Colony-PCR revealed insertion of DNA fragments from the metagenome library (Figure 41).

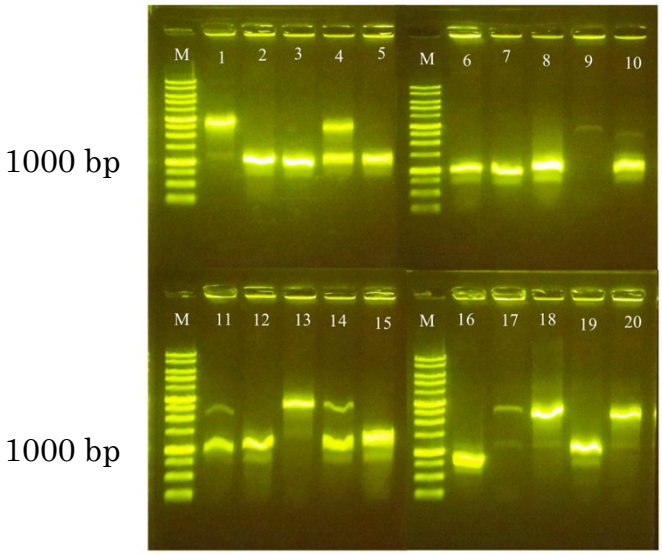

Figure 41. Colony-PCR on 20 positive transformants using M13 primers to validate metagenome insertion. Ten µL of 1 Kb DNA Ready-To-Use Ladder (M), and Colony-PCR products from positive transformants were loaded in 0.7% agarose gel, electrophoresed at 100 V for 40 min. Samples were stained with UltraPower DNA Safe Dye and viewed using Blue Light Transilluminator. Insert was observed to be about 1000 bp–3000 bp.

3.3.4.3 Functional screening of tellurite reduction activity of positive transformants

Identified positive transformants with metagenome fragment insertion were used to investigate possible tellurite-reducing activity of the gene insert. One positive transformant, A1, showed visible tellurite-reducing activity on LB broth amended with 1 mM Na_2TeO_3 (Figure 42, 43).

Figure 42. Functional screening of recombinant cells harboring a metagenome fragment. Assay includes LB media (C1), LB amended with 1 mM Na_2TeO_3 and 1 mM IPTG (C2), LB inoculated with positive transformant (C3), LB amended with 1 mM Na_2TeO_3 and 1 mM IPTG inoculated with positive transformant (A1, A4, A9, A10, A11, A13, A14).

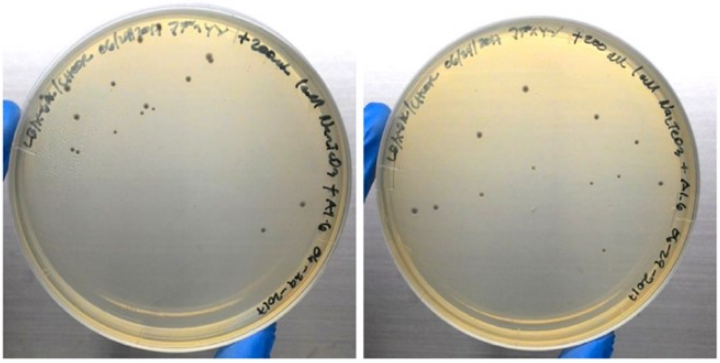

Figure 43. Recombinant cells from sample A1 obtained from functional screening showed tellurite reduction activity on LB/CHL plates amended with 1 mM Na_2TeO_3.

3.3.4.4 Confirmation of metagenome gene insertion on positive transformant A1

RE digestion confirmed the insertion of metagenome fragment in the plasmid extracted from the sample A1 (Figure 44).

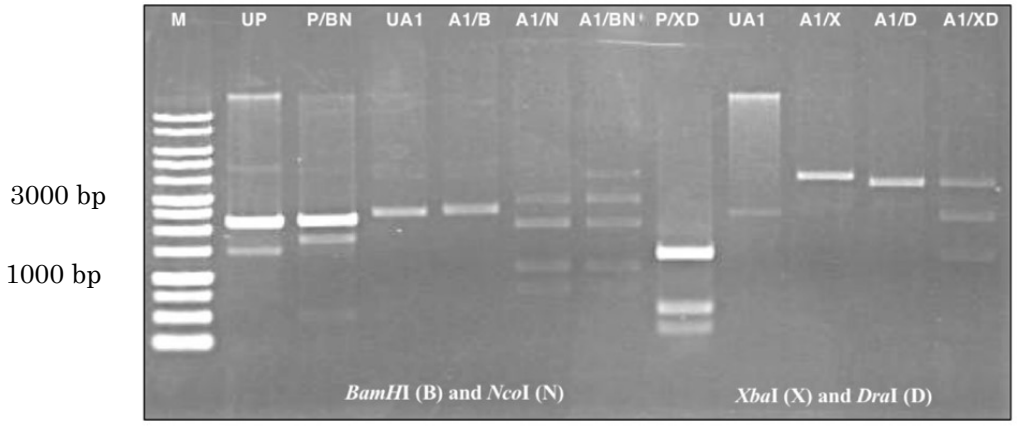

Figure 44. Confirmation of the metagenome fragment insertion by RE digestion. UP: Undigested pHSG398 plasmid vector; P/BN: pHSG398 digested with *Bam*HI and *Nco*I; UA1: Undigested pHSG-A1; A1/B: pHSG-A1 cut with *Bam*HI; A1/N: pHSG-A1 cut with *Nco*I; A1/BN: pHSG-A1 cut with *Bam*HI and *Nco*I; P/XD: pHSG398 digested with *Xba*I and *Dra*I; A1/X: pHSG-A1 cut with *Xba*I; A1/D: pHSG-A1 cut with *Dra*I; A1/XD: pHSG-A1 cut with *Xba*I and *Dra*I. Marker (M) used was 1 Kb DNA Ready-To-Use Ladder.

3.3.4.5 Investigation on tellurite reduction activity of competent cells and plasmid vectors

Tellurite reduction activity of competent cells; DH5α, BL21, and plasmid vectors; pTrc99A, pGGEXP1 was also investigated (Figure 45). There was no visible tellurite reduction activity on the competent cells and plasmid vectors used.

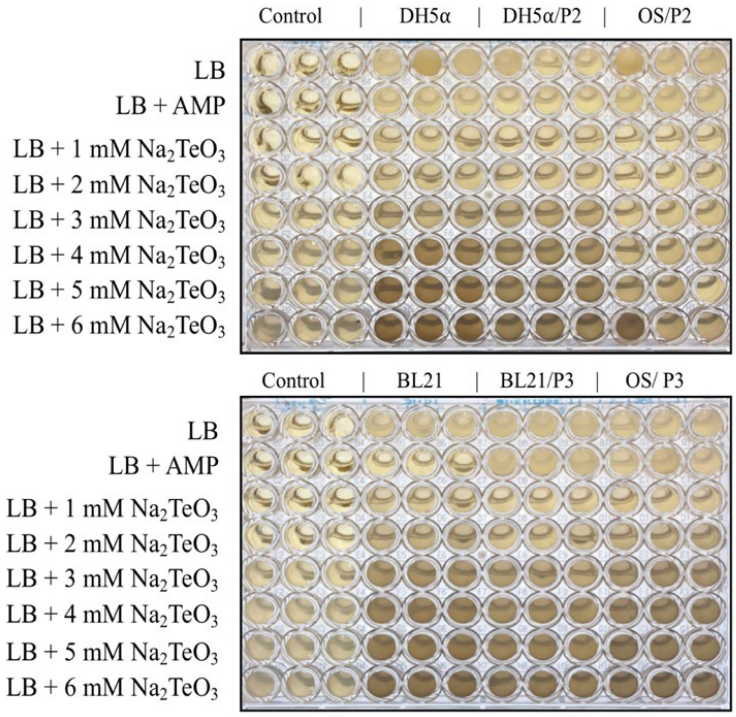

Figure 45. Investigation on tellurite reduction activity of competent cells and plasmid vectors. Competent cells and transformed cells harboring an empty plasmid vector (P2: pTrc99A; P3: pGEX6P1) showed no visible tellurite reduction activity. The assay shows triplicate reactions.

3.3.5 Metagenome fragment shows homology to *P. stutzeri* PAP2 family protein

3.3.5.1 Gene Homology

The nucleotide sequence of the putative tellurite-reducing gene was shown in Figure 46. Conserved domains search using the DNA sequence of the metagenome fragment hinted sequence similarity to transmembrane (TM) type 2 phosphatidic acid phosphatase (PAP2) (Table 21, 22). Structural conservation inquiry using the Protein Data Bank (PDB) further supports structural similarity with the first TM PAP2 type 2 phosphatidylglycerolphosphate phosphatase from

Bacillus subtilis (PDB: 5jikA), and lipid phosphatase from *E. coli* (PDB: 4px7A) (Berman et al., 2000; Berman et al., 2007).

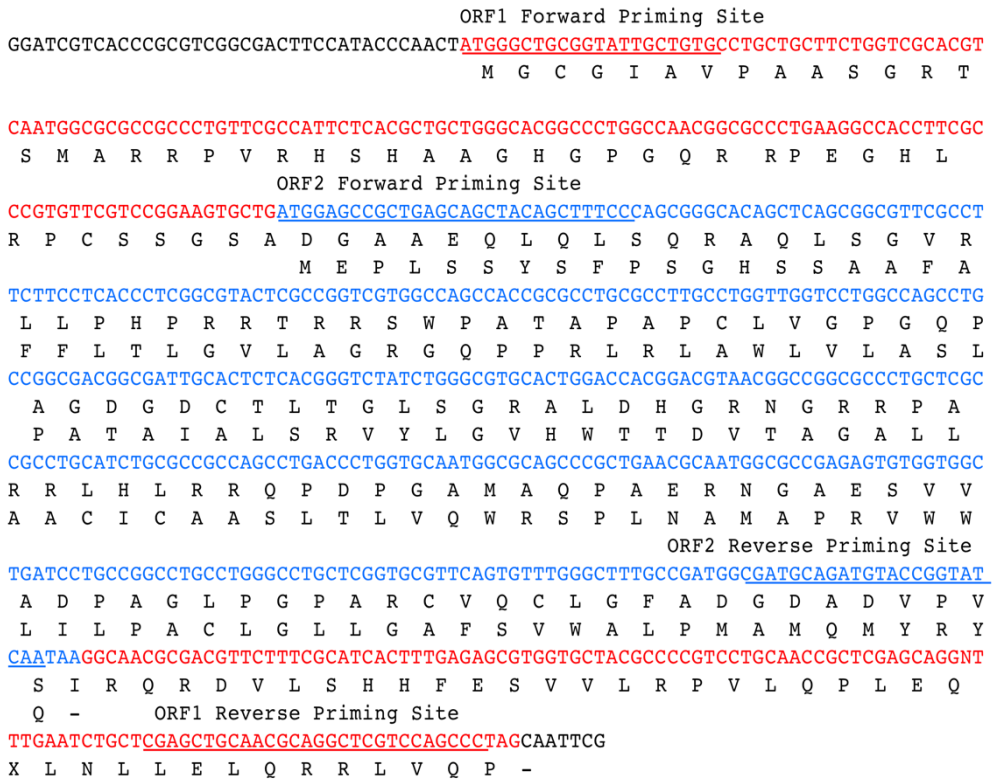

Figure 46. Gene coding sequence (693 bp) of the metagenome fragment which confers tellurite resistance and tellurite reduction activity in recombinant cells. Two overlapping Open Reading Frames (*Ps*-ORF1 and *Ps*-ORF2) were highlighted in red and blue characters, respectively. Deduced amino acid sequences of the two *Ps*-ORFs were also indicated. ORF priming sites for *Ps*-ORF1 and *Ps*-ORF2 were underlined.

Table 21. BLASTN homology search using the DNA sequence of the gene insert (639 bp).

Protein	Identity (%)	E-value	Organism	Accession No.
PAP2 family protein/ DedA family protein	92	0.00	*Pseudomonas stutzeri* CCUG 29243	CP003677.1
PAP2 family protein/ DedA family protein	92	0.00	*P. stutzeri* NCTC10475	LR134482.1
Phosphoesterase	85	0.00	*P. stutzeri* 19SMN4	CP007509.1
Phosphatase PAP2 family protein	83	83-175	*P. stutzeri* DW2-1	CP027543.1
Putative membrane-associated protein	82	2e-161	*P. stutzeri* RCH2	CP003071.1
Phosphatase PAP2 family protein	84	6e-151	*P. stutzeri* SGAir0442	CP025149.2
PAP2 family protein/ DedA family protein	84	3e-149	*P. stutzeri* SLG510A3-8	CP011854.1
PAP2 family protein/ DedA family protein	84	3e-149	*P. stutzeri* CGMCC 1.1803	CP002881.1
PAP2 family protein/ DedA family protein	84	3e-149	*P. stutzeri* DSM 4166	CP002622.1
PAP2 family protein/ DedA family protein	84	3e-149	*P. stutzeri* A1501	CP000304.1
PAP2 family protein/ DedA family protein	84	1e-147	*P. stutzeri* NCTC10450	LR134319.1
Phosphatase PAP2 family protein	84	6e-146	*P. stutzeri* 1W1-1A	CP027664.1
Phosphoesterase	82	3e-129	*Pseudomonas* sp. R2A2	CP029772.1

3.3.5.2 Amino acid sequence homology to PAP2 Super Family protein

Amino acid sequence of the metagenome fragment showed low sequence homology with the PAP2 Superfamily protein. Moreover, the metagenome fragment covers only a fraction about 1/3 region of the whole PAP2 protein (Figure 47). Hence, the truncated fragment may not be able to retain the actual function of the PAP2 protein.

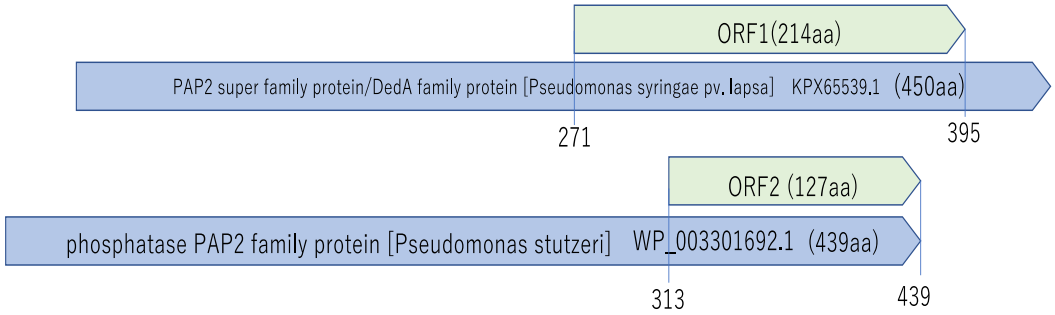

Figure 47. Region of PAP2 protein with sequence homology with the metagenome fragment.

Table 22. BLASTP homology search using translated amino acid sequences of the two overlapping *Ps*-ORFs.

	Protein	Identity (%)	E-value	Organism	Accession No.
Ps-ORF1 (214 aa)	PAP2 Superfamily protein/DedA family protein	38	4e-08	*Pseudomonas syringae pv. lapsa*	KPX65539.1
Ps-ORF2 (127 aa)	Phosphatase PAP2 family protein	100	5e-80	*P. stutzeri*	WP_003301692

3.3.5.3 Gene ontology, structure, and localization

Gene ontology (GO) prediction linked the function of metagenome fragment to a substrate-specific transmembrane transporter (Table 23). Moreover, cellular component predictions revealed high confidence of an integral membrane localization. The gene has one transmembrane domain consisting of alpha helices (Jones et al., 1994). YodM (PDB: 5jki.1.A) was predicted as the closest protein with structural similarity with the metagenome fragment. Some cysteine and histidine residues in metagenome fragment were predicted to function as putative metal-binding sites (Dudev et al., 2003; Babor et al., 2008; Cournia et al., 2015).

Table 23. Prediction of probable biological and molecular functions of the gene insert.

GO term	Activity	Probability (%)
0022891	Substrate-Specific Transmembrane Transporter	99.5
0015077	Monovalent inorganic cation transmembrane transporter	99.3
0008509	Anion transmembrane transporter	99.2
0022857	Transmembrane transporter	99.1
0015293	Symporter activity	98.7
0003824	Catalytic Activity	98.6
0008514	Ion transmembrane transporter	98.3

3.3.6 Validation of metagenome fragment specificity to *P. stutzeri* Hiro-3

3.3.6.1 Validation using Ps-ORF1 specific primers

PCR showed specificity of the metagenome fragment to *P. stutzeri* Hiro-3 (Figure 48).

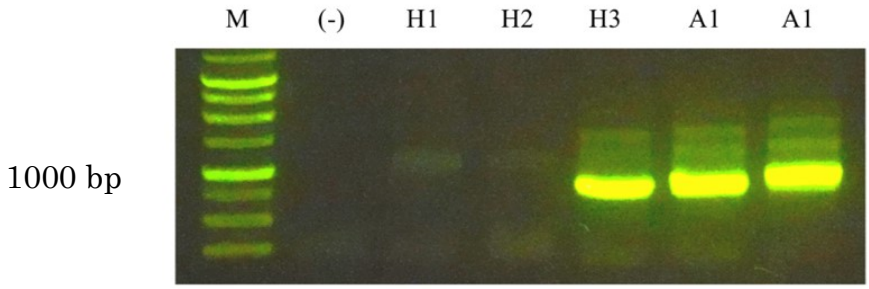

Figure 48. Amplicons were observed in *P. stutzeri* Hiro-3 (H3) and *E. coli* strain A1 (A1) which suggests the probable origin of the metagenome gene fragment. There were no amplicons observed in *S. algae* Hiro-1 (H1) and *P. pseudoalcaligenes* Hiro-2 (H2). Marker (M) used was 1 Kb DNA Ready-To-Use Ladder. Negative control (-) used was UltraPure H_2O.

3.3.6.2 Phylogenetic analysis

Phylogenetic analysis using Maximum-Likelihood tree associated the metagenome fragment with the clustered taxa of *P. stutzeri* (100%) (Figure 49). There are three clusters shown in the cladogram. Two clusters were formed by *P. stutzeri* strains and the other cluster was formed by *Pseudomonas* sp. strains and *P. fluorescens*. Although the metagenome fragment was identified with *P. stutzeri* strains, it was not identified exactly to belong with one of the strains included in the analysis. *Ps*-ORF1 from *P. stutzeri* Hiro-3 was cloned, however it was not sequenced.

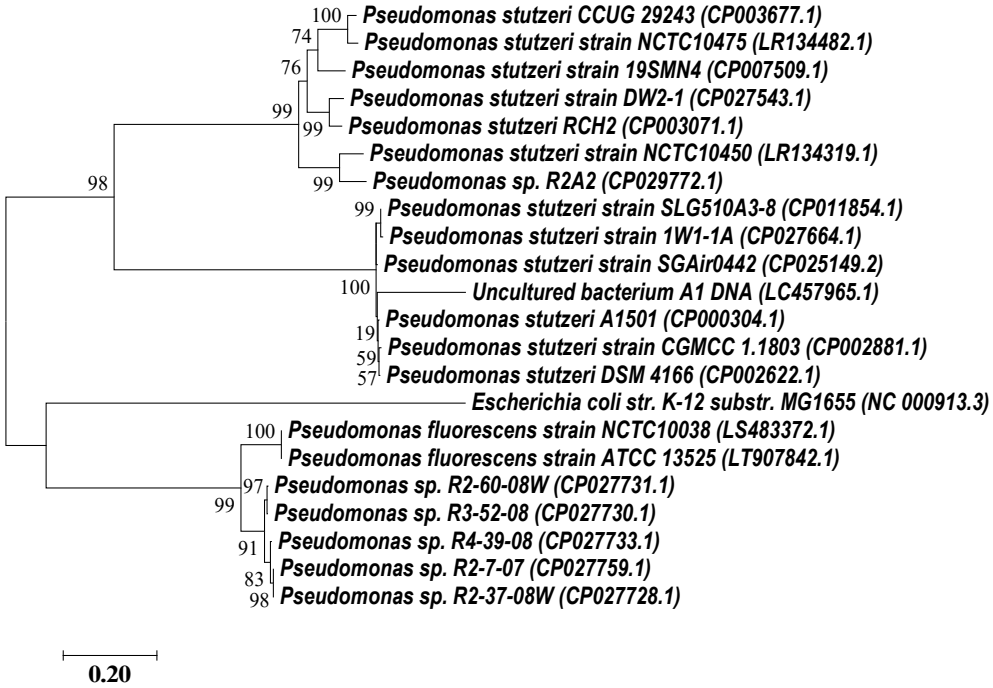

Figure 49. Unrooted Maximum-Likelihood (ML) shows association of metagenome gene fragment from uncultured bacterium A1 DNA with the clustered taxa of *P. stutzeri.* Number at nodes represent bootstrap values from 1000 replications. Scale bar indicates 20% sequence divergence. DedA family protein from *E. coli* str. K-12 substr. MG1655 was used as an outgroup. GenBank Accession numbers were indicated in parentheses.

3.3.7 Determination of responsible ORF reveals tellurite reduction activity of *Ps*-ORF1

3.3.7.1 pTrc99A plasmid vector was used for cloning Ps-ORFs

Vector construct of *Ps*-ORF1 and *Ps*-ORF2 expression clones was shown in Figure 50.

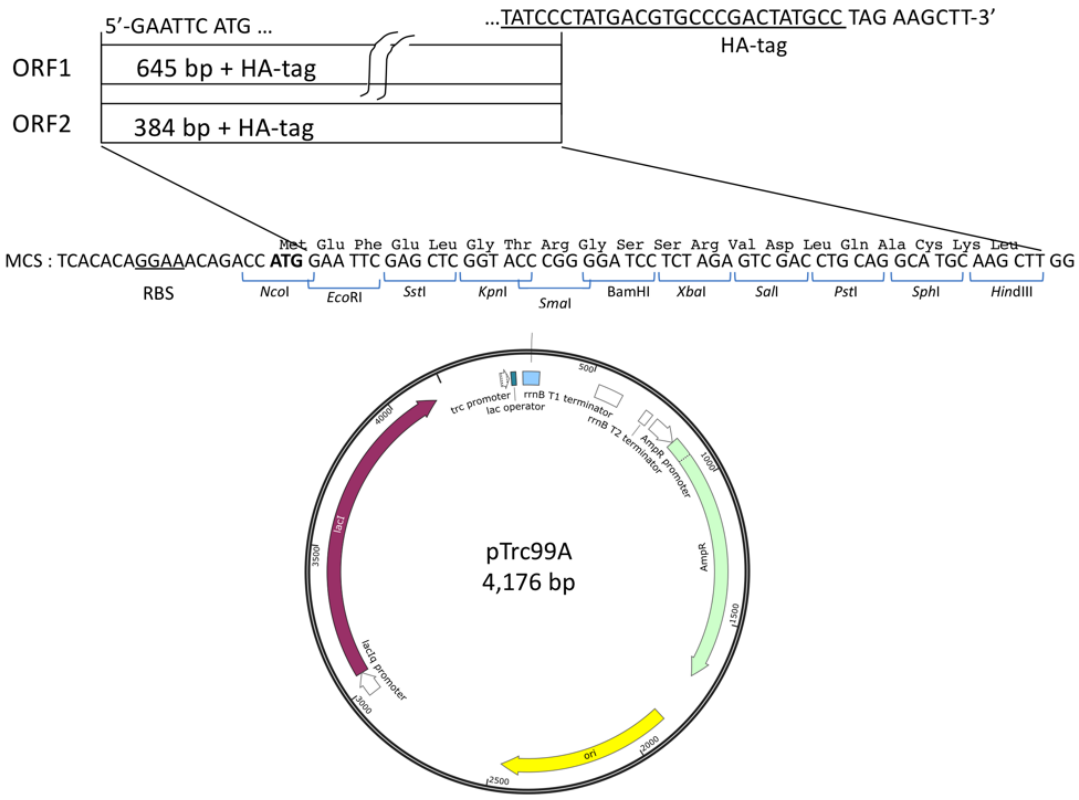

Figure 50. Diagram of plasmid vector construct for *Ps*-ORF1 and *Ps*-ORF2. PCR fragment insertion at *Eco*RI and *Hind*III sites.

3.3.7.2 Optimization of RE digestion on pTrc99A plasmid vector and Ps-ORFs

Optimization of RE digestion on pTrc99A plasmid vector, *Ps*-ORF1, and *Ps*-ORF2 was performed (Figure 51, 52).

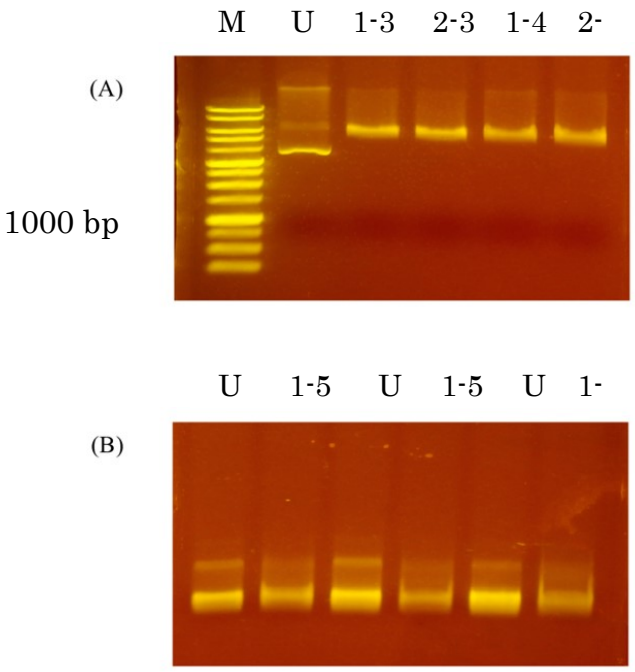

Figure 51. Optimization of RE digestion on pTrcA99 plasmid vector (A) and *Ps*-ORF1 fragments (B). Ten µL of 1 Kb DNA Ready-To-Use Ladder (M), undigested plasmid (U), digested plasmid (A) and *Ps*-ORF-HA-tag fragments (B) were loaded on 0.7% agarose gel, electrophoresed at 100 V for 25 min. Samples were stained with UltraPower DNA Safe Dye and viewed using Blue Light Transilluminator. RE digestion was performed at 37°C for 2 h. The reaction was stopped at 65°C for 20 min. RE digestion was performed with 3 µL (1) or 5 µL (2) RE , in a 50-µL (3) , 45-µL (4), or 55-µL (5) volume per reaction containing 25 µL (3), 30 µL (4) or 40 µL (5) DNA, with 17 µL (3), 5 µL (4), or 10 µL (5) RE buffer. Enzyme inactivation at 65°C for 20 min followed after digestion.

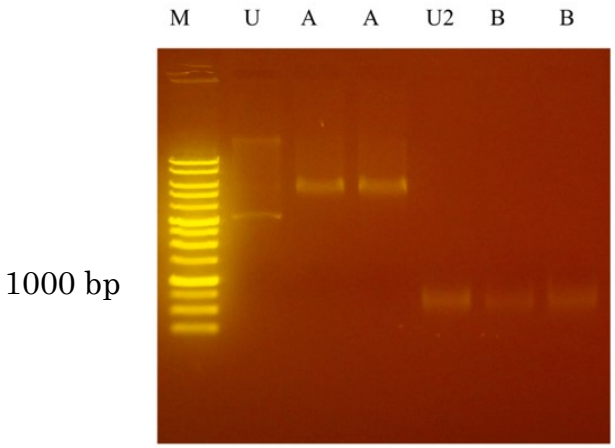

Figure 52. Optimization of RE digestion on pTrcA99 plasmid vector and *Ps*-ORF2 fragments. Ten µL of 1 Kb DNA Ready-To-Use Ladder (M), undigested pTrc99A plasmid (U), undigested *Ps*-ORF2-HA-tag (U2) and digested plasmid (A) and digested *Ps*-ORF2-HA-tag (B) were loaded on 0.7% agarose gel, electrophoresed at 100 V for 25 min. Samples were stained with UltraPower DNA Safe Dye and viewed using Blue Light Transilluminator. RE digestion was performed at 37°C for 2 h. The reaction was stopped at 65°C for 20 min. RE digestion was performed with 3 µL RE in a 50-µL volume per reaction containing 25 µL DNA and 17 µL RE buffer followed by enzyme inactivation at 65°C for 20 min.

3.3.7.3 Amplification of Ps-ORFs

Ps-ORF1 and *Ps*-ORF2 from *E. coli* strain A1 and *P. stutzeri* Hiro-3 were amplified using *Ps*-ORF specific primers (Figure 53, 54).

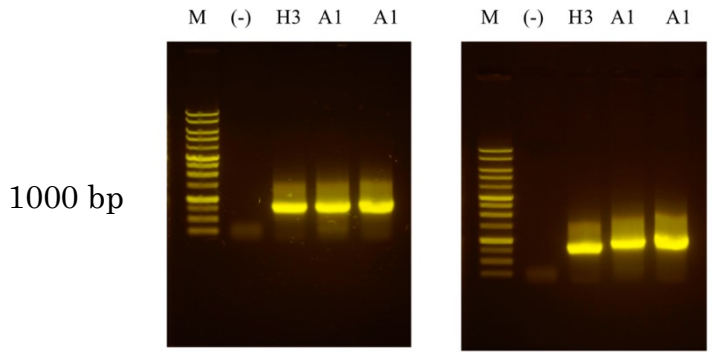

Figure 53. Amplification of *Ps*-ORF1 from *E. coli* strain A1 (A1), and *P. stutzeri* Hiro-3 (H3). Ten µL of 1 Kb DNA Ready-To-Use Ladder (M) and PCR products were loaded on 0.7% agarose gel, electrophoresed at 100 V for 25 min. Samples were stained with UltraPower DNA Safe Dye and viewed using Blue Light Transilluminator. Negative control (-) used was UltraPure H_2O.

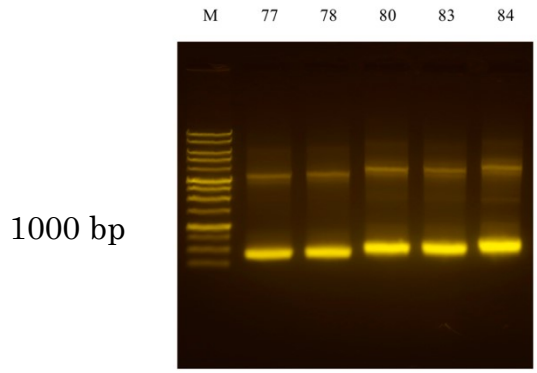

Figure 54. Amplification of *Ps*-ORF2 from *E. coli* strain A1. Ten µL of 1 Kb DNA Ready-To-Use Ladder (M) and PCR products were loaded on 0.7% agarose gel, electrophoresed at 100 V for 30 min. Samples were stained with UltraPower DNA Safe Dye and viewed using Blue Light Transilluminator. Labels 77, 78, 80, 83, and 84 were the annealing temperatures used during PCR.

3.3.7.4 Transformation of Ps-ORFs

Transformation of *Ps*-ORF1 and *Ps*-ORF2 cloning was plated on LB/AMP media (Figure 55, 56).

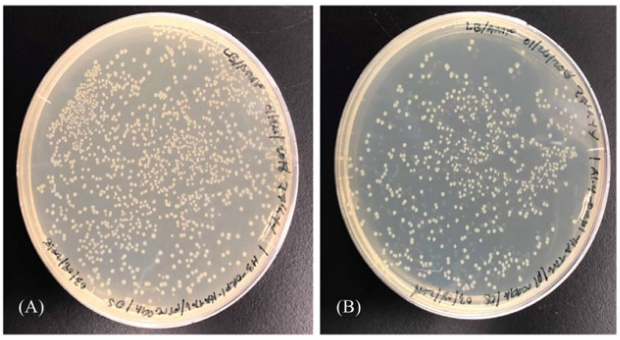

Figure 55. Positive clones harboring the *Ps*-ORF1-HA-tag from *P. stutzeri* Hiro-3 (A) and *E. coli* strain A1 (B) growing on LB/AMP media.

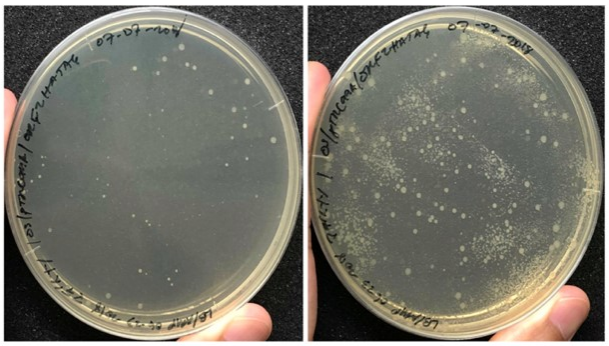

Figure 56. Positive transformants harboring the *Ps*-ORF2-HA-tag ligated fragments from *E. coli* strain A1.

3.3.7.5 Plasmid extraction on Ps-ORF expression clones

Plasmid were extracted on *Ps*-ORF1 positive clones from *P. stutzeri* Hiro-3 and *E. coli* strain A1 (Figure 57). Confirmation of *Ps*-ORFs insertion was also performed using *Ps*-ORF specific primers (Figure 58, 59).

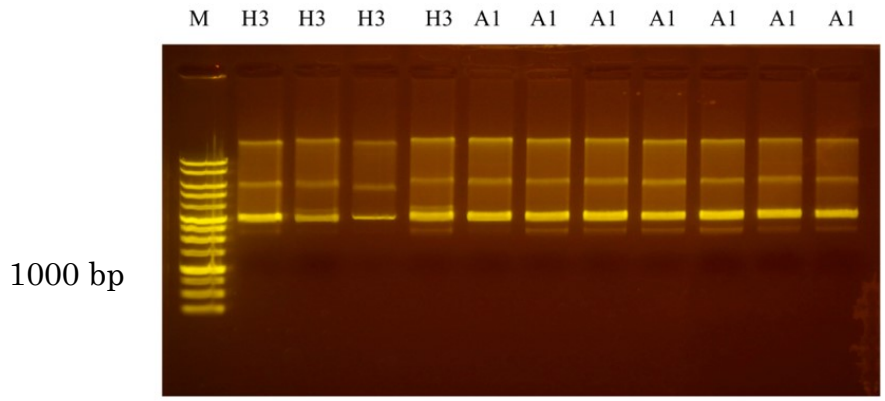

Figure 57. Plasmids extracted from *Ps*-ORF1 expression clones. Plasmid from *P. stutzeri* Hiro-3 (H3) and *E. coli* strain A1 (A1). Ten µL of 1 Kb DNA Ready-To-Use Ladder (M), and plasmid extracted from positive transformants were loaded on 0.7% agarose gel, electrophoresed at 100 V for 25 min. Representative DNA quantity (A260) and quality (A260/A280) were as follows; (H3): 546 ng/µL, 1.818; (A1): 556 ng/µL, 1.886; 504 ng/µL, 1.758.

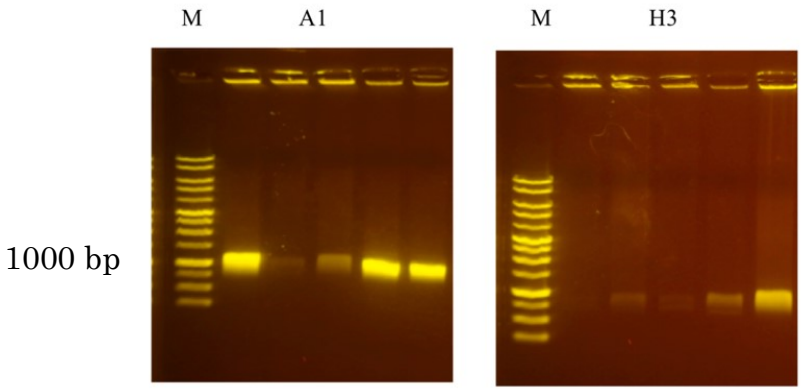

Figure 58. Validation of *Ps*-ORF1 insertion in expression clones. Ten µL of 1 Kb DNA Ready-To-Use Ladder (M), colony-PCR products using *Ps*-ORF1 specific primers on positive transformants of *E. coli* strain A1 (A1) and *P. stutzeri* Hiro-3 (H3) were loaded on 0.7% agarose gel, electrophoresed at 100 V for 25 min. Samples were stained with UltraPower DNA Safe Dye and viewed using Blue Light Transilluminator.

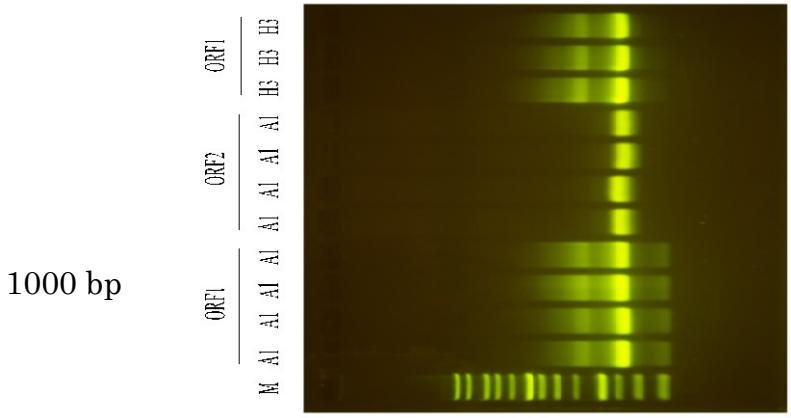

Figure 59. Validation of *Ps*-ORF1 and *Ps*-ORF2 insertion in expression clones. Ten µL of PCR products from *E. coli* strain A1 (A1), and *P. stutzeri* Hiro-3 (H3) were loaded on 0.7% agarose gel, electrophoresed at 100 V for 25 min. Samples were stained with UltraPower DNA Safe Dye and viewed using Blue Light Transilluminator. Marker (M) used was 1 Kb DNA Ready-To-Use Ladder.

3.3.7.6 Tellurite reduction activity of Ps-ORF expression clones

Biochemical assay validated the tellurite reduction activity of the *E. coli* strain A1and *Ps*-ORF1 expression clone (Figure 60, 61). *Ps*-ORF1 from *P. stutzeri* Hiro-3 also showed tellurite reduction activity. There was no activity observed in *Ps*-ORF2 expression clone. Controls which include the wild-type (WT) and WT-harboring the empty plasmid vectors showed no visible growth and no tellurite reduction activity on media amended with 1 mM Na_2TeO_3. These results confirmed that the activity is due to the expression of the metagenome fragment and is not influenced by any other physical factors.

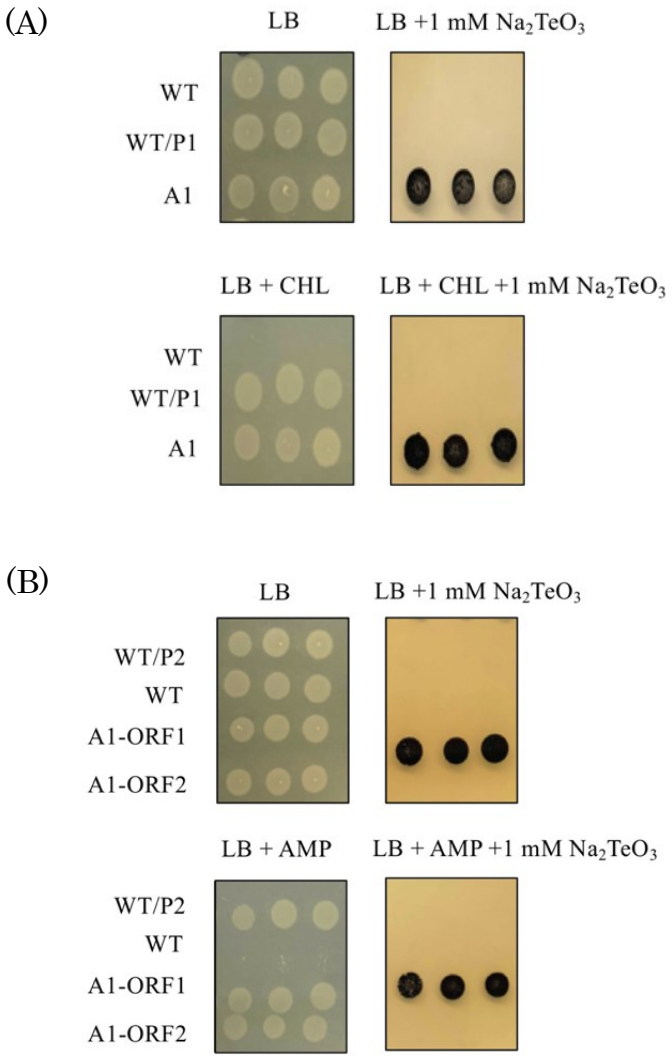

Figure 60. *E. coli* strain A1 (A1) and *Ps*-ORF1 expression clone (A1-ORF1) showed tellurite reduction activity on LB plate amended with 1 mM Na_2TeO_3 (A, B). Wild-type (WT), WT harboring the empty plasmid vector (P1:pHSG398, P2:pTrc99A), and *Ps*-ORF2 expression clone (A1-ORF2) showed no visible tellurite reduction activity. Confluent growths represent triplicate inoculation from three independent sub-cultures.

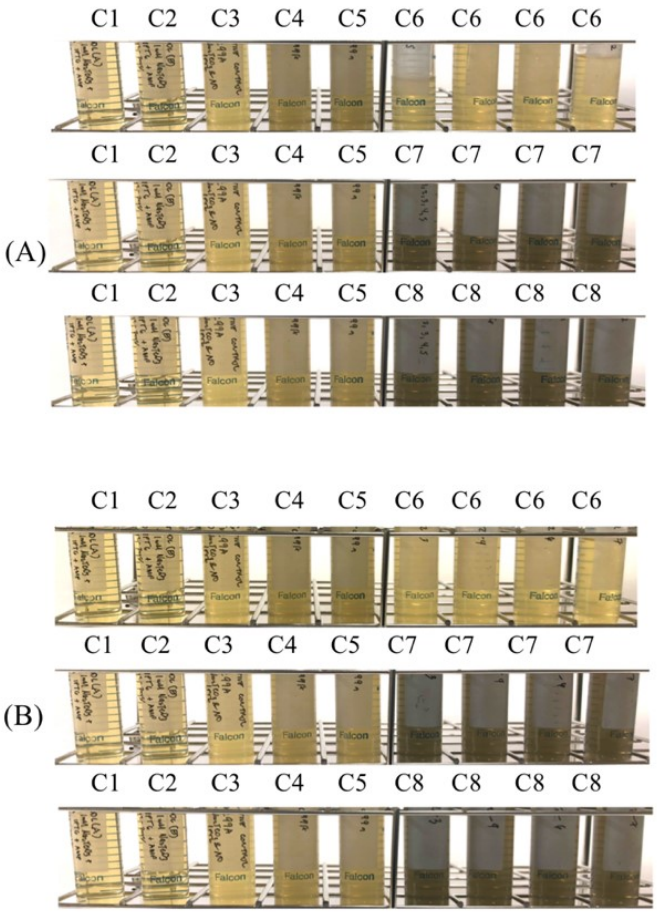

Figure 61. Tellurite reduction activity of expression clones harboring *Ps*-ORF1 from *P. stutzeri* Hiro-3 (A) and *E. coli* strain A1 (B). Tellurite reduction activity of *Ps*-ORF1 expression clone was screened in LB/AMP spiked with 1 mM Na_2TeO_3 and 1 mM IPTG (C1), LB/ AMP spiked with 1 mM Na_2TeO_3 with no IPTG (C2), LB/AMP inoculated with competent cell harboring pTrc99a expression vector (C3), LB/AMP spiked with 1 mM Na_2TeO_3 with 1 mM IPTG inoculated with competent cell harboring pTrc99a expression vector (C4), LB/AMP spiked with 1 mM Na_2TeO_3 with no IPTG inoculated with competent cell harboring pTrc99a expression vector (C5), LB/AMP inoculated with *Ps*-ORF1 expression clones (C6), LB/AMP spiked with 1 mM Na_2TeO_3 with 1 mM IPTG (C7) or without IPTG (C8) inoculated with *Ps*-ORF1 expression clones from *P. stutzeri* Hiro-3, or *E. coli* strain A1.

3.3.8 Characterization of *E. coli* strain A1

3.3.8.1 Colony morphology of E. coli strain A1

E. coli strain A1 formed colonies with round form, entire margin, convex elevation, smooth consistency, and opaque color (Figure 62). These colony characteristics are consistent with the WT culture.

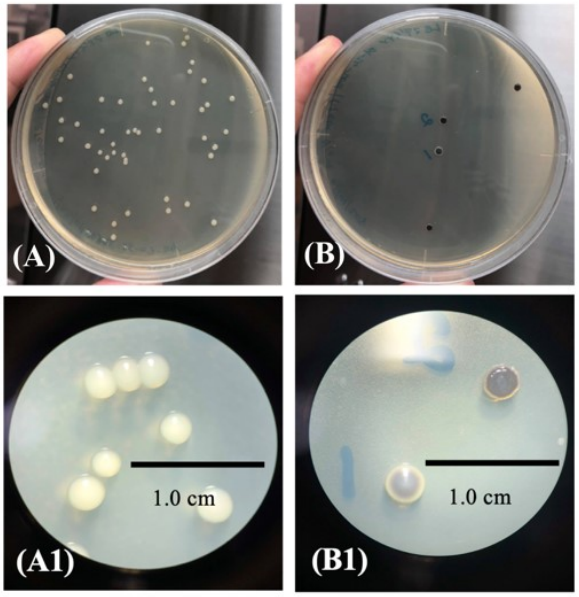

Figure 62. Colony characteristics of the *E. coli* strain A1 on LB agar without Na_2TeO_3 (A, A1) and with 1 mM Na_2TeO_3 (B, B1). Colonies were also observed under stereomicroscope (A1, B1).

3.3.8.2 Growth curve of E. coli strain A1

E. coli strain A1 reaches its stationary growth phase after 16 h incubation at 37°C. Growth curve of *E. coli* strain A1 was presented in Figure 63.

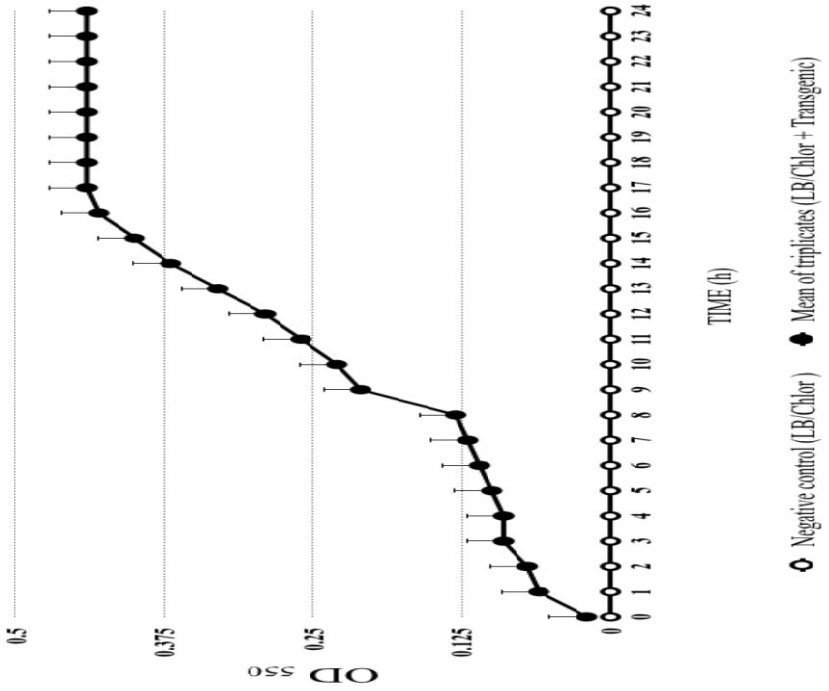

Figure 63. Growth curve of *E. coli* strain A1 in 24-h duration.

3.3.8.3 Tellurite reduction activity of E. coli strain A1

Gradual tellurite reduction was observed on the *E. coli* strain A1 (Figure 64).

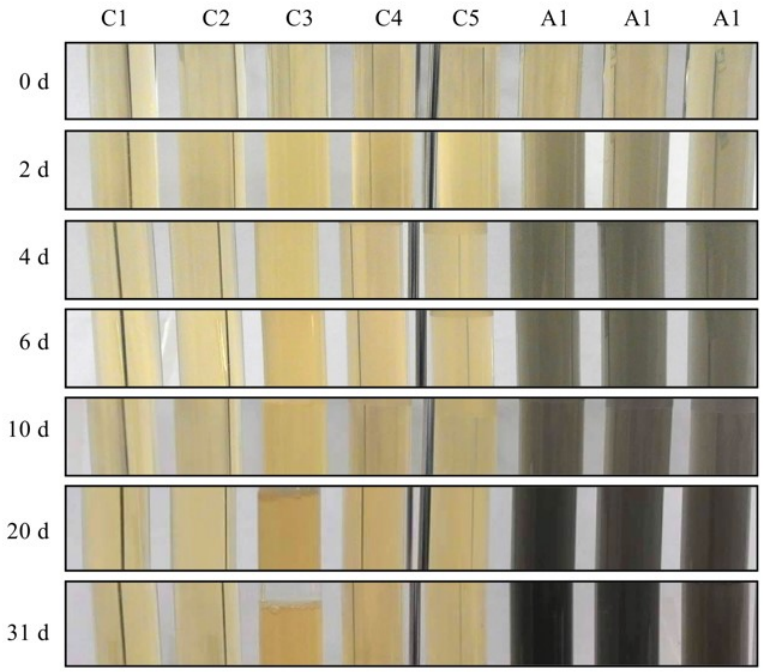

Figure 64. Gradual tellurite reduction activity of the *E. coli* strain A1 at 37°C. Biochemical assay includes LB broth (C1), LB amended with 1 mM Na_2TeO_3 (C2), LB inoculated with wild-type cells (WT) (C3), LB amended with 1 mM Na_2TeO_3 inoculated with WT cells (C4), LB inoculated with *E. coli* strain A1 (C5), LB amended with 1 mM Na_2TeO_3 and 20 µg/mL chloramphenicol inoculated with *E. coli* strain A1 (A1). Days (d) of exposure were indicated.

3.3.8.4 Tellurium crystals of E. coli strain A1

TEM images of recombinant cells exposed with the tellurite ions revealed intracellular tellurium crystals (Figure 65). Crystals outside the cells were also observed which could be crystals released from ruptured cells.

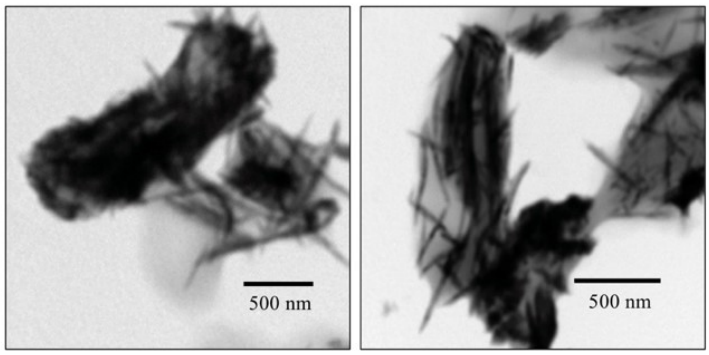

Figure 65. TEM revealed intracellular tellurium crystals formed in the *E. coli* strain A1 cells grown for 101 d. Tellurium crystals sizes are larger than 500 nm.

3.3.8.5 Optimum temperature and pH for growth and tellurite reduction activity

There was no significant difference (*P*-value > .05) observed on growth trends in WT and *E. coli* strain A1 (Figure 66). Highest growth was recorded at 32°C and pH 7.0 in both WT and *E. coli* strain A1 (Figure 66-A). There was no significant difference observed on growth at 32°C and 37°C and at pH 7.0 and pH 9.0 in *Ps*-ORF1 expression clone (Figure 66-A, 66-B). There was no growth recorded on WT when exposed to 1 mM Na_2TeO_3 (Figure 66-D). Tellurite reduction activity was recorded at 32°C and 37°C and at pH 7.0 and pH 9.0 in *E. coli* strain A1 and *Ps*-ORF1 expression clone (Figure 66-D, 66-E). There was no tellurite reduction activity recorded at 4°C and 45°C (Figure 66-D, 66-E, 66-F). There was no tellurite reduction activity observed at pH 10.0 in both *E. coli* strain A1 and *Ps*-ORF1 expression clone (Figure 66-F).

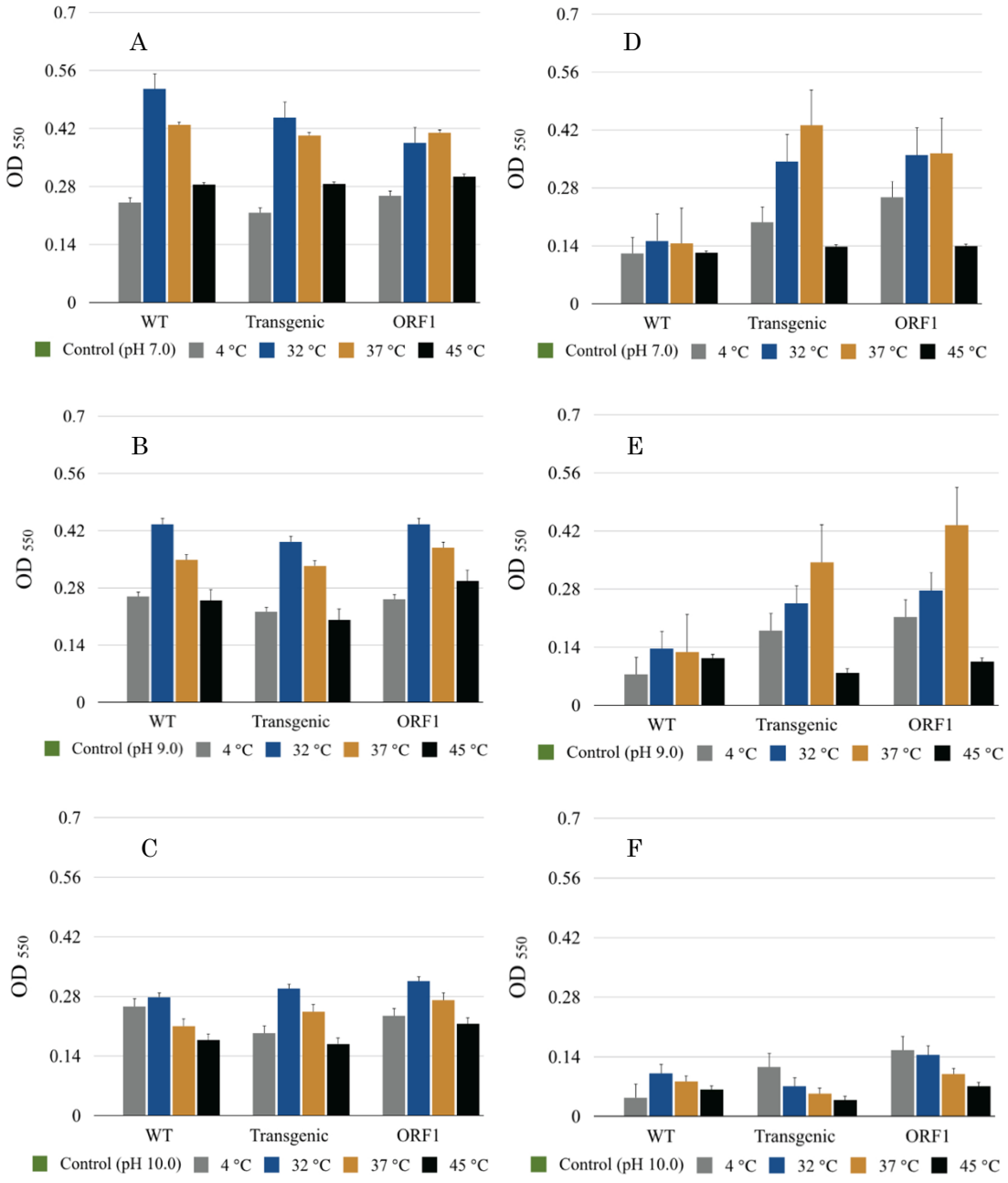

Figure 66. Temperature and pH effects on growth (A, B, C) and tellurite reduction at 1 mM Na_2TeO_3 (D, E, F) of wild-type cells (WT), transgenic cells, and *Ps*-ORF1 expression clone. Colored bars represent growths at different temperatures and pH after 48 h incubation. Error bars indicate standard deviations from triplicate reactions. Control tubes showed no bacterial growths.

3.3.9 Isolation of a chloramphenicol-susceptible strain

3.3.9.1 Isolation of A1 mutant strain

MIC assay using the recombinant culture showed chloramphenicol-susceptible culture with increased resistance at 2 mM Na_2TeO_3 (Figure 67-A). Re-screening of the MIC revealed that the *E. coli* strain A1 has MIC at 2 mM Na_2TeO_3 while the A1 mutant strain has MIC at 3 mM Na_2TeO_3 (Figure 67-B). This result led to the isolation of A1 mutant strain from the recombinant culture (Figure 68).

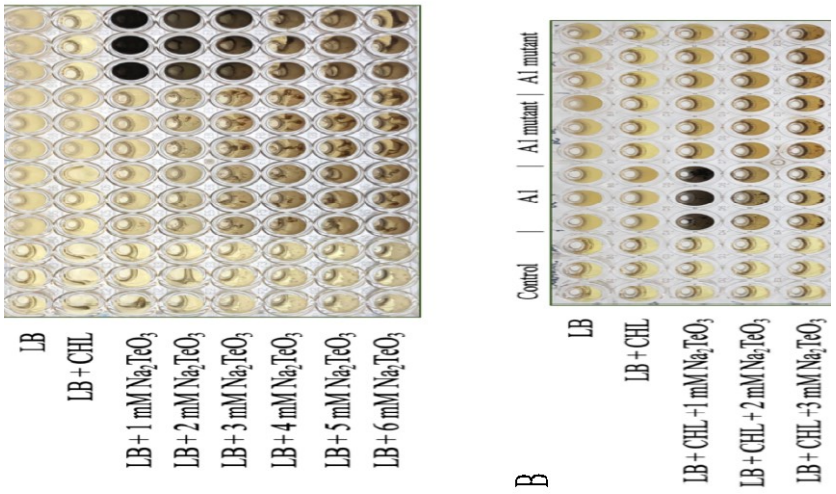

Figure 67. A chloramphenicol-susceptible strain was observed with increased MIC (A). This led to the isolation of a mutant A1 strain with a MIC of 3 mM Na_2TeO_3 (B).

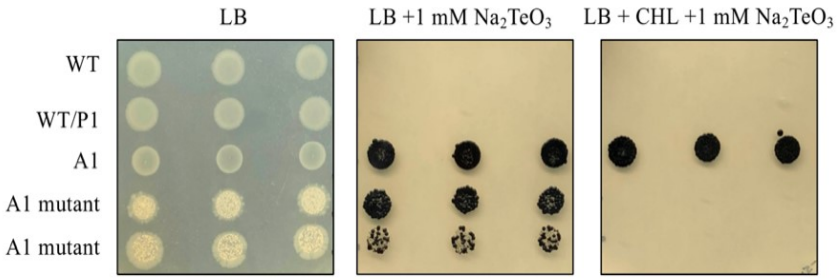

Figure 68. Isolation of chloramphenicol-susceptible A1 mutant strain which showed tellurite reduction activity.

3.3.9.2 Characterization of A1 mutant strain

Growth of the A1 mutant strain was recorded at 32°C and 37°C and at pH 7.0 and pH 9.0 (Figure 69-A). Tellurite reduction activity was recorded at 32°C and 37°C and at pH 7.0, pH 9.0, and pH 10.0 (Figure 69-B).

(A) LB

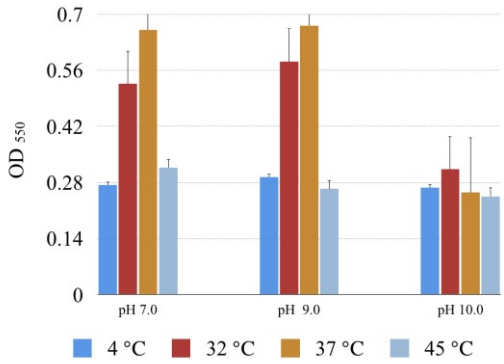

(B) LB Amended with 1 mM Na_2TeO_3

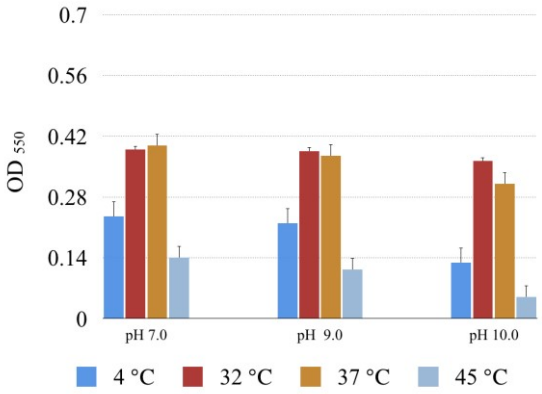

Figure 69. Temperature and pH optimum for growth (A) and tellurite reduction activity (B) of A1 mutant strain.

3.3.9.3 Wider pH tolerance of A1 mutant strain

A1 mutant strain showed wider pH tolerance for tellurite reduction activity (Figure 70).

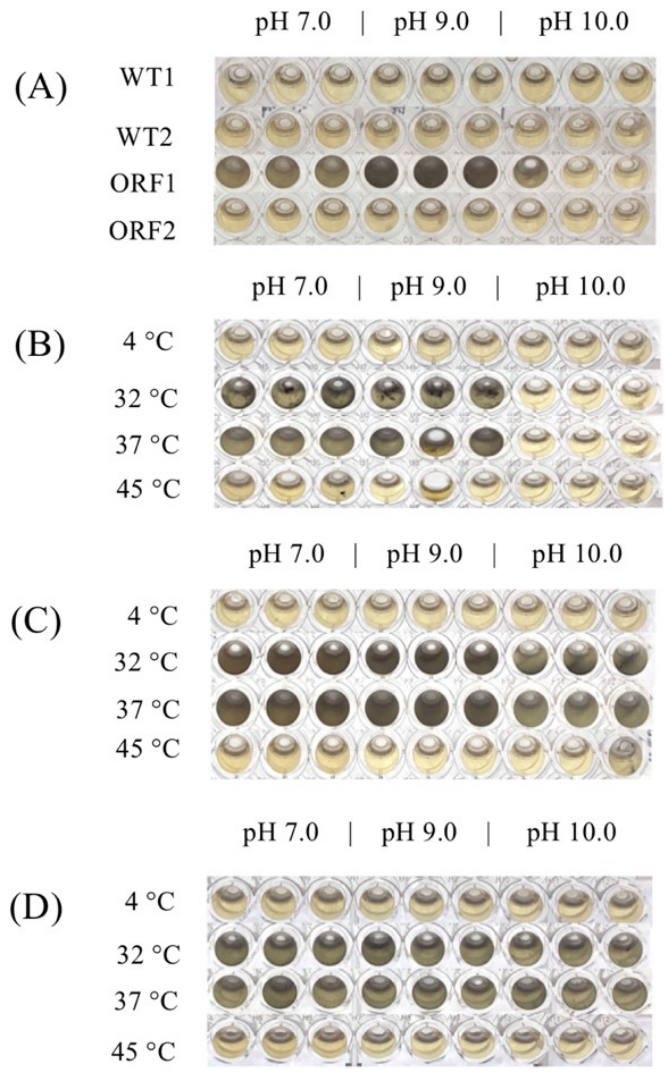

Figure 70. Replication of tellurite reduction assay in LB media amended with 1 mM Na_2TeO_3 on wild-type cells (WT1, WT2) and *Ps*-ORF expression clones (A), *E. coli* strain A1 (B), and chloramphenicol-susceptible A1 mutant strain (C, D).

3.3.9.4 Confirmation of Ps-ORF1 presence in A1 mutant strain

Plasmids were extracted from the A1 mutant strain and revealed less plasmid contents or even loss of plasmid. PCR amplification of *Ps*-ORF1 and *Ps*-ORF2 revealed intact ORFs in the *E. coli* strain A1 (Figure 71-A). Notably, *Ps*-ORF2 amplified from the *E. coli* strain A1 showed larger amplicon size. Since the plasmid is circular, the longer side of the plasmid could have been amplified rather than the actual *Ps*-ORF2. Empty plasmid vector showed no amplicons, thus bands observed on *Ps*-ORF2 in *E. coli* strain A1 are not a product of mis-amplification. In contrast, the A1 mutant strain showed only *Ps*-ORF1 amplicons suggesting a possible integration of the gene in the chromosome of the host cell (Figure 71-B, 71-C). Using the plasmid of A1 mutant, *Ps*-ORF2 was not amplified. There could be some mutation that have occurred on the sequence of *Ps*-ORF2 in the A1 mutant strain. Control empty plasmid vectors showed no bands suggesting the amplicons were not products of non-specific amplification.

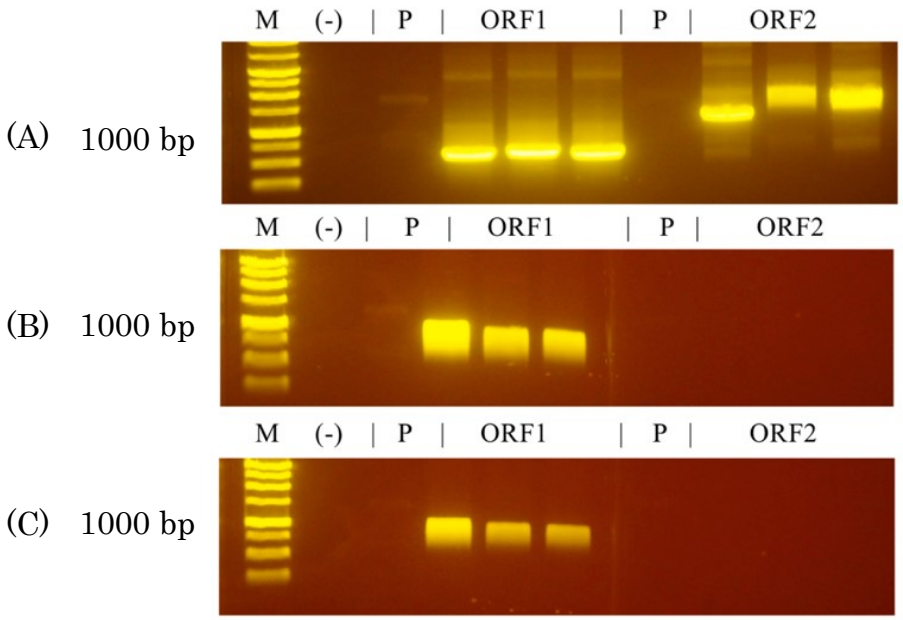

Figure 71. Amplification of *Ps*-ORF1 and *Ps*-ORF2 on *E. coli* strain A1 (A), and A1 mutant strain (B, C). This result suggests a possible difference in the location of the gene. Probable chromosomal integration was hypothesized for A1 mutant strain which showed increased antibiotic sensitivity but retained the tellurite reduction activity and *Ps*-ORF1. Marker (M) used was 1 Kb DNA Ready-To-Use Ladder. Empty plasmid (P) showed no amplicons. Negative control (-) used was UltraPure H_2O.

3.3.10 Temporal aspect of tellurite reduction activity in *E. coli* strain A1, A1 mutant strain, and *Ps*-ORF expression clones

It takes 48 h which coincided with the stationary phase of *E. coli* strain A1, A1 mutant strain, and *Ps*-ORF1 expression clone to observe the growth of black colonies on LB agar media amended with 1 mM Na_2TeO_3 (Figure 72).

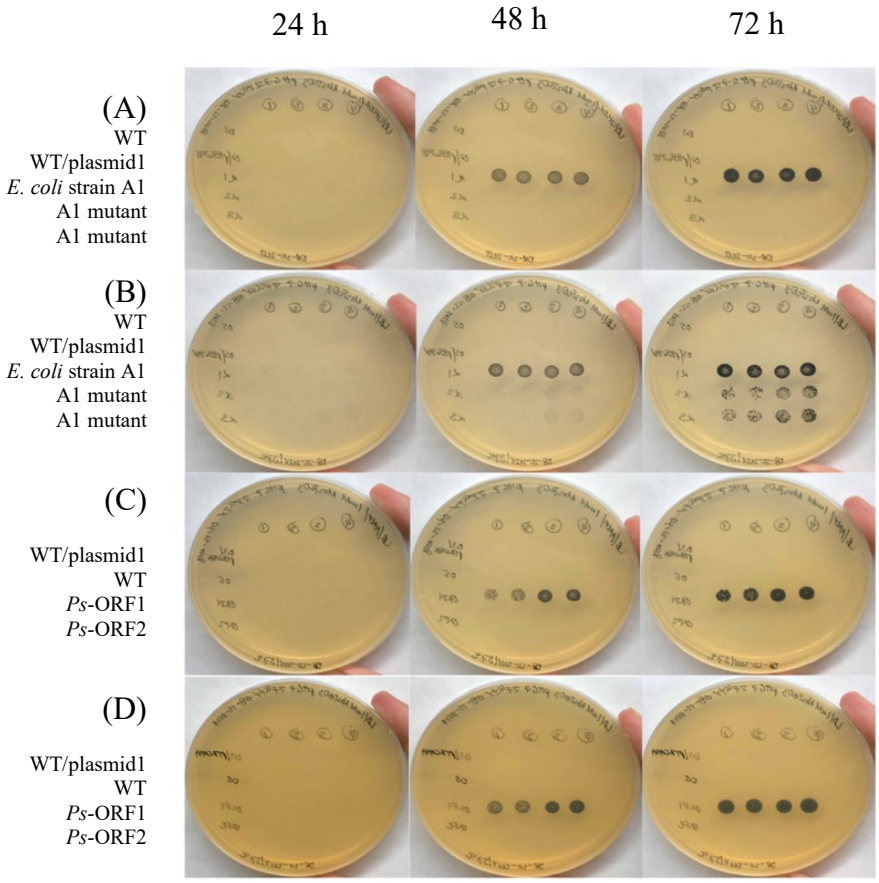

Figure 72. It takes 48 h for the tellurite reduction activity to be observed in *E. coli* strain A1, chloramphenicol-susceptible A1 mutant strain, and *Ps*-ORF1 expression clones (*Ps*-ORF1, *Ps*-ORF2). Assay includes LB/CHL amended with 1 mM Na_2TeO_3 (A), LB amended with 1 mM Na_2TeO_3 (B), LB/AMP amended with 1 mM Na_2TeO_3 (C), and LB amended with 1 mM Na_2TeO_3 (D).

3.3.11 Cell-free tellurite reduction assay

3.3.11.1 Tellurite reduction activity of solubilized cells in LB media

Tellurite reduction activity was observed on solubilized WT cells indicating effects of other unknown tellurite reductases and non-specific enzymes with tellurite reduction activity (Figure 73). Supernatant collected from the cultures which could possibly include extracellularly secreted enzymes showed no visible tellurite reduction activity.

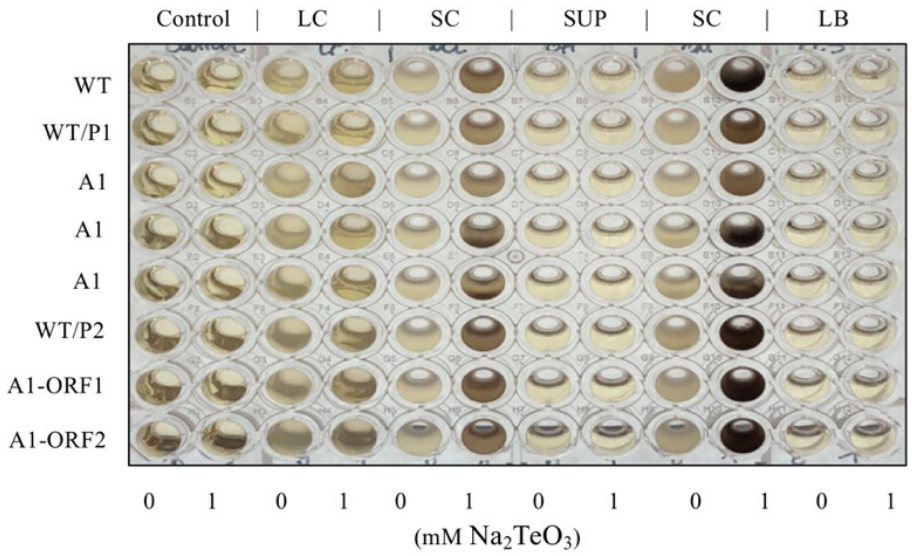

Figure 73. Cell-free tellurite reduction assay. Assay includes solubilized cells (SC), wild-type cells (WT), WT/P1 and WT/P2-harboring empty plasmid vector (P1: pHSG398; P2: pTrc99A), *E. coli* strain A1, A1 mutant strain, and *Ps*-ORF expression clones (A1-ORF1, A1-ORF2). Live-cells (LC), supernatant (SUP), and lysis buffer (LB). SC on lane 6 and lane 10 contains 100 µL and 150 µL solubilized cells, respectively. Control used was LB media. Bacterial concentration was standardized using cultures with similar OD values at 550 nm. Protein concentration was not standardized on this experiment. The image is a representative of three independent experiments with similar results.

3.3.11.2 Tellurite reduction activity of soluble and insoluble fractions from ultracentrifugation in cell lysis solution

Tellurite reduction assay using soluble fraction which contains hydrophilic proteins and insoluble fractions containing hydrophobic proteins from ultracentrifugation showed no visible tellurite reduction activity suggesting that live-intact cells are required to observe the effect of the gene in the recombinant cells (Figure 74).

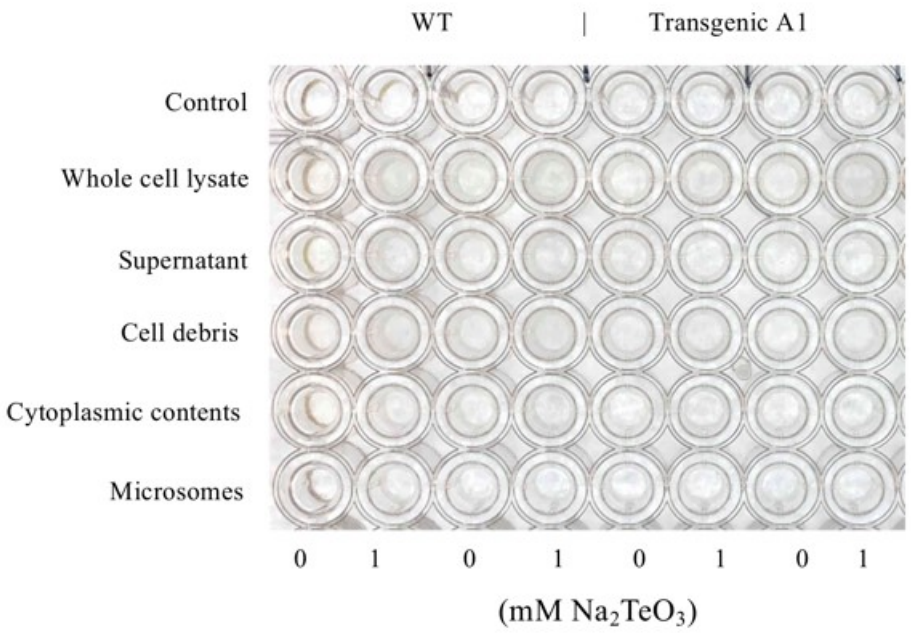

Figure 74. No tellurite reduction activity on soluble and insoluble fractions collected after ultracentrifugation in both wild-type cells (WT) and *E. coli* strain A1 in cell lysis solution amended with 1 mM Na_2TeO_3.

3.3.12 Insights on tellurium recovery using ICP-OES

Figure 75 shows recovered Te from the marine sediment enrichment culture, *S. alage* Hiro-1, *P. pseudoalcaligenes* Hiro-2, *P. stutzeri* Hiro-3, and *E. coli* strain A1. Highest recovery was observed in the marine sediment enrichment culture with 72% (0.16 g/L) recovery at pH 9.0 followed by *P. pseudoalcaligenes* Hiro-2 with 58% (0.13 g/L) at pH 7.0. No significant difference was observed on tellurium recovery on the three new strains at pH 9 with less than 40% recovery. *E. coli* strain A1 has the lowest recovery at 9% (0.02 g/L) probably due to the short time of exposure of one week.

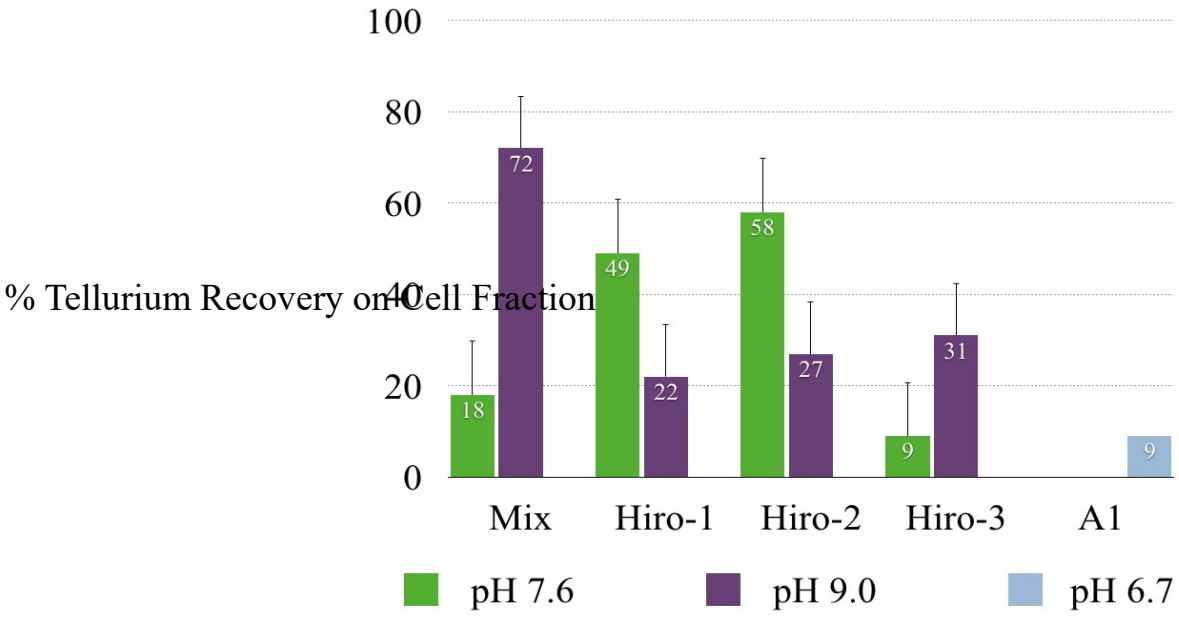

Figure 75. Insights on bacterial tellurium recovery. Marine sediment enrichment culture (Mix), *S. algae* Hiro-1, *P. pseudoalcaligenes* Hiro-2, *P. stutzeri* Hiro-3, and *E. coli* strain A1 was included in the analysis. Standards of known Te concentrations (0.000 mM, 0.100 mM, 1.000 mM, and 10.00 mM) showed exactly the same Te concentration by ICP-OES.

3.4 Discussion

A novel gene was successfully isolated in the marine sediment enrichment culture through metagenome library screening. The metagenome fragment conferring tellurite reduction activity to *E. coli* strain A1 may be derived from the new strain, *P. stutzeri* Hiro-3. Species-specific Te crystal formation was observed between *P. stutzeri* Hiro-3 and *E. coli* strain A1. Te crystals in *P. stutzeri* Hiro-3 showed Te nanorods scattered throughout the cell cytoplasm. Te in the recombinant cells showed similar morphology with the Te crystals from *Erythrobacter litoralis* which can occupy as much as 20%-30% of the cell cytoplasm (Yurkov et al., 1998).

The conservation of amino acid domains with the PAP2 Superfamily protein suggests that the metagenome fragment could have a close evolutionary relationship with the protein family and therefore may share structural and functional attribute as biological molecules (Arenas-Salinas et al., 2016). The recently elucidated PAP2 from *B. subtilis* includes mostly uncharacterized proteins such as PAP2_like_2, PgpB, DedA, and SNARE (Neuwald, 1997; Ghachi et al., 2017). PAP2 shares catalytic residues with haloperoxidases, bacterial acid phosphatases, and ATP diphosphohydrolase (Zhang et al., 2008). A successful purification of PAP2L2 from *Geobacillus toebii* T-85 revealed broad substrate specificity of the integral membrane protein (Zhang et al., 2008). Elucidation of the protein crystal structure of the novel gene can shed valuable information on its relationship with membrane phosphatases.

Amino acid residues associated with metal-binding activities includes cysteine (C), histidine (H), glutamic acid (E), and aspartic acid (D) (Dudev et al., 2003; Babor et al., 2008). Catalytic cysteine residues in some flavoproteins were reported to have a role in the transfer of electrons during the reduction process (Arenas-Salinas et al., 2016). Catalytic function of amino acid residues in the metagenome fragment has not been investigated. Closest enzymes with structural similarity with the metagenome fragment include hydrolases, peroxidases, and oxidoreductases which typically uses NADH or NADPH as a source of electron

for their catalytic activity. One peroxidase which was found to catalyze tellurite reduction in *S. epidermidis* was catalase (Calderón et al., 2006). Expression of catalase also increased resistance to tellurite in recombinant *E. coli* host (Calderón et al., 2006). Oxidoreductases such as nitrate reductase along with terminal oxidases of bacterial respiratory chain was also documented with tellurite reduction activity (Avazeri et al., 1997; Trutko et al., 1998). The source of reducing power, substrate-specificity, selectivity, and inhibition for the catalytic activity of the putative tellurite-reducing gene if present has not been investigated in this thesis.

Instability of plasmid carrying the putative tellurite-reducing gene was observed several times during the conduct of the experiment. Re-screening of the recombinant cells for three times was performed to recover the transgenic cells with tellurite reduction activity. The recombinant culture was cultivated in both LB broth with or without chloramphenicol. The absence of the selective pressure from the antibiotics could have led to the expulsion or degradation of the plasmid containing the chloramphenicol resistance gene (McLoughlin, 1994; Gasiunas et al., 2014). The loss of the pHSG398 plasmid vector resulted in the observed chloramphenicol-susceptibility of the A1 mutant strain. Intuitively, *Ps*-ORF1 in A1 mutant strain could possibly be integrated in the bacterial chromosomal DNA through homologous recombination or by high frequency of recombination (Hfr) (Itaya and Tanaka, 1990; Griffiths et al., 2000; Bennett, 2008; Heap et al., 2012). Homologous recombination was unlikely the cause of mutation because TOP-10 and DH5α competent cells have *rec*A1 which could limit non-specific homologous recombination with the host cell. However, possible mutation on these genes may also be possible. The exact mechanism of mutation remains unclear, nevertheless, the activity imparted by the *Ps*-ORF1 gene in the *E. coli* strain A1 may not be different from that observed in A1 mutant strain.

One possible effect of chromosomal integration is the provision of stronger signals from Shine-Dalgarno (SD) sequence and AUG start codon for the translation of *Ps*-ORF1. This higher translation levels of *Ps*-ORF1 could have led

to the observed elevated tellurite resistance at 2 mM Na_2TeO_3 and tellurite reduction activity even at pH 10.0 in the A1 mutant strain.

Tellurite reduction activity was only observed in the LB media and not in the cell lysis solution. This observation supports earlier findings that tellurite reduction occurs in nutrient medium with yeast extracts and other rich organic compounds but not in media containing acetate, glutamate, or pyruvate as the carbon source. Rich organic medium provides a pool of electron carriers which could shuttle electrons to tellurite during the reduction process (Sepahei and Rashetnia, 2009).

The influx of tellurite ions allows homeostasis enzymes such as glutathione reductase to catalyze the reduction of tellurite ions into pure elemental Te once inside the cell cytoplasm. As observed, *in vitro* assay on the solubilized whole cell lysates suggested that there are other tellurite reductases present in the bacterial cell. Discriminating the effect of *Ps*-ORF1 from other specific and non-specific tellurite reductases remains as a great challenge. Initial attempts to identify the putative TM protein was carried out with immunoprecipitation, however, the results were inconclusive.

3.5 Conclusion

This thesis presents the discovery of a novel gene which function for conferring tellurite resistance to *E. coli* transformant by promoting tellurite reduction within the cells. Growth and tellurite reduction activity of the *E. coli* strain A1 shows thermo-sensitivity and pH-dependent activity. Expression of the putative tellurite-reducing gene in *E. coli* host has significantly increased its tellurite resistance in 1 mM Na_2TeO_3. The observed tellurite resistance in recombinant cells may be due to intracellular sequestration of tellurite ions and through which tellurite is reduced into tellurium by a plethora of homeostasis enzyme once inside the cell. Live-intact cells are required to observe the tellurite reduction activity of the putative tellurite-reducing gene.

A major challenge in employing recombinant bacterial cells in *in situ* bioremediation is the probable risks of introducing antibiotic resistance genes in the wild bacterial population. Thus, the isolation of a chloramphenicol-susceptible A1 strain presents an opportunity for *in situ* application, eliminating the transfer of antibiotic resistance genes in the environment.

Further characterization of the putative tellurite-reducing gene will aid in elucidating the mechanism of tellurite resistance and tellurite reduction activity observed in recombinant cells. Protein isolation and purification will give light on the tellurite reduction activity of the metagenome fragment. The *E. coli* strain A1 showed strong resistance to tellurite ions and might be used to recover Te crystals from environments contaminated with tellurite.

Chapter IV

Conclusion and Recommendations

4.1 Conclusion

New bacterial strains have shown high resistance to tellurite ions which makes them good candidate for future elucidation of tellurite reduction mechanisms on these bacterial species. *S. algae* Hiro-1 showed MIC at 15 mM Na_2TeO_3, while the two pseudomonads showed MIC at 6 mM Na_2TeO_3.

A putative tellurite-reducing gene was successfully unearthed from a marine sediment enrichment culture using metagenome library construction and functional screening. The gene was shown to be specific to *P. stutzeri* by BLAST and by PCR using *Ps*-ORF1 specific primers. The gene has also shown similarity with PAP2 Superfamily Protein from *P. stutzeri*, *B. subtilis*, and *E. coli*. The *E. coli* strain A1 showed MIC at 2 mM Na_2TeO_3. A chloramphenicol-susceptible strain showed MIC at 3 mM Na_2TeO_3 and presents an opportunity for *in situ* bioremediation of tellurite.

The discovery of a putative tellurite-reducing gene can provide novel insights on the tellurite reduction mechanism employed in some bacterial cells. New bacterial strains and recombinant cell with tellurite bioremediation potential can be employed in bioremediation of tellurite from copper-refining acid-mine drainage. Simultaneously, microbial cell-based recovery can provide a sustainable approach to recover tellurium which is a highly valuable metalloid. Recovered tellurium using microbial cells can augment the resource scarcity of this important raw material that is being used in solar cells and other photoelectric devices.

4.2 Recommendations

Further investigations on the tellurium recovery potential of the three new bacterial strains and recombinant strains can jumpstart a microbial cell-based metal recovery strategy. Elucidation of protein crystal structure emerging from the novel gene can reveal its identity and properties that are responsible in the observed tellurite reduction activity.

Literatures Cited

1. AHP Materials (2011) Tellurium-Properties and Applications. Retrieved from https://www.azom.com/article.aspx?ArticleID=5814 Date: July 17, 2019
2. Almagro VM, Blasco R, Huertas MJ, Luque MM, Vivian CM, Castillo F, Roldan MD (2005) Alkaline cyanide biodegradation by *Pseudomonas pseudoalcaligenes* CECT5344. *Biochem Soc Trans* 33:168–169
3. Altschul SF, Gish W, Miller W, Myers EW, Lipman DJ (1990) Basic local alignment search tool. *J Mol Biol* 215: 403-410
4. Amoozegar MA, Ashengroph M, Malekzadeh F, Razavi MR, Naddaf S, Kabiri M (2008) Isolation and initial characterization of the tellurite-reducing moderately halophilic bacterium, *Salinococcus* sp. Strain QW6. *Microbiol Res* 163: 4, 456-465
5. Aradska J, Smidak R, Turkovicova L, Turna J, Lubec G (2013) Proteomic Differences between Tellurite-Sensitive and Tellurite-Resistant *E. coli*. *PLoS ONE*. 8:11, 1-9
6. Arenas FA, Pugin B, Henriquez NA, Arenas-Salinas MA, Diaz-Vasquez WA et al. (2014) Isolation, identification and characterization of highly tellurite-resistant, tellurite-reducing bacteria from Antarctica. *Polar Sci* 8 (1): 40-52
7. Arenas-Salinas M, Perez JI, Morales W, Pinto C, Diaz P, Cornejo FA, et al. (2016) Flavoprotein-Mediated Tellurite Reduction: Structural Basis and Applications to the Synthesis of Tellurium-Containing Nanostructures. *Front Microbiol* 7:1-14
8. Avazeri C, Turner R, Pommier J, Weiner J, Giordano G, Vermeglio A (1997) Tellurite reductase activity of nitrate reductase is responsible for the basal resistance of *Escherichia coli* to tellurite. *Microbiology* 143:1181-1189
9. Ba LA, Doring M, Jamier V, Jacob C (2010) Tellurium: an element with great biological potency and potential. *Org Biomol Chem* 8: 4203-4216

10. Babor M, Gerzon S, Raveh B, Sobolev V, Edelman M (2008) Prediction of transition metal-binding sites from apo protein structures. *Proteins* 70:208-217
11. Baesman SM, Bullen TD, Dewald J, Zhang DH, Curran S, Islam FS, Beveridge TJ, Oremland RS (2007) Formation of tellurium nanocrystals during anaerobic growth of bacteria that use Te oxyanions as respiratory electron acceptors. *Appl Environ Microbiol* 73:2135–2143
12. Baesman SM, Stolz JF, Kulp TR, Oremland RS (2009) Enrichment and isolation of *Bacillus beveridgei* sp. nov., a facultative anaerobic haloalkaliphile from Mono Lake, California, that respires oxyanions of tellurium, selenium, and arsenic. *Extremophiles* 13:695–705
13. Benkert P, Biasini M, Schwede T (2011) Toward the estimation of the absolute quality of individual protein structure models. *Bioinformatics* 27: 343-350
14. Bennett PM (2008) Plasmid encoded antibiotic resistance: acquisition and transfer of antibiotic resistance genes in bacteria. *Br J Pharmacol* 153 (1): 347-357
15. Berman H, Henrick K, Nakamura H, Markley JL (2007) The worldwide Protein Data Bank (wwPDB): ensuring a single, uniform archive of PDB data. *Nucleic Acids Res* 35: 301-303
16. Berman H, Westbrook J, Feng Z, Gilliland G, Bhat TN, Weissig I, et al. (2000) The Protein Data Bank. *Nucleic Acids Res* 28: 235-242
17. Bertani G (1951) Studies on Lysogenesis I. The Mode of Phage Liberation by Lysogenic *Escherichia coli*. *J Bacteriol* 62(3): 293-300
18. Bertoni M, Kiefer F, Biasini M, Bordoli L, Schwede T (2017) Modelling protein quaternary structure of homo- and hetero-oligomers beyond binary interactions by homology. *Sci Rep* 7
19. Bienert S, Waterhouse A, de Beer TAP, Tauriello G, Studer G, Bordoli L, et al. (2017) The SWISS-MODEL Repository- new features and functionality. *Nucleic Acids Res* 45: 313-319

20. Bleiwas DI (2010) Byproduct Mineral Commodities Used for the Production of Photovoltaic Cells. U.S. Geological Survey Circular 1365, 10 p., available at http://pubs.usgs.gov/circ/1365/
21. Borghese R, Baccolini C, Francia F, Sabatino P, Turner RJ, Zannoni D (2014) Reduction of chalcogen oxyanions and generation of nanoprecipitates by the photosynthetic bacterium *Rhodobacter capsulatus*. *J Hazard Mater* 269: 24-30
22. Borsetti F, Borghese R, Francia F, Randi MR, Fedi S, Zannoni D (2003) Reduction of potassium tellurite to elemental tellurium and its effect on the plasma membrane redox components of the facultative phototroph *Rhodobacter capsulatus*. *Protoplasma* 221:152–161
23. Burgess JG, Miyashita H, Sudo H, Matsunaga T (1991) Antibiotic production by the marine photosynthetic bacterium *Chromatium purpuratum* NKPB 031704: Localization of activity to the chromatophores. *FEMS Microbial Let* 84:301-306
24. Calderón IL, Arenas FA, Pérez JM, Fuentes DE, Araya MA, Saavedra CP, et al. (2006) Catalases are NAD(P)H-dependent tellurite reductases. *PLoS ONE* 1(1): 70
25. Castro ME, Molina R, Díaz W, Pichuantes SE, Vásquez CC (2008) The dihydrolipoamide dehydrogenase of *Aeromonas caviae* ST exhibits NADH-dependent tellurite reductase activity. *Biochem. Biophys. Res. Commun* 375: 91–94
26. Chasteen TG, Fuentes DE, Tantalean JC, Vasquez CC (2009) Tellurite: history, oxidative stress, and molecular mechanisms of resistance. *FEMS Microbiol Rev* 33: 820-832
27. Coker VS, Byrne JM, Telling ND, VAN DER Laan G, Lloyd JR, Hitchcock AP, et al. (2012) Characterization of the dissimilatory reduction of Fe (III)-oxyhydroxide at the microbe-mineral interface: the application of STXM-XMCD. *Geobiology* 10 (4): 347-54
28. Csotonyi JT, Stackebrandt E, Yurkov V (2006) Anaerobic respiration on tellurate and other met- alloids in bacteria from hydrothermal vent fields in the eastern Pacific Ocean. *Appl Environ Microbiol* 72:4950–4956

29. Di Tomaso G, Fedi S, Carnevali M, Manegatti M, Taddei C, Zannoni D (2002) The membrane- bound respiratory chain of *Pseudomonas pseudoalcaligenes* KF707 cells grown in the presence or absence of potassium tellurite. *Microbiology* 148(Pt 6):1699–16708
30. Dudev T, Lin YL, Dudev M, Lim C (2003) First-second shell interactions in metal binding sites in proteins: a PDB survey and DFT/CDM calculations. *J Amer Chem Soc* 125: 3168-3180
31. Emsley J (1989). The Elements. New York: Oxford University Press. Retrieved from https://www.encyclopedia.com/science-and-technology/chemistry/compounds-and-elements/tellurium, Date July 17, 2019
32. Felsenstein J (1985) Confidence limits on phylogenies: an approach using the bootstrap. *Evolution* 39:783–791
33. Finn RD, Bateman A, Clements J, Coggill P, Eberhardt RY, Eddy SR, et al. (2014) Pfam: the protein families database. *Nucleic Acids Res* 42: 222-230
34. Finn RD, Coggill P, Eberhardt RY, Eddy SR, Mistry J, Mitchell AL, et al. (2015) The Pfam protein families database: towards a more sustainable future. *Nucleic Acids Res* 44 (1): 279-285
35. Fleming A (1932) On the specific antibacterial properties of penicillin and potassium tellurite. Incorporating a method of demonstrating some bacterial antagonisms. *J Pathol Bacteriol* 35:831–842
36. Gao H, Obraztova A, Stewart N, Popa R, Fredrickson JK, Tiedje JM, Nealson KH, Zhou J (2006) *Shewanella loihica* sp. nov., isolated from iron-rich microbial mats in the Pacific Ocean. *Int J Syst Evol Microbiol* 56:1911–1916
37. Gasiunas G, Sinkunas T, Siksnys V (2014) Molecular mechanisms of CRISPR-mediated microbial immunity. *Cell Mol Life Sci* 71 (3): 449-465
38. Gasteiger E, Gattiker A, Hoogland C, Ivanyi I, Appel RD, Bairoch A (2003) ExPASy: the proteomics server for in-depth protein knowledge and analysis. *Nucleic Acids Res* 31: 3784-3788

39. Ghachi ME, Howe N, Auger R, Lambion A, Guiseppi A, Delbrassine F, et al. (2017) Crystal structure and biochemical characterization of the transmembrane PAP2 type phosphatidylglycerol phosphate phosphatase from *Bacillus subtilis*. *Cell Mol Life Sci* 74 (12): 2319-2332

40. Gorelick N, Hancher M, Dixon M, Ilyushchenko S, Thau D, Moore R (2017) Google Earth Engine: Planetary-scale geospatial analysis for everyone

41. Grandell L, Hook M (2015) Assesing Rare Metal Availability Challenges for Solar Energy Technologies. *Sustainability* 7, 11818-11837

42. Griffiths AJF, Miller JH, Suzuki DT, Lewontin RC, Gelbart WM (2000) An Introduction to Genetic Analysis. 7th edition. New York: WH Freeman. Bacterial conjugation. Available from: https://www.ncbi.nlm.nih.gov/books/NBK21942/

43. Guex N, Peitsch MC, Schwede T (2009) Automated comparative protein structure modeling with SWISS-MODEL and Swiss-PdbViewer: A historical perspective. *Electrophoresis* 30: 162-173

44. Heap JT, Ehsaan M, Cooksley CM, Ng YK, Cartman ST, Winzer K, et al. (2012) Integration of DNA into bacterial chromosomes from plasmids without a counter-selection marker. *Nucleic Acids Res* 40 (8): 59

45. Hill SM, Jobling MG, Lloyd BH, Strike P, Ritchie DA (1993) Functional expression of the tellurite resistance determinant from the IncHI-2 plasmid pMER610. *Mol Gen Genet* 241:203-212

46. Holt HM, Gahrn-Hansen B, Bruun B (2005) *Shewanella algae* and *Shewanella putrefaciens*: clinical and microbiological characteristics. *Clin Microbiol Infect* 11:347–352

47. Horwitz JP, Chua J, Curby RJ, Tomson AJ, Da Rooge MA, Fisher BE, et al. (1964) Substrates for cytochemical demonstration of enzyme activity. I. Some substituted 3-indoyl-β-D-glycopyranosides. *J Med Chem* 7:574-575

48. Iravani S (2014) Bacteria in Nanoparticle Synthesis: Current Status and Future Prospects. *Int Sch Res Notices* 2014:1-18

49. Itaya M and Tanaka T (1990) Gene-directed mutagenesis on the chromosome of *Bacillus subtilis* 168. *Mol Gen Genet* 223: 268-272

50. Jobling MG and Ritchie DA (1987) Genetic and physical analysis of plasmid genes expressing inducible resistance of tellurite in *Escherichia coli*. *Mol Gen Genet* 208: 288-293
51. Jobling MG and Ritchie DA (1988) The nucleotide sequence of a plasmid determinant for resistance to tellurium anions. *Gene* 66:245-258
52. Jones DT (1999) Protein secondary structure prediction based on position-specific scoring matrices. *J Mol Biol* 292 (2): 195-202
53. Kehres DG, Zaharik ML, Finlay BB, Maguire ME (2000) The NRAMP proteins of *Salmonella typhimurium* and *Escherichia coli* are selective manganese transporters involved in the response to reactive oxygen. *Mol Microbiol* 36 (5): 1085-100
54. Kelley LA and Sternberg MJE (2009) Protein structure prediction on the web: a case study using the Phyre server. *Nat Protoc* 4: 363-371
55. Kim D, Baik KS, Kim MS, Jung BM, Shin TS, Chung GH, Rhee MS, Seong CH (2007) *Shewanella haliotis* sp. nov., isolated from the gut microflora of abalone, *Haliotis discus hannai*. *Int J Syst Evol Microbiol* 57:2926–2931
56. Kimura M (1980) A simple method for estimating evolutionary rate of base substitutions through comparative studies of nucleotide sequences. *J Mol Evol* 16:111-120
57. Klaus-Joerger T, Joerger R, Olsson E, Granqvist C (2001) Bacteria as workers in the living factory: metal-accumulating bacteria and their potential for materials science. *Trends Biotechnol* 19 (1): 15-20
58. Klonowska A, Heulin T, Vermeglio A (2005) Selenite and tellurite reduction by *Shewanella oneidensis*. *Appl Environ Microbiol* 71:5607–5609
59. Korbekandi H, Iravani S, Abbasi S (2009) Production of nanoparticles using organisms. *Crit Rev Biotechnol* 29(4): 279-306
60. Kumar S, Stecher G, Tamura K (2016) MEGA7: Molecular Evolutionary Genetics Analysis Version 7.0 for Bigger Datasets. *Mol Biol Evol* 33 (7): 1870-4

61. Lalucat J, Bennasar A, Bosch R, García-Valdés E, Palleroni NJ (2006) Biology of *Pseudomonas stutzeri. Microbiol Mol Biol Rev* 70, 510-547
62. Lovley DR (1993) Dissimilatory metal Reduction. *Annu Rev Microbiol* 47: 263-290
63. Makui H, Roig E, Cole ST, Helmann JD, Gros P, Cellier MF (2000) Identification of the *Escherichia coli* K-12 Nramp orthologue (MntH) as a selective divalent metal ion transporter. *Mol Microbiol* 35 (5): 1065-78
64. Mal J, Nancharaiah YV van Hullebusch ED, Lens PN (2016) Metal chalcogenide quantum dots: biotechnological synthesis and applications. *RSC Advances.* 47
65. Maltman C, Donald LJ, Yurkov V (2017) Tellurite and Tellurate Reduction by the Aerobic Anoxygenic Phototroph *Erythromonas ursincola* Strain KR99 is carried out by a Novel Membrane Associated Enzyme. *Microorganisms* 5(2):20
66. Marchler-Bauer A, Bryant SH (2004) CD-Search: protein domain annotations on the fly. *Nucleic Acids Res* 32: 327-31
67. Marchler-Bauer A, Bo Y, Han L, He J, Lanczycki CJ, Lu S, et al. (2017) CDD/SPARCLE: functional classification of proteins via subfamily domain architectures. *Nucleic Acids Res* 45 (1): 200-203
68. Marchler-Bauer A, Derbyshire MK, Gonzales NR, Lu S, Chitsaz F, Geer LY, et al. (2015) CDD: NCBI's conserved domain database. *Nucleic Acids Res* 43: 222-6
69. Marchler-Bauer A, Lu S, Anderson JB, Chitsaz F, Derbyshire MK, DeWeese-Scott C, et al. (2011) CDD: a Conserved Domain Database for the functional annotation of proteins. *Nucleic Acids Res* 39: 225-9
70. Martinez-Finley EJ, Chakraborty S, Fretham S, Aschner M (2012) Admit One: How Essential and Nonessential metals Gain Entrance into the Cell. *Metallomics* 4 (7): 593-605
71. Mayers B, Xia Y (2002) One-dimensional nanostructures of trigonal tellurium with various morphologies can be synthesized using a solution-phase approach. *J Mater Chem* 12: 1875-1881

72. McLoughlin AJ (1994) Plasmid stability and ecological competence in recombinant cultures. *Biotechnol Adv* 12 (2): 279-324
73. Monias B (1928) Classification of *Bacterium alcaligenes pyocyaneum* and *fluorescens*. *J Infect Dis* 43(4):330–334
74. Moore M and Kaplan S (1992) Identification of intrinsic high-level resistance to rare-earth oxides and oxyanions in members of the class Proteobacteria: characterization of tellurite, selenite, and rhodium sesquioxide reduction in *Rhodobacter sphaeroides*. *J Bacteriol* 174:1505-1514
75. Moore MD, Kaplan S (1994) Members of the family Rhodospirillaceae reduce heavy metal oxy-anions to maintain redox poise during photosynthetic growth. *ASM News* 60:17–24
76. Mori T, Iwamoto K, Wakaoji S, Araie H, Kohara Y, Okamura Y (2016) Characterization of a novel gene involved in cadmium accumulation screened from sponge-associated bacterial metagenome. *Gene* 576 (2): 618-625
77. Moyes RB, Reynolds J, Breakwell DP (2009) Prelimibnary Staining of Bacteria: Simple Stains. *Curr Protoc Microbiol* 15 (1): 3-5
78. Narayanan KB and Sakthivel N (2010) Biological synthesis of metal nanoparticles by microbes. *Adv Colloid Interface Sci* 156 (1-2): 1-13
79. Nei M, Kumar S (2000) Molecular evolution and phylogenetics. Oxford University Press, New York
80. Neuwald AF (1997) An unexpected structural relationship between integral membrane phosphatases and soluble haloperoxidases. *Protein Sci* 6, 1764-1767
81. Nozue H, Hayashi T, Hashimoto Y, Ezaki T, Hamasaki K, Ohwada K, Terawaki Y (1992) Isolation and characterization of *Shewanella alga* from human clinical specimens and emendation of the description of *S. alga* Simidu et al., 1990, 335. *Int J Syst Bacteriol* 42:628–634
82. Okamura Y, Kimura T, Yokouchi H, Meneses-Osorio M, Katoh M, Matsunaga T, et al. (2010) Isolation and characterization of a GDSL

esterase from the metagenome of a marine sponge-associated bacteria. *Mar Biotechnol* 12 (4): 395-402

83. Oremland RS, Herbel MJ, Blum JS, Langley S, Beveridge TJ, Ajayan PM, Sutto T, Ellis AV, Curran S (2004) Structural and spectral features of selenium nanospheres produced by Se-respiring bacteria. *Appl Environ Microbiol* 70:52–60
84. Passerini A, Lippi M, Frasconi P (2011) MetalDetector v2.0: Predicting the Geometry of Metal Binding Sites from Protein Sequence. *Nucleic Acids Res* 39 (2): 288-292
85. Pérez JM, Calderón IL, Arenas FA, Fuentes DE, Pradenas GA, Fuentes EL, et al. (2007) Bacterial toxicity of potassium tellurite: unveiling an ancient enigma. *PLoS ONE* 2:2
86. Pugin B, Cornejo FA, Muñoz-Diaz P, Muñoz-Villagrán CM, Vargas-Pérez JI, Arenas FA, Vásquez CC (2014) Glutathione reductase-mediated synthesis of tellurium-containing nanostructures exhibiting antibacterial properties. *Appl Environ Microbiol* 80:7061–7070
87. Ralston-Barrett E, Palleroni NJ, Duodoroff M (1976) Phenotypic Characterization and Deoxyribonucleic Acid Homologies of the "*Pseudomonas alcaligenes*" Group. *Int J Syst Bacteriol* 26, 421-426
88. Romero JM, Orejas RD, Lorenzo VD (1998) Resistance to tellurite as a selection marker for genetic manipulations of *Pseudomonas* strains. *Appl Environ Microbiol* 64:4040–4046
89. Rosselló-Mora RA, Lalucat J, Dott W, Kämpfer P (1994) Biochemical and chemotaxonomic characterization of *Pseudomonas stutzeri* genomovars. *J Appl Bacteriol* 76, 226-233
90. Roy A, Kucukural A, Zhang Y (2010) I-TASSER: a unified platform for automated protein structure and function prediction. *Nat Protoc* 5: 725-738
91. Rzhetsky A, Nei M (1992) A simple method for estimating and testing minimum evolution trees. *Mol Biol Evol* 9:945–967

92. Sabaty M, Avazeri C, Pignol D, Vermeglio A (2001) Characterization of the reduction of selenate and tellurite by nitrate reductases. *Appl Environ Microbiol* 67:5122–5126
93. Saitou N, Nei M (1987) The neighbor-joining method: A new method for reconstructing phyloge- netic trees. *Mol Biol Evol* 4:406–425
94. Sanders ER (2012) Aseptic Laboratory Techniques: Plating Methods. *J Vis Exp* 63:3064, 1-18
95. Schaad NW, Sowell G, Goth RW, Colwell RR, Webb RE (1978) *Pseudomonas pseudoalcaligenes* subsp. *citrulli* subsp. nov. *Int J Syst Bacteriol* 28:117–125
96. Simidu U, Kita-Tsukamoto K, Yasumoto T, Yotsu M (1990) Taxonomy of four marine bacterial strains that produce tetrodotoxin. *Int J Syst Bacteriol* 40:331–336
97. Simon FS, Prinz WC (1973) Tellurium, in Brobst, D.A. and Pratt, W.P. eds., United States mineral resources: U.S. Geological Survey Professional Paper 820, p. 627-630, available at http://pubs.er.usgs.gov/usgspubs/ pp/pp820/
98. Sepahei A, Rashetnia V (2009) Tellurite resistance and reduction during aerobic and anaerobic growth of bacteria isolated from Sarchesme Copper Mine. *Iran J Environ Health Sci Eng*. 6:4, 253-260
99. Smith AC, Hussey MA (2005) Gram Stain Protocols. *ASM,* 1-9
100. Tamura K, Stecher G, Peterson D, Filipski A, Kumar S (2013) MEGA6: molecular evolutionary genetics analysis version 6.0. *Mol Biol Evol* 30:2725–2729
101. Taylor DE (1999) Bacterial tellurite resistance. *Trends Microbiol* 7:111–115
102. Taylor DE, Rooker M, Keelan M, Ng LK, Martin I, Perna NT, et al. (2002) Genomic variability of O islands encoding tellurite resistance in enterohemorrhagic *Escherichia coli* O157:H7 isolates. *J Bacteriol* 184, 4690-4698
103. Thapa S, Li H, Joshua O, Bhatti HS, Zhou S (2017) Metagenomics Prospective in Bio-mining The Microbial Enzymes. *J Genes Proteins* 1:1

104. Thompson JD, Higgins DG, Gibson TJ (1994) CLUSTALW: improving the sensitivity of progressive multiple sequence alignment through sequence weighting, position-specific gap penalties and weight matrix choice. *Nucleic Acids Res* 22(22): 4673-4680

105. Tremaroli V, Fedi S, Zannoni D (2007) Evidence for a tellurite-dependent generation of reactive oxygen species and absence of a tellurite-mediated adaptive response to oxidative stress in cells of *Pseudomonas pseudoalcaligenes* KF707. *Arch Microbiol* 187 (2): 127-35

106. Trouba J (2019) Tellurium as a By-product of Copper Refining. Critical Materials Institue, Colorado School of Mines.

107. Trüper HG and de' Clari L (1997) Taxonomic note: necessary correction of specific epithets formed as substantives (nouns) 'in apposition'. *Int J Syst Bacteriol* 47, 908-909

108. Trutko SM, Akimenko VK, Suzina NE, Anisimova LA, Shlyapnikov MG, Baskunov BP, Duda VI, Boronin AM (2000) Involvement of the respiratory chain of gram-negative bacteria in the reduction of tellurite. *Arch Microbiol* 173:178–186

109. Trutko SM, Suzina NE, Duda VI, Akimenko VK, Boronin AM (1998) Participation of the bacterial respiratory chain in reduction of potassium tellurite. *Dokl Akad Nauk* 358 (6): 836-838

110. Tucker FL, Walper JF, Appleman MD, Donohue J (1962) Complete reduction of tellurite to pure tellurium metal by microorganisms. *J Bacteriol* 83:1313–1314

111. Turner MS, Tan YP, Giffard PM (2007) Inactivation of an Iron transporter in *Lactobacillus lactis* Results in Resistance to Tellurite and Oxidative Stress. *Appl Environ Microbiol* 73(19): 6144-6149

112. Turner RJ (2001) Tellurite toxicity and resistance in gram-negative bacteria. *Recent Res Dev Microbiol* 5:69–77

113. Turner RJ, Aharonowitz Y, Weiner JH, Taylor DE (2001) Glutathione is a target in tellurite toxicity and is protected by tellurite resistance determinants in *Escherichia coli*. *Can J Microbiol* 47: 33–40

114. Turner RJ, Borghese R, Zannoni D (2012) Microbial processing of tellurium as a tool in biotechnology. *Biotechnol Adv* 30:954–963

115. Venkateswaran K, Dollhopf ME, Aller R, Stackebrandt E, Nealson KH (1998) *Shewanella amazonensis* sp. nov., a novel metal-reducing facultative anaerobe from Amazonian shelf muds. *Int J Syst Bacteriol* 48:965–972

116. Vincze T, Posfai J, Roberts RJ (2003) NEBcutter: a program to cleave DNA with restriction enzymes. *Nucleic Acids Res* 31 (13): 3688-3691

117. Waterhouse A, Bertoni M, Bienert S, Studer G, Tauriello G, Gumienny R, et al. (2018) SWISS-MODEL: homology modelling of protein structures and complexes. *Nucleic Acids Res* 46 (1): 296-303

118. Whelan KF, Colleran E, Taylor DE (1995) Phage inhibition, colicin resistance, and tellurite resistance are encoded by a single cluster of genes on the IncHI1 plasmid R478. *J Bacteriol* 177:5016-5027

119. Yang J, Yan R, Roy A, Xu D, Poisson J, Zhang Y (2015) The I-TASSER Suite: Protein structure and function prediction. *Nat Methods* 12:7-8

120. Yanisch-Perron C, Vieira J, Messing J (1985) Improved M13 phage cloning vectors and host strains: nucleotide sequences of the M13mpl8 and pUC19 vectors. *Gene* 33 (1): 103-119

121. Yurkov VV, Beatty JT (1998) Aerobic anoxygenic phototrophic bacteria. *Microbiol Mol Biol Rev* 62 (3): 695-724

122. Zhang Y (2008) I-TASSER server for protein 3D structure prediction. *BMC Bioinformatics* 9, 40

123. Zhang Y, Yang Z, Huang X, Peng J, Fei X, Gu S, et al. (2008) Cloning, expression, and characterization of a thermostable PAP2L2, a new member of the type-2 phosphatidic acid phosphatase family from *Geobacillus toebii* T-85. *Biosci Biotechnol Biochem* 72(12): 3134-41

124. Zhang X, Jiao S, Tu J, Li-Song W, Xiao X. et al. (2019). Rechargeable ultrahigh-capacity tellurium-aluminum batteries. *Energy and Environ Sci* 6

Acknowledgements

This PhD Thesis was made into fruition through the Top Global University Project of the Ministry of Education, Culture, Sports, Science and Technology (MEXT) Japan. To the Graduate Committee of the Graduate School of Advanced Sciences of Matter (AdSM), Hiroshima University, I could have not completed my PhD requirements without your kindest consideration for allowing me to have an on-line public presentation of my thesis amidst a global pandemic.

To Prof. YOSHIKO OKAMURA and Ms. TERUMI NAKADATE, for their relentless guidance and academic support all throughout my PhD training, a sincere gratitude for all your help. The new tellurite-reducing bacterial strains, novel gene conferring tellurite reduction activity, and a chloramphenicol-susceptible A1 strain will never be isolated and discovered without the generosity of Dr. TAKESHI TERAHARA of the Tokyo University of Marine Science and Technology for providing the marine sediment that was used all throughout this thesis.

To Prof. LAWRENCE LIAO, CHAROSE PEREZ, CZARINA LABAYO, and DAVE ANGELES, I appreciate every moment we spend together in Saijo.

To my siblings, FARIDA, DARWIN, and NERIZA, who are always there to support me in pursuing my dreams, THANK YOU from the bottom of my heart. To my mother, GLORIA PASCUAL MUNAR, your unconditional love and prayers always brings peace, protection, and comfort to my soul, THANK YOU with all my heart. To my father, ARTEMIO DELA CRUZ MUNAR, you are my inspiration, my role model, and my HERO, thank you for the guidance from above. You are forever in my heart.

AD MAJOREM DEI GLORIAM

公表論文
（Articles）

(1) Biomineralization of Metallic Tellurium by Bacteria Isolated from Marine Sediment Off Niigata Japan

Munar MP, Matsuo T, Kimura H, Takahashi H, Okamura Y

In: Endo K, Kogure T, Nagasawa H (eds)

Biomineralization, Springer, Singapore. 31, 291- 301 (2018)

DOI**:** https://doi.org/10.1007/978-981-13-1002-7_31

(2) Discovery of a Novel Gene Conferring Tellurite Tolerance Through Tellurite Reduction to *Escherichia coli* Transformant in Marine Sediment Metagenome Library

Munar MP, Takahashi H, Okamura Y

Marine Biotechnology 21, 762-772 (2019)

DOI: https://doi.org/10.1007/s10126-019-09922-w